

**A novel role for Ral in response to mitochondrial depolarization**

Sarah Rachel Pollock  
Churchville, PA

M.S. Biological & Physical Sciences, University of Virginia, 2015  
B.A. Biology, Minor in English, Franklin & Marshall College, 2013

A dissertation presented to the Graduate Faculty of the University of Virginia in  
Candidacy for the Degree of Doctor of Philosophy

Department of Microbiology, Immunology and Cancer Biology

University of Virginia  
May 2019

**Thesis Abstract:**

Healthy mitochondria use an electrochemical gradient across the inner mitochondrial membrane (IMM) to generate energy in the form of ATP. A variety of endogenous and exogenous factors can lead to transient or sustained depolarization of the IMM, including mitochondrial fission events, expression of uncoupling proteins, electron transport chain (ETC) inhibitors, or chemical uncouplers. This depolarization in turn leads to a variety of physiological responses, ranging from selective mitochondrial clearance (mitophagy) to cell death. There are multiple types of mitophagy including PINK1-Parkin mitophagy in which the kinase, PINK1 accumulates on outer mitochondrial membrane (OMM) and results in Parkin (an E3 ubiquitin ligase) translocation from the cytosol to the OMM to recruit the autophagy machinery. How cells recognize and ultimately respond to depolarized mitochondria remains incompletely understood. We found that the small Ras-like GTPases, RalA and RalB relocate to depolarized mitochondria in a clathrin-dependent process. Furthermore, both genetic and pharmacologic inhibition of RalA and RalB leads to an increase in the activity of the atypical I $\kappa$ B kinase TBK1 both basally and in response to mitochondrial depolarization. We also observed this phenotype following inhibition of Ral relocation. Collectively, these data suggest a model in which RalA and RalB inhibit TBK1 and that relocation of Ral (both RalA and RalB) to depolarized mitochondria facilitates TBK1 activation through release of this inhibition. We also found that RalA, but not RalB, participates in Parkin recruitment during PINK1-Parkin mitophagy as RalA knockdown or knockout results in impaired Parkin translocation from the cytosol to depolarized mitochondria. Since the mechanism underlying Parkin recruitment remains unclear,

our findings underscoring the importance of RalA provide new insight into Parkin relocalization. Additionally, pharmacologic and genetic impairment of clathrin-mediated endocytosis (CME) decreases Parkin recruitment, suggesting that CME not only regulates Ral relocalization, but also affects Parkin trafficking. Collectively, our findings point to a novel role for RalA and RalB in response to mitochondrial depolarization.

### **Acknowledgements:**

First I have to thank my mentor, Dave Kashatus for all of his support throughout these past several years. Dave, thank you for your guidance, patience, and for helping me grow into an independent scientist! Thank you for giving me opportunities to share my work at scientific conferences and for encouraging me to explore my ideas for experiments even if they do not always work. I was fortunate to conduct my dissertation research in your lab.

Thank you to my current and former labmates, Sarb, Ali, Saad, and Aldo. You are some of the hardest working people I know. Thank you for making the lab a great environment to work in and for thoughtful scientific discussions. Thank you also to my former undergraduate student, Austin for your instrumental work in helping me with my project.

Thank you to my lab manager, Jen for your constant support both in and outside of the lab. I am grateful for your training. You initially trained me when I first joined the lab in February 2014. I have grams = moles x molecular weight x

liters forever memorized. Thank you also for letting me share my love of dance with you in our few trips to the Charlottesville Salsa Club. Finally, thank you for always inviting me to Sally's dance performances—you know that I truly enjoy them.

I also want to thank my committee members, Dean Kedes, Amy Bouton, Young Hahn, Jim Casanova, and Zhen Yan. Thank you for pushing me to think critically about science. You all have been encouraging throughout numerous committee meetings, especially when I decided to change the focus of my project in my fifth year of graduate school. I am proud of the work that I am leaving behind.

I would not have conducted my doctoral work at UVA had it not been for my undergraduate mentor, Beckley Davis. Beckley, thank you for telling me to apply to UVA and for introducing me to research. I knew nothing about cell culture and experimental design prior to joining your lab.

Of course, I have to thank my parents for their unwavering support throughout my entire education. Without you pursuing my Ph.D. in Microbiology would not have been possible. Thank you for sharing my excitement as my research progressed.

I also need to thank all of the friends I made during graduate school for bringing strength, humor and joy into my life. Keren, thank you for being by my side ever since we first moved to Charlottesville. Graduate school would not have been nearly as great without all of our adventures. Janet and Aiola, you two constantly make me laugh and I am grateful for our friendship. Andrew, thank you for becoming my dance partner and practicing tango, bachata and salsa with me.

Rachel, thank you for cheering for me and for our weekly phone calls that became routine since you left town.

In addition to the friends I made at UVA, I am thankful for the friends who have supported me long before I moved to Charlottesville. Carrie, Ryan, and Ian, thank you for 15 years of friendship and for staying in touch no matter where we live. Ian, thank you also for driving from Pittsburgh to visit me in Charlottesville. Evan, thank you for all our outings. I am thrilled that you were able to join me at UVA after we graduated from F&M.

## Table of Contents

<b>THESIS ABSTRACT:</b> .....	<b>II</b>
<b>ACKNOWLEDGEMENTS:</b> .....	<b>III</b>
<b>LIST OF FIGURES</b> .....	<b>VII</b>
<b>APPENDIX</b> .....	<b>134</b>
<b>REFERENCES</b> .....	<b>140</b>
<b>CHAPTER ONE: INTRODUCTION TO RAL PROTEINS</b> .....	<b>1</b>
<b><i>SECTION A: THE FUNDAMENTALS OF RAL PROTEINS</i></b> .....	<b>1</b>
HISTORICAL BACKGROUND: .....	1
RAL IN DEVELOPMENT: .....	5
RAL AND CANCER: .....	7
THERAPEUTIC TARGETING OF RAL:.....	9
RAL EFFECTORS:.....	11
RAL AND TBK1: .....	15
SUMMARY: .....	17
FIGURES .....	19
<b><i>SECTION B: LINKING RAL PROTEINS WITH MITOPHAGY</i></b> .....	<b>21</b>
INTRODUCTION TO AUTOPHAGY: .....	21
RAL PROTEINS AND AUTOPHAGY:.....	25
OVERVIEW OF MITOCHONDRIA: .....	25
INTRODUCTION TO MITOPHAGY:.....	30
PINK1-PARKIN MITOPHAGY:.....	32
SUMMARY: .....	34
FIGURES .....	36
<b>CHAPTER TWO: UNDERSTANDING THE ROLE OF RAL PROTEINS IN RESPONSE TO MITOCHONDRIAL DEPOLARIZATION</b> .....	<b>38</b>
INTRODUCTION .....	38
RALA AND RALB RELOCALIZE TO MITOCHONDRIA IN RESPONSE TO MITOCHONDRIAL DEPOLARIZATION.....	40
RALA-GTP LEVELS DECREASE FOLLOWING OA AND CCCP TREATMENT .....	43
PHOSPHORYLATION OF NEITHER SERINE 194 NOR SERINE 183 IS REQUIRED FOR RALA RELOCALIZATION FOLLOWING MITOCHONDRIAL DEPOLARIZATION .....	44
CLATHRIN-MEDIATED ENDOCYTOSIS FACILITATES RAL RELOCALIZATION TO DEPOLARIZED MITOCHONDRIA.....	45
RALA AND RALB NEGATIVELY REGULATE TBK1 ACTIVITY.....	47
DISCUSSION .....	49
FUTURE DIRECTIONS .....	53
MATERIALS AND METHODS .....	62
FIGURES .....	74
<b>CHAPTER THREE: A NOVEL ROLE FOR RALA DURING PINK1-PARKIN MITOPHAGY</b> .....	<b>93</b>

INTRODUCTION .....	93
BOTH RALA AND RALB COLOCALIZE WITH PARKIN FOLLOWING MITOCHONDRIAL DEPOLARIZATION.....	94
ALA KNOCKDOWN RESULTS IN IMPAIRED PARKIN RECRUITMENT.....	94
RALB KNOCKDOWN DOES NOT IMPAIR PARKIN RECRUITMENT .....	96
ALA KNOCKOUT RESULTS IN IMPAIRED PARKIN RECRUITMENT .....	96
IMAGING FLOW CYTOMETRY CONFIRMS THAT SHALA HELA CELLS EXHIBIT IMPAIRED PARKIN RECRUITMENT .....	97
EXPRESSION OF GFP-ALA RESCUES PARKIN RECRUITMENT IN SHALA HELA CELLS .....	98
CLATHRIN-MEDIATED ENDOCYTOSIS FACILITATES PARKIN RECRUITMENT FOLLOWING MITOCHONDRIAL DEPOLARIZATION .....	98
DISCUSSION .....	101
FUTURE DIRECTIONS .....	105
MATERIALS AND METHODS .....	108
FIGURES .....	115
<b>CHAPTER FOUR: CONCLUSIONS.....</b>	<b>127</b>

## LIST OF FIGURES

Figure 1.1. RalA and RalB structures.....	19
Figure 1.2. Therapeutic strategies for targeting Ral in cancer.....	20
Figure 1.3. Overview of the role of mitochondrial depolarization in mitochondrial dynamics and mitophagy. ....	36
Figure 1.4. Schematic of PINK1-Parkin mitophagy.....	37
Figure 2.1. Both RalA and RalB are recruited to depolarized mitochondria. ....	74
Figure 2.2. OA, Valinomycin and CCCP induce mitochondrial depolarization and RalA relocalization.....	76
Figure 2.3. GFP does not relocalize to depolarized mitochondria.....	77
Figure 2.4. RalA GTP-loading decreases following mitochondrial depolarization, but does not regulate RalA localization. ....	78
Figure 2.5. Phosphorylation of RalA on Ser194 or Ser183 does not regulate RalA subcellular localization in response to mitochondrial damage.....	80
Figure 2.6. Clathrin-mediated endocytosis facilitates RalA and RalB recruitment to depolarized mitochondria. ....	81
Figure 2.7. shAP50 cells exhibit impaired clathrin-mediated endocytosis. ....	83
Figure 2.8. shAP50 cells exhibit impaired RalA and RalB localization to depolarized mitochondria. ....	84
Figure 2.9. RalA and RalB negatively regulate TBK1 activity.....	86
Figure 2.10. RalA and RalB relocalization to depolarized mitochondria occurs upstream of TBK1 activation.....	87
Figure 2.11. Ral relocalization affects TBK1 activity.....	89
Figure 2.12. shRalA/RalB cells exhibit decreased STING levels.....	90
Figure 2.13. GST-RalA-GTP and GST-RalA-GDP interact similarly with GFP-TBK1...	91

Figure 2.14. Stable expression of Flag RalA restores TBK1 inhibition in shRalA/RalB HeLa cells .....	92
Figure 3.1. RalB and Parkin relocalize in response to OA, Valinomycin and CCCP ..	115
Figure 3.2. Genetic inhibition of RalA results in impaired Parkin recruitment following mitochondrial depolarization.....	116
Figure 3.3. RalB knockdown does not affect Parkin recruitment following mitochondrial depolarization .....	118
Figure 3.4. RalA KO MEFs exhibit impaired Parkin recruitment in response to mitochondrial depolarization .....	119
Figure 3.5. RalA KO MEFs exhibit comparable levels of phospho-ubiquitin (Ser65) following CCCP treatment compared to RalA FL/FL MEFs .....	120
Figure 3.6. Imaging flow cytometry confirms that shRalA HeLa cells exhibit impaired Parkin recruitment.....	121
Figure 3.7. Expression of GFP-RalA rescues Parkin recruitment in shRalA HeLa cells .....	122
Figure 3.8. Clathrin-mediated endocytosis facilitates Parkin recruitment to depolarized mitochondria .....	123
Figure 3.9. shAP50 cells exhibit impaired Parkin recruitment to depolarized mitochondria .....	124
Figure 3.10. Rab7 colocalizes with mitochondria, RalA and Parkin following mitochondrial depolarization .....	125
Figure 3.11. Rab5 is recruited to depolarized mitochondria with Parkin.....	126

## **Chapter One: Introduction to Ral Proteins**

Part of this chapter has been adapted from: Pollock S.R., Kashatus D.F. (2018) Ral. In: Choi S. (eds) Encyclopedia of Signaling Molecules. Springer, Cham.

### ***Section A: The Fundamentals of Ral Proteins***

#### **Historical Background:**

Ral proteins, RalA and RalB, are members of the Ras family of small GTPases. Ral proteins are activated by guanine nucleotide exchange factors (GEFs) that catalyze the exchange of GDP for GTP and facilitate the binding of Ral to its various downstream effector proteins. GTPase-activating proteins (GAPs) stimulate the hydrolysis of GTP to GDP, which inactivates Ral.

The discovery that many tumors contained a transforming Ras allele (*HRAS*, *KRAS* and *NRAS*) in the 1980s spurred interest in identifying new members of the Ras family. In 1986, Pierre Chardin and Armand Tavittian synthesized a 20-mer oligonucleotide probe corresponding to a conserved region of Ras proteins to identify novel Ras genes by screening a simian B-cell line cDNA library <sup>1</sup>. The screen resulted in the discovery of an open reading frame that shared a high degree of homology with the three Ras genes and was consequently named Ral (Ras-like). The probe identified two RNAs that differed in length, resulting from alternative processing <sup>1</sup>. The cDNA of this simian Ral was subsequently used as a probe to isolate human RalA cDNA from a human pheochromocytoma library <sup>2</sup>. Additionally, this screen identified cDNA that encoded for a related protein, RalB.

RalA and RalB are closely related, sharing 85% amino acid sequence identity. Moreover, RalA and RalB share 50% amino acid sequence identity with Ras proteins. Although mammals encode both Ral isoforms, invertebrates such as *Drosophila melanogaster* and *Caenorhabditis elegans* harbor only one Ral gene<sup>3</sup>. Ral genes have only been identified in multicellular organisms, but no Ral orthologues have been found in yeast. In humans, RalA and RalB are located on chromosomes 7 and 2, respectively<sup>4</sup>.

Both Ral proteins share similar structural organization (Figure 1.1). Ral proteins contain an N-terminal 11 amino acid stretch followed by four conserved GTP-binding regions and a C-terminal hypervariable domain that terminates in a CAAX motif (C = cysteine, A = aliphatic amino acid, X = any amino acid) that can be post-translationally modified<sup>5</sup>. RalA and RalB share similar CAAX motifs that terminate in Cys-Cys-Ile-Leu and Cys-Cys-Leu-Leu, respectively. In contrast to Ras proteins that are preferentially farnesylated, Ral proteins are geranyl-geranylated<sup>6</sup>. The CAAX motif undergoes three sequential posttranslational modifications: 1. prenylation 2. proteolysis and 3. carboxymethylation.

Geranylgeranyltransferase-I (GGTaseI) transfers a 20-carbon geranylgeranyl moiety on the first cysteine residue. Following prenylation, Ral localizes to the endoplasmic reticulum where Ras converting endopeptidase 1 (RCE1) cleaves the terminal AAX tripeptide<sup>7</sup>. Isoprenylcysteine carboxymethyltransferase (ICMT) then methylates the lipid-modified cysteine. An alternative posttranslational modification exists where the CAAX motif bypasses proteolysis and carboxymethylation, ultimately resulting in palmitoylation at the second cysteine of

either RalA or RalB CAAX motifs (Cys-Cys-Ile-Leu or Cys-Cys-Leu-Leu, respectively<sup>8</sup>. The precise role of these two different post-translational modifications remains unclear. Both RalA and RalB require RCE1 to localize to the plasma membrane. However, RalA requires ICMT for localization to recycling endosomes, whereas RalB requires ICMT for targeting to the plasma membrane<sup>9</sup>. Moreover, palmitoylation is important for RalB, but not RalA, localization to the plasma membrane.

The most significant sequence divergence between RalA and RalB is in their 30 amino acid hypervariable C-terminal domain<sup>2</sup>. These C-terminal sequences contain distinct sites for post-translational modifications that allow Ral to associate with different membranes. To investigate how differences in the C-terminus affect the biological functions of RalA and RalB, earlier investigations tested the effects of fusing the C-terminal amino acids of RalA to the N-terminal portion of RalB or fusing the C-terminal amino acids of RalB to the N-terminal portion of RalA. These studies revealed that the C-terminus of RalA, but not the C-terminus of RalB is sufficient to promote RalA-driven polarized delivery of membrane proteins and to facilitate RalA-mediated tumorigenesis<sup>10,11</sup>.

The C-terminus likely facilitates different biological functions for Ral proteins by mediating changes in subcellular localization. RalA and RalB are phosphorylated on different sites within their C-termini. Aurora A phosphorylates RalA on Ser194, promoting a shift in RalA subcellular distribution and potentially enhancing RalA activity, as ectopically expressed Aurora A increases RalA activity in a GST-RalBP1-RalBD pulldown assay<sup>12</sup>. RalA is also phosphorylated on Ser183, possibly by PKA<sup>13</sup>.

The tumor suppressor, PP2A $\beta$ , dephosphorylates RalA on both Ser183 and 194, inactivating RalA <sup>14</sup>. In contrast to RalA, PKC $\alpha$  phosphorylates RalB on Ser198 and promotes RalB relocalization to perinuclear regions and anchorage-independent growth in bladder cancer cells <sup>13</sup>. PKC $\alpha$  also phosphorylates RalB on Ser192 <sup>15</sup>. The phosphatase that dephosphorylates RalB on Ser198 and 192 has not yet been discovered. It is not understood exactly how phosphorylation changes RalA and RalB subcellular localization. However, investigators have hypothesized that the addition of a negatively charged phosphate group neutralizes the charge of the polybasic region, enabling dissociation from the plasma membrane and relocalization to other membranes, similar to KRas translocation <sup>16</sup>.

In addition to phosphorylation, Ral proteins can undergo nondegradative ubiquitination <sup>17</sup>. Monoubiquitination of RalA (but not RalB), results in enrichment of RalA in lipid rafts within the plasma membrane. Furthermore, de-ubiquitination of RalA in raft microdomains dissociates RalA from the plasma membrane. The discovery that Ral proteins experience reversible ubiquitination prompted inquiry into the enzymes that regulate Ral ubiquitination. Consequently, it was found that the ubiquitin-specific protease USP33 interacts with both RalA and RalB, which appear to be direct targets of USP33 <sup>18</sup>. However, RalB demonstrates higher affinity for USP33 than RalA when RalB is GDP-bound. Ubiquitination of RalB at Lys47 modulates the ability of RalB to interact with two of its downstream effectors: Sec5 and Exo84. Therefore, nondegradative ubiquitination differentially regulates the functions of RalA and RalB.

Ral activity is not only affected by GDP/GTP cycling and post-translational modifications, but is also altered by calcium and calmodulin. RalA and RalB contain a calmodulin-binding site in their C-termini and a calcium-independent binding site in their N-termini<sup>19</sup>. High intracellular calcium levels promote Ral activity as demonstrated by increased *in vitro* Ral GTP-binding<sup>20,21</sup>. How calcium levels activate Ral has not been elucidated. However, one possibility is that phosphorylation by calcium-dependent kinases may regulate RalGEF or RalGAP activity.

Ral binding to calmodulin requires prenylation of the C-terminal CAAX motif<sup>22</sup>. Calmodulin-binding to Ral is important for thrombin-induced activation of Ral in human platelets. Interestingly, RalA has a higher binding affinity for calmodulin than RalB, which possibly indicates the functional differences between RalA and RalB in calcium- and calmodulin-mediated signaling pathways.

### **Ral in Development:**

Given that RalA and RalB are members of the Ras family of small GTPases, most research focuses on understanding the role of Ral proteins in cancer. However, we cannot appreciate the role of Ral proteins in cancer without understanding their contributions during development. Ral is expressed ubiquitously in tissues, but levels are highest in the brain, testis and platelets<sup>23-25</sup>. Zhao and Rivkees characterized the spatial and temporal patterns of RalA and RalB expression in mice during embryogenesis from E9.5 to E16 and showed that RalA and RalB expression first emerges in the brain and gut<sup>26</sup>.

RalA null mice are embryonic lethal, while RalB null mice display no apparent phenotype <sup>27</sup>. To determine why RalA null mice are embryonic lethal, embryos from RalA<sup>+/-</sup> crosses were examined and several embryos between E10.5 and E19.5 exhibited exencephaly: a disorder where the brain resides outside of the skull. Failure of neural tube closure causes exencephaly, indicating that RalA plays a role in neural tube closure. Moreover, RalA and RalB appear to share some functions during development because RalA<sup>-/-</sup>; RalB<sup>-/-</sup> mice are embryonic lethal.

The role of Ral in development has also been studied in *Drosophila melanogaster*. *Drosophila* only have one Ral gene, which is essential for viability <sup>28</sup>. The development of *Drosophila* bristles and hairs is commonly used as a model for studying regulation of the cytoskeleton because these phenotypes are easy to observe. Consequently, one group sought to identify the role of Ral in development by examining the effects of different Ral mutants in transgenic *Drosophila* on bristle and wing hair formation. A dominant negative *Drosophila* homologue of Ral, DRal<sup>S25N</sup>, results in loss of bristles on the nota by impairing bristle shaft initiation <sup>29</sup>. Moreover, expression of DRal<sup>S25N</sup> results in multiple wing hairs shorter than those in wild type *Drosophila*, suggesting disturbed organization of the actin cytoskeleton. Single large bundles of F-actin (referred to as prehair) form in each wing cell. *Drosophila* expressing DRal<sup>S25N</sup> exhibit an abnormal number of prehairsts and irregular prehair morphology, suggesting that Ral is involved in the initiation of hair development <sup>29</sup>.

Interestingly, mutating genes encoding JNKK and JNK suppresses the DRal<sup>S25N</sup> induced bristle phenotype and expression of constitutively active Ral,

DRal<sup>G20V</sup>, inhibits JNK phosphorylation <sup>29</sup>. Consequently, these data suggest that Ral controls changes in cell shape by inhibiting the JNK pathway. Consistent with the observed JNK phosphorylation in *Drosophila*, depletion of RalA in HeLa cells increases JNK phosphorylation, further supporting that Ral is a negative regulator of JNK <sup>28</sup>. Given that JNK and p38 MAP kinase are often coactivated in mammals in response to various stresses such as TNF, the effect of Ral on p38 MAP kinase phosphorylation was investigated. RalA depletion in HeLa cells impairs TNF-induced p38 MAP kinase activation, indicating that RalA positively regulates p38 MAP kinase. While the full molecular details of the RalA-JNK signaling axis remain to be fully elucidated, epistasis experiments demonstrated that Ral regulates cell-death through the JNK pathway during embryogenesis <sup>28</sup>. Furthermore, the exocyst was identified as a point of crosstalk between Ral and JNK signaling.

In addition to Ral's role in development in mice and *Drosophila*, Ral is also involved in human development. A study identified mutations within the GTP/GDP-binding region of RalA in ten probands that were associated with speech and motor delays as well as facial dysmorphism, short stature, and low weight <sup>30</sup>. Interestingly, all RalA mutations, except for one, decreased GTPase activity and RalA effector-protein binding. This finding implicates RalA in facilitating human development and provides insight into RASopathies, which are diseases that arise due to mutations in RAS/MAPK signaling proteins.

### **Ral and Cancer:**

Given that Ral proteins function downstream of Ras and that four RalGEFs bind directly to activated Ras, a lot of research has focused on the role of Ral in Ras-driven tumorigenesis. Interestingly, activating mutations of Ral have not been identified in human cancers. Despite this, several studies point to aberrant activation of Ral in human cancer tissues and cell lines. For example, increased Ral activation has been found in bladder, colon, pancreatic and brain cancers<sup>31-34</sup>. The mechanism of Ral activation in cancer remains an ongoing investigation. However, aberrant activation of Ral in different cancers may be caused by altered expression of its regulators such as GAPs, GEFs and deregulation of known Ral-regulating kinases.

RalA and RalB have both distinct and redundant roles in cancer, which reflects the complexity of their function. RalA is required for cellular proliferation and anchorage-independent proliferation in human tumor cell lines, while RalB is required for survival of transformed cells<sup>35</sup>. Chris Counter's group used siRNA to deplete RalA or RalB levels in human cells and found that constitutively GTP-bound RalA, but not RalB is sufficient to transform human cells<sup>11</sup>. Further highlighting the importance of RalA in the initiation of tumorigenesis, RalA, but not RalB is required for the establishment of *K-Ras* mutation-positive human pancreatic tumors in immunocompromised mice<sup>31</sup>.

In contrast to the findings in human cell lines, analysis of RalA and RalB knockout mice demonstrated that elimination of RalA and RalB in a mouse model of non-small cell lung carcinoma (NSCLC) did not impair KRas<sup>G12D</sup>-driven tumors, suggesting that both RalA and RalB are dispensable for tumorigenesis, at least in

this model <sup>27</sup>. The apparent discrepancy in these data may reflect species-specific differences in Ral's function in tumorigenesis because human and mouse cells exhibit distinct effector requirements during Ras-driven oncogenesis <sup>36</sup>.

Alternatively, the differences may reflect variations in experimental design, since much of the previous analysis of Ral function in cancer has employed siRNA-mediated knockdown or expression of dominant negative mutants, both of which can have inherent off-target effects complicating data interpretation.

The RalGEF pathway promotes tumor invasion and metastasis. RalA is predominantly associated with anchorage independent survival and cellular proliferation, but RalB appears to play more of a role in metastasis. RalB mediates trafficking of Multiple Myeloma cells and promotes invasion and metastasis of glioma cells <sup>37,38</sup>. Although RalB appears to be more involved in metastasis, this effect may be tumor-type specific. For instance, in human prostate cancer cells, RalA, but not RalB is required for bone metastasis <sup>39</sup>. In contrast, knockdown of neither RalA nor RalB affects metastasis of MDA-MB-231 cells, a human breast cancer cell line in athymic nude mice <sup>39</sup>. Collectively, these data suggest that the role of RalA or RalB in metastasis is tumor-type specific and scientists should be cautious about assigning particular functions in cancer to either Ral protein.

### **Therapeutic Targeting of Ral:**

With the notorious struggle to directly target Ras in different Ras-driven cancers, there is growing interest in targeting Ral proteins as potential cancer therapeutics. Ras is difficult to target because it does not contain an obvious drug-

binding pocket and functions as a signaling node. However, targeting Ral proteins may be more promising than that of Ras (Figure 1.2). Both RalA and RalB are substrates of geranylgeranyltransferase I (GGTase-I). Inhibition of Ral geranylgeranylation affects anchorage-independent and -dependent tumor cell growth <sup>6</sup>, indicating that GGTase-I inhibitors may be useful in targeting Ral. However, it would be difficult to selectively target Ral with GGTase-I inhibitors since they target additional small GTPases such as RhoA.

In 2014, *Yan et al.*, discovered two chemical inhibitors of Ral that inhibited tumor xenograft growth similar to depleting Ral in human lung cancer cell lines: RBC8 and BQU57. Importantly, these Ral inhibitors are selective for Ral over other GTPases such as RhoA and Ras. However, RBC8 and BQU57 are first generation tools and it is not known how effective they would be in clinical trials.

Helen Mott's group recently developed a stapled peptide approach for inhibiting Ral <sup>40</sup>. Stapled peptides contain a chemically synthesized brace, which stabilizes the  $\alpha$ -helical confirmation of the peptides. The introduction of a staple improves the ability of the peptide to penetrate the cell and helps protect the peptide from protease degradation. The future of stapled peptides as cancer therapeutics appears promising as stapled peptides designed to reactivate p53 are currently undergoing phase I clinical trials, while another stapled peptide designed to act as a long acting growth releasing hormone (GHRH) agonist has already passed phase I trials. Stapled peptides were designed to inhibit Ral based on the RalB-RalBP1 Ral-Binding Domain, so the peptides exhibit a higher affinity for RalB than RalA <sup>40</sup>. Consequently, the ability of the stapled peptides to inhibit Ral activity was

only tested for RalB and not RalA. RalB becomes active in response to nutrient starvation and is both necessary and sufficient for autophagy. Mott's group found that one of their stapled peptides against Ral (referred to as SP1), inhibited GFP-LC3 (an autophagosome marker) turnover in HeLa cells that stably express GFP-LC3. Nutrient starvation failed to reverse SP1-inhibition of GFP-LC3 turnover, demonstrating that SP1 inhibits RalB. Further investigation is required to examine how SP1 will function as a possible cancer therapeutic in a mouse model of Ras-driven tumorigenesis.

In addition to targeting Ral for use as a cancer therapy, it is also possible that Ral may be used as a biomarker for certain cancers such as hepatocellular carcinoma and prostate cancer <sup>41,42</sup>. Patients with cancer often mount an immune response, which is likely driven by tumor-associated antigens (TAAs). Consequently, there is a change in autoantibody production against TAAs, enabling TAAs to be used as biomarkers for cancer. Studies have found that patients with prostate cancer or hepatocellular carcinoma tend to have elevated autoantibody production against RalA <sup>41,42</sup>. Moreover, examining both RalA autoantibody and PSA levels significantly increases prostate cancer detection. Therefore, combining Ral with other established biomarkers might further increase our ability to detect at least a subset of cancers.

### **Ral Effectors:**

Ral's function depends upon the numerous effector proteins to which Ral binds in a GTP-dependent manner via its effector-binding loop. This section highlights several Ral effectors, though it is not a comprehensive list.

## Well-Characterized Effectors

The following described effector proteins are commonly studied and implicate both RalA and RalB in membrane remodeling, cell polarity, endocytosis and exocytosis. It is important to recognize these effector proteins because they mediate Ral's potential functions.

### *RalBP1*

The first Ral binding partner identified was RalBP1 (synonyms: RLIP76 and Rip1) <sup>43-45</sup>. RalBP1 is a large protein that has a vast array of functions ranging from receptor-mediated endocytosis to facilitating mitochondrial fission during mitosis <sup>46,47</sup>. RalBP1 binds GTP-bound Ral <sup>48</sup>. Even though RalA and RalB are 100% identical in their contact sites for binding RalBP1, the binding surfaces on RalBP1 that contact RalA and RalB are not identical <sup>49</sup>. For example, an L492A mutation reduces RalA binding more than RalB. Functionally, RalBP1 exhibits GAP activity toward CDC42 and Rac1, which stimulate filopodia and lamellipodia formation, respectively. Therefore, a RalBP1-Ral interaction implicates Ral in regulating actin cytoskeleton changes.

The Ral-RalBP1 interaction has also been implicated in receptor-mediated endocytosis. Specifically, RalBP1 binds two Eps homology (EH) domain-containing proteins: POB1 and Reps15. RalBP1 also binds to the  $\mu$ 2 subunit of AP2, which recruits clathrin to sites of endocytosis <sup>46,50,51</sup>. However, it remains unclear as to whether Ral promotes or inhibits endocytosis. Overexpression of wild-type RalA and the EGF receptor (EGFR) in rat fibroblasts results in reduced EGF-induced EGFR internalization, suggesting that RalA negatively regulates receptor-mediated

endocytosis<sup>52</sup>. However, expression of either constitutively active Ral (Ral<sup>G23V</sup>) or inactive Ral (Ral<sup>S28N</sup>) in two different cell lines inhibits EGFR internalization, suggesting GDP/GTP cycling may be important for RalA's regulation of EGFR internalization<sup>50</sup>. Additional studies will be required to determine the precise role of the Ral-RalBP1 interaction in endocytosis.

In addition to mediating endocytosis, RalBP1 functions as an ATP-dependent transporter, potentially contributing to multidrug resistance<sup>53</sup>. ATP-dependent transporters can pump drugs out of cells, which results in multidrug resistance due to decreased intracellular drug concentrations. RalBP1 is overexpressed in different human cancers such as colorectal and breast cancer. However, it remains unclear how RalBP1 contributes to Ral's tumorigenic potential.

#### *The Exocyst*

The exocyst is an octameric protein complex that tethers vesicles to the plasma membrane and regulates exocytosis. Both RalA and RalB interact with two subunits of the exocyst, Sec5 and Exo84 in a GTP-dependent manner<sup>54,55</sup>. However, RalA has a higher affinity for the exocyst than RalB due to distinct amino acid sequences in RalA that are distal to the effector-binding domain. The exocyst targets the glucose transporter, Glut4, to the plasma membrane and insulin-induced activation of RalA stimulates Glut4 trafficking to the plasma membrane in adipocytes<sup>56</sup>. It must be noted though that the exocyst not only facilitates insulin secretion, but also regulates all types of secretion. The exocyst is not only involved in exocytosis, but also regulates cell polarity and membrane remodeling. RalA's

association with the exocyst enhances basolateral delivery of membrane components in epithelial cells <sup>10</sup>.

The Ral-Exocyst complex also plays a role in innate immunity. Knockdown of Sec5 or RalA results in impaired cytotoxicity in NK cells, suggesting that Ral-mediated exocyst assembly is required for NK cells to efficiently kill target cells <sup>57</sup>. The RalB and Sec5 complex has also been implicated in innate immunity. A RalB-Sec5 interaction recruits and activates the I $\kappa$ B family member kinase, TBK1, which in turn promotes activation of the immune response to virus exposure <sup>58</sup>.

Additionally, RalB interactions with the exocyst have functions outside of regulating exocytosis. For example, RalB and its effector, Exo84 help activate autophagosome assembly to mediate the cellular starvation response <sup>59</sup>.

### Other Ral-binding Proteins

In addition to well-characterized effectors, other Ral-binding proteins dictate Ral's function. It is important to consider other possible effects of these Ral-binding proteins on Ral's function, which range from transcriptional regulation to filopodia formation.

#### *Phospholipase D (PLD)*

Ral interacts with PLD1 in a nucleotide-independent manner, but it is not known if Ral binds PLD2. PLD is a lipase that catalyzes the hydrolysis of phosphatidylcholine to choline and phosphatidic acid. Phosphatidic acid acts as a second messenger to facilitate vesicle budding and transport. The Ral-PLD1 complex is associated with a small GTPase, Arf, which in turn promotes PLD1 activity <sup>60</sup>. Arf-

induced PLD1 activation is involved in receptor-mediated endocytosis and exocytosis <sup>52,61</sup>.

### *ZONAB*

RalA interacts with the Y-box transcription factor, ZO-1-associated nucleic-acid binding protein (ZONAB) in a GTP and cell-density-dependent manner <sup>62</sup>. High cell density and cell cycle arrest cause RalA to relocate to the plasma membrane where it colocalizes with ZONAB. Relocalization of ZONAB from the nucleus to the plasma membrane relieves its transcriptional repression.

### *Filamin*

RalA binds filamin in a GTP-dependent manner <sup>63</sup>. RalA-induced filopodia formation requires filamin binding. Moreover, a constitutively active form of RalA changes the cellular distribution of filamin and recruits it into the cytoskeleton. Interestingly, increased filopodia formation can promote cell migration and is a characteristic of invasive carcinoma cells <sup>64</sup>. Consequently, RalA-induced filopodia formation could be another link between RalA and cancer.

### *PKC $\eta$*

RalA binds to the C-terminus of PKC $\eta$ , which is a kinase required for keratinocyte differentiation <sup>65</sup>. PKC $\eta$  binding to RalA results in activation of RalA and actin depolymerization. However, the mechanism behind how RalA activation contributes to keratinocyte differentiation remains unclear.

### **Ral and TBK1:**

Ral's interaction with Sec5 and Exo84 link Ral activity to that of TANK-binding kinase 1 (TBK1) activity, a non-canonical I $\kappa$ B kinase that regulates a variety of cellular processes including autophagy and the inflammatory response. TBK1 generally becomes active when it undergoes trans-autophosphorylation in its activation loop at Ser 172 <sup>66</sup>. Subcellular localization of TBK1 and various adapter proteins regulate its function as local clustering of TBK1 promotes autophosphorylation.

However, the mechanism of TBK1 activation may be context dependent as a previous study found that depolarization-induced TBK1 activation requires PINK1 <sup>67</sup>. Moreover, HeLa cells pre-treated with the TBK1 inhibitor, MRT and depolarized with oligomycin and antimycin A did not impair phosphorylation of TBK1, suggesting that TBK1 activation is not autocatalytic following mitochondrial depolarization <sup>68</sup>. MRT targets the kinase dimer interface, thus preventing TBK1 activation. Antimycin A inhibits complex III of the electron transport chain, while oligomycin inhibits ATP synthase. The combinatorial use of antimycin A and oligomycin collapses the proton gradient across the inner mitochondrial membrane.

Following activation, TBK1 can phosphorylate a variety of target proteins including p62, Akt, IRF-3 and IRF-7 <sup>66,69</sup>. Nonsense, frameshift, and missense mutations in TBK1 can result in impaired autophagy and are linked to amyotrophic lateral sclerosis (ALS) <sup>70</sup>.

Expression of a constitutively active RalB mutant results in a Sec5-dependent increase in TBK1 activity during oncogene activation to promote tumor cell survival <sup>58</sup>. Moreover, viral infection also results in RalB mediated Sec5-dependent increase

in TBK1 activity <sup>18</sup>. TBK1 phosphorylation of Exo84 leads to dissociation of the RalA/Exo84 complex to promote Glut4 trafficking during insulin signaling <sup>71</sup>.

Therefore, Ral has context-dependent effects on TBK1.

Interestingly, ubiquitination of Ral dictates the effector that it binds, which subsequently regulates a particular cellular process. Deubiquitinase USP33 regulates RalB ubiquitination on Lys 47 and determines whether RalB binds Exo84 or Sec5 <sup>18</sup>. Nutrient starvation triggers deubiquitination of RalB on Lys 47, which enables RalB to interact with Exo84, forming a complex with Beclin-1 that results in autophagosome formation <sup>18</sup>. In contrast, viral infection promotes RalB ubiquitination, resulting in a RalB-Sec5 interaction that causes TBK1 to activate IRF-3, initiating an inflammatory response <sup>18</sup>. In summary, context-dependent signals regulate ubiquitination of RalB to determine the effector protein to which it binds and subsequent cellular effect.

### **Summary:**

Our understanding of RalA and RalB function and regulation has steadily increased since the discovery of Ral in 1986. However, further research is required to formally determine why RalA and RalB have the same set of effectors and yet, function differently. Moreover, it remains to be understood exactly how RalA and RalB contribute to tumor growth downstream of Ras activation. There is mounting evidence that Ral proteins function as drivers in Ras-mediated tumorigenesis. However, is the role of different Ral proteins tumor-type specific and if so, what drives this preference for one Ral protein over another? With recent advancements

in Ral inhibition such as stapled peptides and small molecule inhibitors, we should be able to distinguish RalA and RalB functions in Ras-driven cancers. Additionally, advancements in genetic modification such as CRISPR will aid our understanding of RalA and RalB function and regulation. Other questions remain as well, such as, what distinct roles are played by the multiple RalGEFs and RalGAPs and do other yet to be discovered kinases and phosphatases regulate Ral activity? As our knowledge about Ral regulation and function expands, we can hopefully develop new methods to target the Ral pathway in Ras-driven cancers.

## Figures

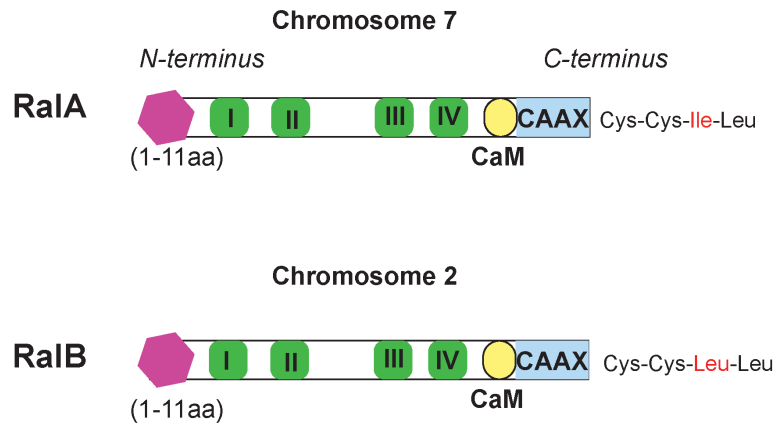


**Figure 1.1.** RalA and RalB structures. The four GTP motifs are labeled I-IV. Both RalA and RalB contain a calmodulin-binding site (CaM) in their C-terminus. Differences in the CAAX motif between RalA and RalB are highlighted in red.

## Therapeutic Targeting of Ral

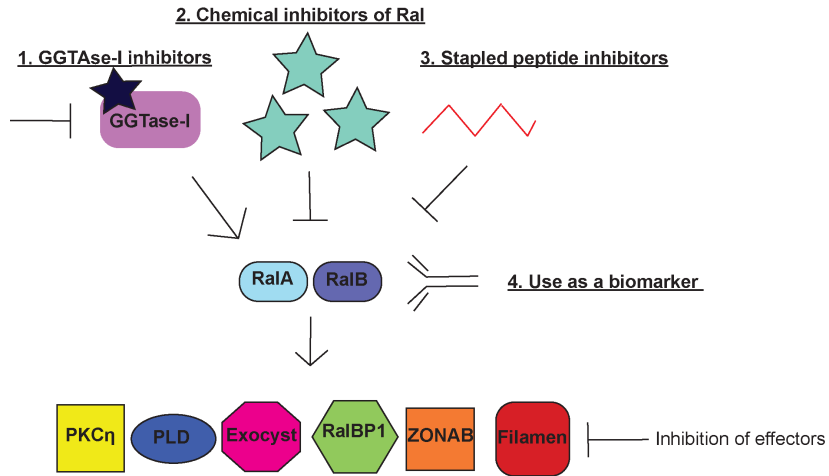


**Figure 1.2.** Therapeutic strategies for targeting Ral in cancer.

## **Section B: Linking Ral Proteins with Mitophagy**

### **Introduction to Autophagy:**

Autophagy is the degradation of cytoplasmic components at the lysosome and is important in response to nutrient starvation, hypoxia and during development. The word “autophagy” is derived from Greek and means “eating of self.” At any give time, autophagy occurs basally in numerous cell types to maintain cellular health. The autophagy pathway is conserved from yeast to mammals.

During autophagy, a membrane is isolated to form the phagopore that ultimately gives rise to an autophagosome, which is a double-membrane-bound organelle. The source of the membrane used to generate autophagosomes remains unknown. In mammalian cells, it has been shown that the membrane for the autophagosome may come from other membranes such as the Endoplasmic Reticulum (ER), Golgi, mitochondria, plasma membrane and recycling endosomes <sup>72</sup>. Similarly, it is not understood how membrane is isolated to form the autophagosome in yeast. Autophagosomes in yeast have been reported to occur as a punctate spot next to a vacuolar membrane termed the “phagopore assembly site” (PAS) <sup>73</sup>. It is not known if formation near the vacuole has any purpose and PAS structures have not been observed in mammalian cells. Mammalian cells exhibit multiple sites of autophagosome formation.

Autophagosome formation consists of three distinct stages in both yeast and mammalian cells: 1. Initiation, 2. Nucleation and 3. Expansion <sup>72</sup>. During initiation, a signal is transmitted to the membrane source where the isolated membrane

undergoes nucleation. Additional initiating complexes are also recruited such as the ULK complex (contains ULK1, ULK2, ATG13, FIP200 and ATG101) and Beclin-1 complex (contains VPS34, p150, ATG15 and Beclin-1) <sup>72</sup>. Although yeast and mammals share numerous autophagy-related genes (ATG) that regulate the autophagy pathway, mammals have specific factors that are not present in yeast such as Beclin-1.

Following initiation, nucleation isolates the membrane from the originating membrane source. The ULK complex and Beclin-1 complex phosphorylate unknown proteins and generate an autophagosome-specific pool of phosphatidyl-inositol-3-phosphate (PtdIns(3)P) <sup>72</sup>. The production of PtdIns(3)P results in the recruitment of Atg18 in yeast or WIPI2 in mammals and Atg2 <sup>74</sup>. A previous study found that loss of Atg2 inhibits autophagosome closure, but it remains unknown exactly how PtdIns(3)P contributes to autophagosome formation <sup>72</sup>.

Once initiation has occurred, the isolated membrane undergoes expansion (growth that occurs due to lipid recruitment) until autophagosome formation is complete. During expansion, the ATG16L1 complex functions as a ubiquitin-protein ligase (E3) ligase-like enzyme to conjugate Atg9 in yeast or LC3 in mammals to phosphatidylethanolamine (PE) <sup>75,76</sup>. Lipidation of Atg9 or LC3 mediates association with the autophagosome <sup>72</sup>. The ATG16L1 complex is released from the autophagosome before vacuole fusion <sup>77</sup>.

Before the isolated membrane closes, ATG proteins bound to the membrane dissociate. LC3 remains bound to the membrane and is often used as a marker to identify autophagosomes in mammalian cells. LC3 exists as a cytosolic form termed,

“LC3-II,” or the lipidated form (PE-LC3) referred to as LC3-II. LC3-II interacts with adaptor molecules to facilitate their degradation <sup>78</sup>. These interactions occur through LC3-interacting (LIR) motifs <sup>79</sup>. In contrast to LC3, Atg8 localizes to both the inner and outer membrane of the phagopore, resulting in a portion of Atg8 delivered with the autophagosome to the vacuole <sup>80</sup>. Consequently, Atg8 marks both the phagopore and mature autophagosome.

Membrane closure to form the autophagosome sequesters part of the cytoplasm. Once the autophagosome is fully formed, it fuses with the endo-lysosomal system. Fusion of the autophagosome directly with the lysosome results in the formation of the autolysosome where lysosomal proteases degrade the sequestered cytoplasmic material <sup>72</sup>. Autophagosomes traffic to lysosomes along microtubules <sup>81</sup>. In contrast to directly fusing with the lysosome, the autophagosome can fuse with a late endosome forming the amphisome. The amphisome then fuses with the lysosome <sup>82</sup>. It is unclear which mode of entry to autolysosome formation (direct or indirect) is favored in mammalian cells, while yeast cells may prefer direct fusion of the autophagosome with the lysosome <sup>83</sup>.

Rab proteins, SNAREs, and tethering factors mediate fusion of the autophagosome with the lysosome <sup>84</sup>. Both Rab7 and Rab33b contribute to fusion. Knockdown of Rab7 in HeLa cells results in accumulation of late autophagic vacuoles (autophagosomes that have fused with late endosomes or lysosomes), suggesting that Rab7 is involved in fusion of autophagosomes with lysosomes <sup>85</sup>. In addition to Rab7, Rab33b facilitates fusion of the autophagosome with the lysosome. Rab33b is localized at the Golgi and interacts with ATG16L1, mediating

autophagosome formation<sup>86</sup>. Not only is Rab33b involved in autophagosome formation, but is also involved in autophagosome fusion since overexpression of its GAP ornithine aminotransferase-like 1 (OATL1) inhibits autophagosome-lysosome fusion<sup>86</sup>.

SNAREs (Soluble *N*-ethylmaleimide-sensitive factor activating protein receptor) are also involved in autophagosome—lysosome fusion<sup>87</sup>. There are over 60 SNARE proteins that are categorized based on their localization (v-SNAREs on donor vesicles and t-SNAREs on target vesicles)<sup>84</sup>. SNAREs in two adjacent membranes form stable complexes that bring membranes closer to each other<sup>87</sup>. Moreover, tethering factors further facilitate autophagosome—lysosome fusion. Tethers physically connect vesicles with their target membranes. Tethers can bind SNAREs to aid SNARE complex assembly and also can be Rab effectors<sup>74</sup>.

In addition to Rab proteins, SNAREs, and tethers, it is increasingly appreciated that phosphoinositides (PIs) participate in autophagosome—lysosome fusion<sup>84</sup>. PI4P (phosphatidylinositol (4)-phosphate) is required for fusion as a previous study found that depletion of PI4P in HeLa cells blocks autophagosome—lysosome fusion<sup>88</sup>. Moreover, the level of phosphatidylinositol (3,5)-bisphosphate [PI(3,5)P<sub>2</sub>] in the lysosomal membrane is important for autophagosome—lysosome fusion<sup>89</sup>. There are numerous PIs involved in autophagosome—lysosome fusion, however the exact role of each PI in this process remains to be discovered.

Although there are different means by which autophagosome—lysosome fusion may occur, the ultimate result is degradation of sequestered cytoplasmic material. Autophagy is comprised of numerous proteins and molecular events, but it

can be simplified into four key steps: 1. Isolation of a membrane, 2. Formation of the autophagosome, 3. Autophagosome—lysosome fusion and 4. Degradation of autophagosomal contents. Proper functioning autophagy is vital for cellular health. Further understanding the autophagy pathway is important because numerous diseases are associated with alterations to autophagy including human cancers, cardiac diseases (i.e. Danon disease) and neurodegenerative diseases such as Alzheimer's disease <sup>90</sup>.

### **Ral Proteins and Autophagy:**

Ral proteins facilitate autophagy through their interactions with components of the exocyst, Sec5 and Exo84. For example, Ral is required for larval salivary gland degradation in *Drosophila* <sup>91</sup>. Additionally, in response to nutrient starvation the RalB-Exo84 effector protein complex promotes autophagosome formation <sup>59</sup>. RalB binding to Exo84 results in the assembly of an active ULK1-Beclin1-VPS34 complex, which facilitates induction of autophagy <sup>59</sup>. This function appears specific to RalB during nutrient starvation as amino acid depletion activates RalB (increased GTP-loading), but not RalA <sup>59</sup>. Consequently, Ral proteins regulate autophagy through their effectors.

### **Overview of Mitochondria:**

Mitochondria are double-membrane-bound organelles best known for their role in producing energy for cells in the form of adenosine triphosphate (ATP). The

origins of mitochondria began roughly two billion years ago. Scientists hypothesize that a eukaryotic cell engulfed an aerobic prokaryote, resulting in an endosymbiotic relationship <sup>92</sup>. This was advantageous because mitochondria increased the number of proteins that a cell expresses by four to six orders of magnitude <sup>93</sup>. Mitochondria also enabled cells to have enough energy to produce increased numbers of proteins.

A unique feature of mitochondria is that they contain their own circular DNA, which reflects their derivation from prokaryotes. The human mitochondrial genome encodes for 13 proteins, 22 transfer RNAs and two mitochondrial ribosome-coding RNAs <sup>92</sup>. Mitochondrial DNA (mtDNA) resides in the matrix, which is the site where oxidative metabolism occurs. Given that mtDNA only encodes for 13 proteins, the majority of mitochondrial proteins are nucleus-encoded and imported into the mitochondria. Most mitochondrial proteins are imported by the Translocase of the Outer Membrane (TOM complex) <sup>94</sup>. Intermembrane space proteins are not imported by the TOM complex, but instead pass through the Mitochondrial Intermembrane space import and Assembly (MIA) machinery <sup>94</sup>.

Proteins involved in ATP synthesis and electron transport reside in the inner mitochondrial membrane. The inner mitochondrial membrane forms folds known as cristae that extend into the matrix. Cristae increase surface area to maximize ATP synthesis. A proton gradient exists across the inner mitochondria membrane and forms as hydrogen is pumped out of the matrix due to the passing of an electron along the electron transport chain <sup>92</sup>. The potential energy stored in the proton gradient drives ATP synthesis. A collapse of the proton gradient (mitochondrial depolarization) can suggest damaged mitochondria that are no longer able to

generate ATP. Mitochondrial depolarization occurs in a variety of circumstances, including mitochondrial dynamics (Figure 1.3).

Mitochondrial dynamics refers to the cycles of fusion and fission that mitochondria experience. Mitochondria are not static organelles. Instead, mitochondria fuse with each other or separate from each other through a process called mitochondrial fission. The sections below further describe details regarding both mitochondrial fusion and fission. Stress induces changes in mitochondrial morphology. For example, mitochondria increasingly become fused when they are forced to rely on oxidative phosphorylation <sup>95</sup>. Additionally, mitochondria become fused in response to nutrient starvation, allowing for complementation or sharing of material between mitochondria. Alternatively, mitochondria experience fission when damaged, facilitating autophagic removal.

Conserved dynamin-related proteins regulate mitochondrial dynamics <sup>92</sup>. During mitochondrial fission, DRP1 in mammals (Dnm1 in yeast) is recruited to mitochondria where it forms a helical structure that constricts the mitochondria orthogonal to its long axis <sup>92</sup>. As a consequence of mitochondrial fission, mitochondria experience transient depolarization. One daughter mitochondria experiences a greater extent of transient depolarization than the other <sup>96</sup>. The mitochondrion that experiences a greater extent of depolarization undergoes a recovery period before it re-enters the fusion-fission cycle (Figure 1.3). Therefore, mitochondrial depolarization regulates the order in which mitochondria are able to experience fission and fusion. Once mitochondria undergo fission they can

experience biogenesis due to importing proteins from the cytosol and importing lipids from the ER.

Mitofusions 1 and 2 (Mfn1 and Mfn2) regulate fusion between outer mitochondrial membranes. In contrast OPA1 (Mgm1 in yeast) mediates fusion between inner mitochondrial membranes<sup>97</sup>. There are multiple forms of OPA1 such as long and short forms due to alternative splicing and proteolytic cleavage<sup>97</sup>. OPA1 not only regulates mitochondrial fusion, but also maintains cristae morphology. Coordinating fusion of both the inner and outer mitochondrial membranes is crucial for generating fused mitochondria.

Mitochondrial dynamics helps maintain mitochondrial homeostasis. Mitochondria are not made *de novo*. Consequently, mitochondrial fission during cell division ensures the generation of daughter mitochondria<sup>98</sup>.

Although mitochondria are commonly referred to as the “powerhouse of the cell” for producing ATP, mitochondria have other important roles. These include regulating intracellular calcium levels, governing lipid homeostasis, and maintaining pro-apoptotic proteins such as cytochrome *c*, Smac and Omi<sup>99</sup>. Mitochondria take up calcium through their mitochondrial Calcium Uniporter (mCU), which catalyzes passive uptake of calcium across the inner mitochondrial membrane<sup>100</sup>. Importantly, calcium uptake is driven by negative mitochondrial membrane potential across the inner mitochondrial membrane<sup>100</sup>. Mitochondrial-mediated buffering of calcium levels is essential for cellular health because calcium acts as a widely used second messenger in the cell. Therefore, inappropriate calcium signaling can impair cell viability.

Sustained increases in calcium in the mitochondrial matrix results in cell death. Elevated mitochondrial calcium levels trigger the opening of the mitochondrial permeability transition pore (PTP), which releases cytochrome *c* and induces apoptosis <sup>100</sup>. Cytochrome *c* release from mitochondrial intermembrane/intercristae spaces initiates apoptosis by aiding allosteric activation of apoptosis-protease activating factor 1 (Apaf-1), which generates the apoptosome <sup>101</sup>. The apoptosome or “wheel of death” activates an initiator caspase (pro-caspase-9) and the resulting downstream molecular events lead to cell death.

Consequently, mitochondria regulate apoptosis through harboring pro-apoptotic proteins. Cytochrome *c* not only participates in apoptosis, but also maintains cellular health. Loss of cytochrome *c* in mice is embryonic lethal <sup>101</sup>. Cytochrome *c* is important for the cell because it serves as an electron transport between complex III and IV of the electron transport chain. Other pro-apoptotic proteins that mitochondria contain include Smac and Omi. Similar to cytochrome *c*, second mitochondria-derived activator of caspase (Smac) promotes caspase activation to facilitate apoptosis when it is released into the cytosol. Smac binds inhibitor of apoptosis proteins (IAPs) in the cytosol and releases their inhibition of apoptosis <sup>102</sup>. Interestingly, Smac also functions outside of apoptosis as it previously was shown to mediate phospholipid synthesis <sup>103</sup>. Release of Omi (a serine protease) into the cytosol also promotes apoptosis by activating caspases through binding IAPs <sup>104</sup>. To summarize, mitochondria regulate apoptosis through releasing various pro-apoptotic proteins into the cytosol.

In addition to ATP production, regulating apoptosis and maintaining calcium levels, mitochondria also orchestrate cellular lipid homeostasis. Mitochondria regulate membrane phospholipid synthesis such as PE, phosphatidylcholine (PC) and cardiolipin <sup>105</sup>. Additionally, mitochondria degrade fatty acids acting at the site of  $\beta$ -oxidation and import a variety of lipids <sup>106</sup>. Lipid import and export from mitochondria occurs through several potential modes including contact-sites (i.e. ER-mitochondria contact sites) and mitochondrial-derived vesicles <sup>106</sup>. Lipid trafficking and production at mitochondria are important for mitochondrial membrane composition and mitochondrial function. For instance, decreased cardiolipin and PE levels result in decreased mitochondrial membrane potential, which impairs protein import into mitochondria <sup>107</sup>. In conclusion, mitochondria perform diverse functions aside from their best-known role in ATP production.

### **Introduction to Mitophagy:**

In contrast to bulk degradation (macroautophagy), there are selective forms of autophagy such as xenophagy (degradation of pathogens), pexophagy (degradation of peroxisomes), and mitophagy (degradation of mitochondria). All selective forms of autophagy utilize the autophagy machinery for clearance. However, specific signaling pathways give rise to selective forms of autophagy. The rest of this section will focus on mitophagy given its relevance to my research.

Because mitochondria perform numerous important roles (i.e. regulating intracellular calcium levels, maintaining pro-apoptotic proteins, orchestrating lipid homeostasis and generating ATP), mitochondrial quality is vital for cellular health.

Over time, mitochondria accumulate damage, which may be in the form of misfolded proteins, damaged mtDNA, and damaged mitochondrial lipids. Mitophagy selectively removes damaged mitochondria from cells, ensuring that cells maintain a healthy population of mitochondria to sustain proper cellular functions. Additionally, mitophagy occurs during reticulocyte maturation and during egg fertilization to eliminate paternal mtDNA.

There are several types of mitophagy, which differ in terms of how they achieve mitochondrial clearance: Nix and Bnip3 mediated mitophagy, Type 1, Type 2 and Type 3 mitophagy as well as PINK1-Parkin mitophagy <sup>108,109</sup>. It is likely that various types of mitophagy exist to respond differently depending on the initiating stimuli. Hypoxia, for example, induces expression of both Nix and Bnip3 through hypoxia-inducible factor-1 (HIF-1) <sup>110</sup>. Increased Nix and Bnip3 levels facilitate mitophagy <sup>111</sup>. Nix interacts with LC3 and may be involved in recruiting the autophagy machinery. Additionally, Nix is specifically involved in mitophagy during erythroid development because Nix deficient mice exhibit impaired erythroid development <sup>111</sup>. Increased Bnip3 expression can cause mitochondrial depolarization, subsequently resulting in mitophagy <sup>111</sup>. Furthermore, in muscle wasting disorders where autophagy contributes to pathogenesis, both Bnip3 and Nix are upregulated, implicating them in autophagy <sup>111</sup>.

One way of broadly categorizing different types of mitophagy is with Type 1, Type 2, and Type 3 mitophagy. Nutrient deprivation can induce Type 1 mitophagy where preautophagic structures (PAS) sequester mitochondria for removal. In contrast, mitochondrial damage (e.g. photodamage) results in Type 2 mitophagy

where mitochondrial depolarization occurs, but a PAS does not form and mitochondrial fission is not evident <sup>108</sup>. During Type 3 mitophagy, mitochondrial-derived vesicles bud off from mitochondria, become internalized into multivesicular bodies and then fuse with lysosomes for degradation <sup>108</sup>.

PINK1-Parkin mitophagy occurs in response to mitochondrial depolarization where Parkin, an E3 ubiquitin ligase, localizes to depolarized mitochondria and initiates recruitment of the autophagy machinery. PINK1-Parkin mitophagy itself can be classified as Type 2 mitophagy. A proteomics screen identified RalA as a possible Parkin-interacting protein <sup>112</sup>. Therefore, RalA may participate in PINK1-Parkin mitophagy. The next section further describes PINK1-Parkin mitophagy given the possible relevance to Ral proteins.

### **PINK1-Parkin Mitophagy:**

PINK1-Parkin mitophagy (Figure 1.4) was discovered in HeLa cells in 2008 <sup>109</sup>. Both PINK1 and Parkin loss-of-function mutations have been identified in patients with Parkinson's disease with Parkin mutations comprising half of known cases of autosomal-recessive parkinsonism <sup>113</sup>. Consequently, understanding the relevance of this pathway in humans may provide new therapeutic insights into treating Parkinson's disease.

Under normal conditions, PINK1 (a serine-threonine kinase) is constitutively imported into the inner mitochondrial membrane and degraded by PARL, a rhomboid protease <sup>95</sup>. Mitochondrial depolarization prevents PINK1 import and subsequent degradation, resulting in PINK1 stabilization on the outer mitochondrial

membrane (OMM). Following mitochondrial depolarization, PINK1 stabilization on the OMM recruits Parkin through two different phosphorylation events: 1. Phosphorylation of ubiquitin chains on Ser65 and 2. Phosphorylation of Parkin in the UBL (ubiquitin-like) domain on Ser65<sup>114-116</sup>. Parkin is autoinhibited by several mechanisms and must undergo a conformational change to become active. Parkin contains a cysteine residue (Cys<sup>431</sup>) that is critical for passing the ubiquitin molecule to its target protein<sup>117,118</sup>. However, Cys<sup>431</sup> is occluded by an interaction between Parkin's RING0 and RING2 domains<sup>118</sup>. Additionally, the repressor element of Parkin (REP) further autoinhibits Parkin by blocking the E2-binding site involved in ubiquitination<sup>118</sup>. PINK1 phosphorylation of Parkin in its UBL domain and phosphorylation of ubiquitin that binds Parkin causes Parkin to undergo a conformational change, releasing Parkin's autoinhibition. Moreover, phosphorylated ubiquitin binding to Parkin results in a feedforward mechanism of Parkin activation.

Once Parkin is at the OMM, it ubiquitinates mitochondrial proteins and results in the recruitment of autophagy receptors for mitochondrial clearance<sup>119</sup>. Although PINK1 kinase activity is required for Parkin recruitment, it remains unclear how Parkin traffics to PINK1 at the OMM from the cytosol following activation by phosphorylated ubiquitin chains<sup>114</sup>. The current dogma in the field is that Parkin randomly diffuses throughout the cytosol where Parkin eventually encounters PINK1 since Parkin is cytoplasmic prior to mitochondrial depolarization.

TBK1 becomes active following mitochondrial depolarization and phosphorylates four autophagy receptors during PINK1-Parkin mitophagy: 1. OPTN, 2. NDP52, 3. TAX1BP1 and 4. p62<sup>68,120</sup>. These autophagy receptors contain an LC3

interaction region (LIR), which allows them to bind ATG8 family proteins and a ubiquitin chain-binding domain. PINK1 is required for TBK1 activation following mitochondrial depolarization as shRNA depletion of PINK1 in SH-SY5Y cells prevents depolarization-induced TBK1 activation <sup>68</sup>. In addition to PINK1, TBK1 activation following mitochondrial depolarization also requires OPTN and NDP52 because double knockout OPTN and NDP52 HeLa cells exhibit decreased TBK1 activity <sup>68</sup>. Interestingly, in HeLa cells only NDP52 and OPTN are required for mitophagy <sup>68</sup>. TBK1 phosphorylates OPTN on multiple sites including Ser177, Ser155 and Ser473 <sup>120,121</sup>. TBK1 phosphorylation of OPTN's UBAN domain on Ser473 enables OPTN to bind polyubiquitinated chains, creating an amplification loop to recruit and retain OPTN/TBK1 at depolarized mitochondria <sup>120</sup>.

TBK1 also phosphorylates Rab7a on Ser72 in response to mitochondrial depolarization <sup>67</sup>. HeLa cells that inducibly express Parkin and express a Rab7a phosphorylation mutant exhibit impaired mitophagy, suggesting that phosphorylation of Rab7a on Ser72 is required for mitophagy. Specifically, phosphorylation of Rab7a is required for Atg9a recruitment to depolarized mitochondria <sup>67</sup>. Further elucidating how TBK1 phosphorylation of Rab7a mediates PINK1-Parkin mitophagy will be important for understanding neurodegenerative disorders like Parkinson's disease where genes with well-defined roles in endocytosis (i.e. Synj1, GAK, and LRRK2) are mutated <sup>122-124</sup>.

## **Summary:**

Ral proteins promote autophagy through the effector proteins to which they bind. Given that Ral proteins are involved in autophagy, it is possible that Ral may mediate mitophagy as mitophagy utilizes the autophagy machinery. Eliminating damaged mitochondria from cells is crucial for cellular health. Mitochondria not only provide energy for cells in the form of ATP, but also regulate intracellular calcium levels, maintain lipid homeostasis and facilitate apoptosis. Damaged mitochondria can release pro-apoptotic proteins, lose metabolic function, and generate reactive oxygen species. Consequently, it is understandable that impaired mitophagy is associated with different neurodegenerative disorders and human cancers. There are several types of mitophagy, but PINK1-Parkin mitophagy is one of the most well-characterized forms. There is significant interest to further elucidate mechanisms that regulate PINK1-Parkin mitophagy given that mutations in PINK1 and Parkin are linked to patients with Parkinson's disease. Additionally, loss-of-function mutations in Parkin are associated with different cancers<sup>125</sup>. Moreover, there can be dysregulation at the expression level of both PINK1 and Parkin, which may contribute to human cancers<sup>126-128</sup>.

## Figures

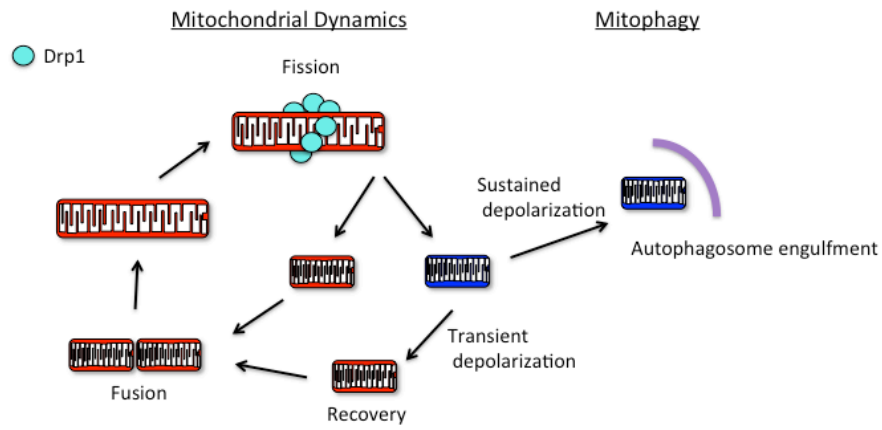


**Figure 1.3.** Overview of the role of mitochondrial depolarization in mitochondrial dynamics and mitophagy.

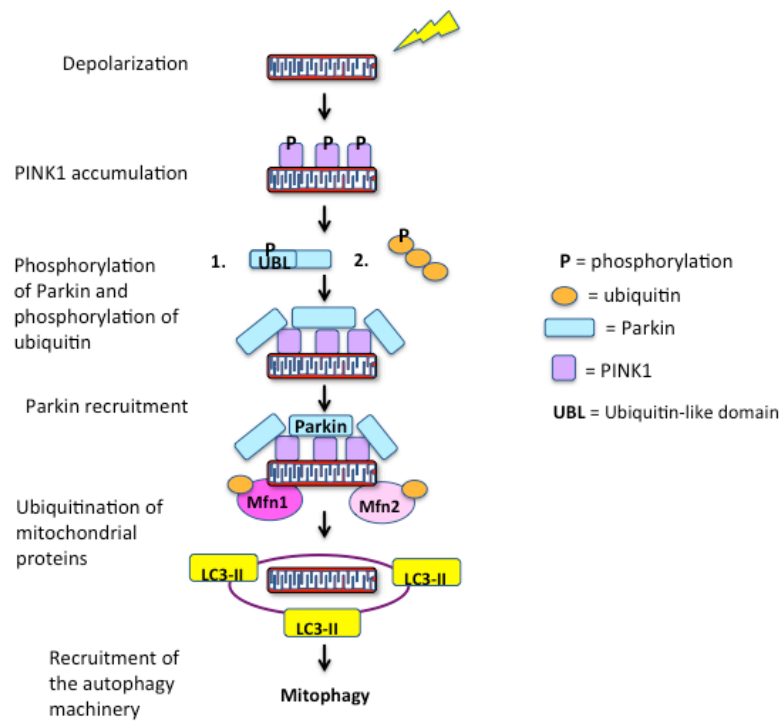


**Figure 1.4.** Schematic of PINK1-Parkin mitophagy.

## **Chapter Two: Understanding the Role of Ral Proteins in Response to Mitochondrial Depolarization**

Part of this chapter has been adapted from: Pollock S.R, Schinlever A.R, Rohani A, Kashatus J.A, Kashatus DF (2019) RalA and RalB relocalization to depolarized mitochondria depends on clathrin-mediated endocytosis and facilitates TBK1 activation. PLoS ONE 14(4): <https://doi.org/10.1371/journal.pone.0214764>

### **Introduction**

The Ras-related small GTPases RalA and RalB are directly activated downstream of active Ras. Interest in Ral proteins has grown in recent years as a number of studies have demonstrated aberrant activation of Ral in several human cancer tissues and cell lines <sup>31-33,129</sup>. Importantly, genetic or pharmacologic inhibition of Ral blocks tumor growth in a variety of models <sup>11,27,130</sup>, suggesting that Ral may be an attractive therapeutic target for human cancer.

RalA and RalB share 80% sequence identity at the amino acid level and function through the engagement of a shared set of effector proteins. Despite this, RalA and RalB exhibit both redundant and distinct functions, and this specificity may be regulated through distinct post-translational modifications and subcellular localization. A key Ral effector is RalBP1, a large multifunctional protein that regulates endocytosis and mitotic mitochondria fission <sup>47</sup> among other cellular processes. Other Ral effectors include Sec5 and Exo84, components of the exocyst complex <sup>54,55</sup> that regulate exocytosis in polarized cells, but can also contribute to both cell survival and autophagy <sup>59,131</sup>. Sec5 and Exo84 also link Ral activity to that of Tank-binding kinase 1 (TBK1), a non-canonical I $\kappa$ B kinase that regulates a variety of cellular processes including autophagy and the inflammatory response. Several

reports link overexpression of a constitutively active RalB mutant to a Sec5-dependent increase in TBK1 activity in the context of viral infection and oncogene activation<sup>18,58</sup>. Moreover, TBK1 phosphorylation of Exo84 leads to dissociation of the RalA/Exo84 complex to promote Glut4 trafficking during insulin signaling<sup>71</sup>.

TBK1 is also recruited to mitochondria to promote mitophagy, the selective autophagic removal of damaged mitochondria from the cell<sup>132</sup>. Mitochondria accumulate damage through a variety of both normal and pathological processes. Damaged mitochondria must be removed to maintain cellular health and are associated with a variety of diseases, including neurodegenerative diseases such as Parkinson's disease and ALS<sup>113,133</sup>. Given that Ral signals to affect autophagy, it is possible that Ral may also be implicated in mitophagy.

Mitochondrial depolarization, which is the collapse of the proton gradient across the inner mitochondrial membrane, can induce changes in mitochondrial dynamics and mitophagy<sup>96</sup>. Mitochondrial membrane potential drives ATP synthesis. Consequently, sustained changes in mitochondrial membrane potential indicate damaged mitochondria, resulting in mitophagy<sup>134</sup>. In contrast, transient mitochondrial depolarization induces changes in mitochondrial dynamics and regulates the timing in which mitochondria are able to enter the fission-fusion cycle<sup>134</sup>.

Although mitochondrial depolarization can lead to these changes in mitochondrial dynamics and mitophagy, the molecular response to depolarization is not well understood. Given that changes in mitochondrial dynamics and mitophagy are associated with neurodegenerative diseases and cancers, it is imperative that we

elucidate the cellular response to mitochondrial depolarization. Moreover, the fact that Ral is involved in mitochondrial dynamics <sup>47</sup> and may be involved in mitophagy, potentially implicates Ral during mitochondrial depolarization. Therefore, we sought to determine Ral's role in response to mitochondrial depolarization.

We demonstrate that both RalA and RalB relocate to depolarized mitochondria. We find that pharmacologic inhibition of clathrin-mediated endocytosis (CME) impairs RalA and RalB localization to depolarized mitochondria, suggesting that CME facilitates Ral trafficking following mitochondrial depolarization. Consistent with this finding, genetic inhibition of CME results in impaired RalA recruitment to depolarized mitochondria. Additionally, we demonstrate that both pharmacologic and genetic inhibition of both RalA and RalB leads to increased TBK1 activity, suggesting that Ral negatively regulates TBK1 activity. Collectively, our data support a model where RalA and RalB localize to depolarized mitochondria potentially through CME and regulate TBK1 activity.

### **RalA and RalB relocate to mitochondria in response to mitochondrial depolarization**

To identify whether RalA is involved in the cellular response to mitochondrial depolarization, we examined RalA localization in HeLa cells that transiently express mito-BFP and GFP-RalA. Mitochondrial depolarization was induced for 3 hours using three different chemical means: 1. oligomycin (ATP synthase inhibitor) and antimycin A (inhibits complex III of the electron transport chain) (OA), 2. CCCP (protonophore) and 3. valinomycin (potassium-specific

ionophore). In untreated cells, RalA localized to both internal structures and the plasma membrane (Figure 2.1A). Following treatment with OA, CCCP and valinomycin, RalA relocalized to mitochondria or punctate structures adjacent to mitochondria, which became fragmented and accumulated in a perinuclear fashion (Figure 2.1A). This RalA relocalization is consistent with the three distinct methods of depolarization, though we detected some differences in the nature of the colocalization that may reflect different effects the drugs have on mitochondrial structure. For example, cells treated with OA and valinomycin mainly exhibited distinct ring-like structures of RalA around the mitochondria (Figures 2.1A and 2.1B). In contrast, cells treated with CCCP tended to display perinuclear RalA puncta adjacent to mitochondria (Figures 2.1A and 2.1B). We do not understand the functional consequences of RalA adjacent to mitochondria compared to forming ring-like structures around mitochondria or appearing directly colocalized with mitochondria.

Instances where RalA appeared directly colocalized with mitochondria in response to OA treatment can be quantified by calculating the percent overlap of RalA with mitochondria. However, percent overlap is not an appropriate quantification method for instances where RalA is in the proximity of mitochondria when cells are treated with valinomycin or CCCP. Therefore, we quantified the spatial relationship of RalA to mitochondria by using a proximity index score to measure the distance of RalA to mitochondria. We observed a statistically significant increase in RalA proximity to mitochondria following CCCP and OA treatment (Figure 2.1C). We also observed an increase in RalA proximity to mitochondria

following valinomycin treatment, although this was not statistically significant (p-value = 0.06) (Figure 2.1C).

We next examined if the RalA homologue RalB also relocalizes to depolarized mitochondria by examining HeLa cells that transiently express mito-BFP and GFP-RalB. Prior to mitochondrial depolarization, RalB localized primarily to membrane-bound compartments within the cytoplasm, similar to RalA, with some RalB at mitochondria (Figures 2.1D and 2.1E). Interestingly, like RalA, RalB relocalized to mitochondria following 3 hours of treatment with OA, CCCP or valinomycin. Once again, we observed differences in the appearance of RalB localization to mitochondria depending on the depolarization method. Cells treated with OA and valinomycin largely exhibited ring-like structures of RalB around mitochondria with some direct colocalization (Figures 2.1D and 2.1E). Cells treated with CCCP mainly displayed RalB puncta adjacent to mitochondria (Figures 2.1D and 2.1E), which was similar to RalA localization in response to CCCP treatment. We also observed statistically significant increases in RalB proximity to mitochondria following OA, CCCP and valinomycin treatment (Figure 2.1F).

To confirm that OA, CCCP and valinomycin induce mitochondrial depolarization, we repeated the above experiments in HeLa cells that stably or transiently express mCherry-Parkin and transiently express mito-BFP and/or GFP-RalA. We used mCherry-Parkin as a positive control for mitochondrial depolarization as Parkin translocates from the cytosol to mitochondria in response to mitochondrial depolarization<sup>109</sup>. In response to OA, CCCP and valinomycin, Parkin was recruited to the mitochondria indicating that mitochondrial

depolarization is induced (Figures 2.2A, 2.2B and 2.2C). Moreover, RalA relocalization to depolarized mitochondria occurred in a similar fashion to cells that lack exogenous Parkin, indicating that Parkin expression does not affect RalA redistribution (Figures 2.2A, 2.2B and 2.2C). Importantly, GFP alone remains cytosolic before and after OA treatment, indicating that the signal promoting GFP-RalA mitochondrial redistribution is within the Ral sequence (Figure 2.3A). Collectively, these data indicate that both RalA and RalB relocalize to depolarized mitochondria.

### **RalA-GTP levels decrease following OA and CCCP treatment**

To further examine RalA activity in response to mitochondrial depolarization, we next sought to determine how depolarization affects RalA-GTP loading. RalA-GTP levels significantly decrease over 80 minutes of OA treatment (Figure 2.4A). We used OPA1 as a readout to confirm mitochondrial depolarization since OPA1 is preferentially processed into its shorter isoform following depolarization (Figures 2.4A and 2.4B) <sup>135</sup>. We observed similar decreases in RalA-GTP levels following CCCP treatment (Figure 2.4B). Moreover, RalA-GTP levels remain decreased over 3 hours of mitochondrial depolarization (Appendix A).

Changes in RalA-GTP levels may be a direct consequence of the loss in mitochondrial activity, as decreased ATP synthesis should result in decreased cellular GTP levels. Alternatively, RalA relocalization may alter its proximity to its guanine nucleotide exchange factors (GEFs) or GTPase activating proteins (GAPs). To determine if RalA-GTP loading affects its relocalization following mitochondrial

depolarization, we co-transfected shRala HeLa cells (Figure 2.4C) that stably express mCherry-Parkin with mito-BFP and shRNA resistant GFP-RalA<sup>Q72L</sup> (constitutively GTP-bound) or GFP-RalA<sup>S28N</sup> (constitutively GDP-bound) <sup>46,136,137</sup>. Following OA treatment, both GFP-RalA<sup>S28N</sup> and GFP-RalA<sup>Q72L</sup> mutants relocalized with Parkin to the mitochondria (Figures 2.4D, 2.4E and 2.4F). These data indicate that nucleotide-binding neither positively nor negatively regulates RalA localization following mitochondrial depolarization. Further, the data suggest that direct effectors of Ral, which bind to the GTP-bound form, are not required for Ral relocalization.

### **Phosphorylation of neither serine 194 nor serine 183 is required for RalA relocalization following mitochondrial depolarization**

Phosphorylation of the C-terminal hypervariable domain of RalA has been shown to regulate its localization, potentially due to the negatively charged phosphate group neutralizing the charge of the polybasic region <sup>47,138</sup>. Neutralizing the charge changes RalA's affinity for membranes, similar to what has been demonstrated for KRas <sup>16</sup>. RalA is phosphorylated on serine 194 and serine 183 by Aurora A and potentially PKC, respectively <sup>12,13</sup>. PP2A A $\beta$  dephosphorylates RalA on serine 194 and serine 183 <sup>14</sup>.

To identify if phosphorylation of RalA regulates RalA relocalization in response to mitochondrial depolarization, we co-transfected mito-BFP and shRNA resistant S183A, S194A or S194A/S183A mutants of GFP-RalA into shRala HeLa cells stably expressing mCherry-Parkin and treated with OA for 3 hours. Prior to

mitochondrial depolarization, we observed that S183A, S194A and S194A/S183A mutants of GFP-RalA localize to distinct structures within the cell with some RalA localized to mitochondria (Figures 2.5A and 2.5B). However, after 3 hours of OA treatment, all phospho-RalA mutants exhibited a more pronounced perinuclear punctate phenotype and relocalized with Parkin to mitochondria (Figures 2.5A and 2.5B). Moreover, all three phospho-RalA mutants exhibited statistically significant colocalization with depolarized mitochondria (Figure 2.5C). This suggests that phosphorylation of serine 194 and serine 183 are not required for RalA mitochondrial localization following mitochondrial depolarization.

### **Clathrin-mediated endocytosis facilitates Ral relocalization to depolarized mitochondria**

Ral relocalization has previously been shown to be induced by specific post-translational modifications<sup>139</sup>, but as a membrane-anchored protein, it can also relocalize throughout the cell by trafficking through the endo-lysosomal system<sup>140</sup>. As such, we next sought to determine whether endocytic trafficking is required for depolarization-induced RalA relocalization. RalA was previously identified at sites of clathrin-mediated endocytosis (CME) and its binding partners RalBP1 and PLD are both involved in endocytosis<sup>50,52,141</sup>. Furthermore, a growing number of studies have demonstrated delivery of specific proteins to mitochondria via endocytic trafficking, including Drp1 and XIAP<sup>142,143</sup>. Thus, to determine whether CME plays a role in the recruitment of Ral to mitochondria following mitochondrial depolarization, we treated HeLa cells transiently expressing mito-BFP and GFP-RalA

or GFP-RalB with OA and Pitstop 2, a cell-permeable CME inhibitor, either alone or in combination. Importantly, Pitstop 2 abolished uptake of fluorescently tagged transferrin, indicating that it effectively inhibits CME at the dose we are using (Figure 2.6A).

While untreated cells and those treated with Pitstop 2 alone did not exhibit striking RalA and RalB localization at the mitochondria, we observed robust redistribution of RalA and RalB to mitochondria following 1 hour of OA treatment (Figures 2.6B, 2.6C, 2.6D and 2.6E). Interestingly, cells treated with both OA and Pitstop 2 failed to exhibit Ral localization at mitochondria and in fact, Ral localization in Pitstop 2 treated cells appeared shifted towards the plasma membrane (Figures 2.6B, 2.6C, 2.6D and 2.6E). These data suggest that CME may facilitate both RalA and RalB recruitment to depolarized mitochondria.

Given that clathrin has additional roles outside of CME, and that any pharmacologic inhibitor will exhibit some degree of off-target effects, we examined RalA relocation in HeLa cells that stably expressed an shRNA targeting AP50, the  $\mu 2$  subunit of AP2 that is required for clathrin recruitment to sites of endocytosis. We confirmed that shAP50 cells exhibited impaired CME through analysis of transferrin uptake (Figures 2.7A, 2.7B and 2.7C). As expected, both untreated shScramble and shAP50 cells exhibit RalA and RalB localized to structures present throughout the cytoplasm (Figures 2.8A and 2.8C). However, following 3 hours of OA treatment, shAP50 cells exhibited significantly impaired RalA and RalB relocation to depolarized mitochondria compared with shScramble control cells (Figures 2.8A, 2.8B, 2.8C and 2.8D). Collectively, these findings are consistent with

the observed loss of Ral recruitment in cells treated with both OA and Pitstop 2. This supports the notion that CME plays a role in RalA and RalB localization to mitochondria in response to mitochondrial depolarization.

### **RalA and RalB negatively regulate TBK1 activity**

Given that RalA and RalB both localize to mitochondria following mitochondrial depolarization, we sought to understand Ral's function in these conditions. Previous studies found that Tank-binding kinase 1 (TBK1), a non-canonical I $\kappa$ B kinase, is recruited to depolarized mitochondria where it phosphorylates autophagy receptors to promote mitophagy<sup>68,120</sup>. Given that both RalA and RalB are implicated in TBK1 signaling<sup>18,58,71</sup> and that TBK1 exerts signaling effects in response to mitochondrial depolarization, we postulated that RalA and RalB may affect TBK1 activity in response to mitochondrial depolarization.

We studied TBK1 activity in response to CCCP treatment in HeLa cells stably expressing shRNA targeting a scramble control sequence or RalA and RalB. As expected, following 1 hour of CCCP treatment shScramble HeLa cells exhibited increased TBK1 activity, which decreased over 8 hours (Figure 2.9A). In contrast to shScramble cells, shRalA/RalB double knockdown cells exhibited increased TBK1 activity both basally and in response to CCCP (Figures 2.9A and 2.9B). We also observed this phenotype, though to a lesser extent in single shRalA or shRalB HeLa cells (Figure 2.9C) indicating that RalA and RalB act similarly in regulating TBK1 activity. Moreover, shRalA/RalB HeLa cells generated with different shRNA constructs (shRalA-2/RalB-2 cells) also exhibited increased basal TBK1 activity

(Appendix B). This increase in TBK1 activity is not to the same extent that we observed in shRala/RalB HeLa cells likely corresponding with the fact that the knockdown of RalA is not as efficient. These data suggest that RalA and RalB negatively regulate TBK1 activity.

To validate our finding that shRala/RalB HeLa cells exhibit increased TBK1 activity both basally and following mitochondrial depolarization, we performed a rescue experiment by stably expressing Flag RalA in shRala/RalB double knockdown cells (Figure 2.9D). Consistent with the idea that RalA and RalB act redundantly in negatively regulating TBK1 activity, we found that re-expression of Flag RalA was sufficient to reduce TBK1 activity in shRala/RalB cells (Figure 2.9D).

To further confirm whether Ral negatively regulates TBK1 activity, we treated HeLa cells over 2 hours with BQU57, a Ral inhibitor (Figure 2.9E). BQU57 inhibits both RalA and RalB by locking them in a GDP-bound state. We verified that BQU57 inhibits RalA-GTP levels over 2 hours (Appendix C). We anticipated that inhibiting Ral would phenocopy the elevated phospho-TBK1 levels observed in shRala/RalB cells (Figures 2.9A and 2.9B) because RalA-GTP levels decreased following mitochondrial depolarization (Figures 2.9A and 2.9B) and TBK1 activity rose in response to depolarization (Figure 2.9A). Consistent with this, TBK1 activity increased over 2 hours of BQU57 treatment (Figures 2.9E and 2.9F). Collectively, these data suggest that RalA and RalB negatively regulate TBK1 activity.

We next sought to determine if TBK1 activity affects RalA and RalB relocalization. To address this, we induced mitochondrial depolarization in HeLa cells transiently expressing GFP-RalA or GFP-RalB and mito-BFP with OA in the

presence or absence of BX795, a TBK1 inhibitor (Figure 2.10A and 2.10C). Both GFP-RalA and GFP-RalB relocalized to depolarized mitochondria in the presence of BX795, suggesting that Ral relocalization is independent of TBK1 activity (Figure 2.10A, 2.10B, 2.10C and 2.10D).

We next hypothesized that Ral relocalization following depolarization may affect its ability to inhibit TBK1 activity. To test this, we depolarized mitochondria in HeLa cells with CCCP in the absence and presence of Pitstop 2 and measured TBK1 phosphorylation. Consistent with a model in which Ral relocalization releases it from inhibiting TBK1, cells treated with both Pitstop 2 and CCCP, which failed to relocalize Ral to mitochondria (Figures 2.6B, 2.6C, 2.6D and 2.6E) also failed to exhibit increased TBK1 activity (Figures 2.11A and 2.11B). Importantly, treatment with Pitstop 2 alone did not affect TBK1 activity (Figures 2.11A and 2.11B). Collectively, these data support a model where RalA and RalB inhibit TBK1 under basal conditions and their relocalization following mitochondrial depolarization releases the inhibition, allowing TBK1 activity to increase (Figure 2.11C).

## **Discussion**

Mitochondrial depolarization initiates a number of different cellular processes, including changes in mitochondrial dynamics and mitophagy. In this chapter we show that both RalA and RalB relocalize to depolarized mitochondria (Figures 2.1A, 2.1C, 2.1D and 2.1F). We previously demonstrated that RalA localizes to mitochondria during mitosis<sup>47</sup> and our data here suggest that the roles of Ral proteins in regulating mitochondrial structure and function are more widespread.

We find that RalA-GTP levels decrease in response to mitochondrial depolarization. However, neither RalA nucleotide-binding nor phosphorylation on serine 183 or serine 194 are required for RalA redistribution to depolarized mitochondria. In contrast, we find that CME facilitates Ral localization following mitochondrial depolarization. It remains to be determined whether Ral directly associates with endosomes and how endocytic trafficking delivers Ral to mitochondrial membranes. It is possible that RalA and RalB associate with the endosomal pathway through direct protein-protein interactions. Additionally, post-translational modifications other than the ones tested in this paper may contribute to Ral's trafficking and localization. For instance, both RalA and RalB undergo nondegradative ubiquitination that has previously been shown to regulate localization<sup>17</sup>. Specifically, de-ubiquitination of RalA promotes its relocalization from the plasma membrane to lipid raft microdomains.

Surprisingly, we find that RalA and RalB inhibit TBK1, both basally and in response to mitochondrial depolarization. Previous studies showed that Ral GTPases promote TBK1 activity and are required for TBK1 function<sup>58,71</sup>. Our data suggest the relationship between Ral and TBK1 is likely more complex and may depend on context-specific factors that are biological or experimental. For instance, previous studies did not use a genetic approach like we did to study the relationship between Ral proteins and TBK1. These studies also used different reagents and cell lines. Further experiments are necessary to determine why our results differ from other studies.

Interestingly, we observe that CME participates both in TBK1 activation and Ral relocalization in response to mitochondrial depolarization. As such, we propose a model in which Ral inhibition of TBK1 activity is location-dependent. In other words, redistribution of Ral is a mechanism through which its inhibition of TBK1 can be removed (Figure 2.11C). It is tempting to speculate that this mechanism also involves the disruption of a protein complex between Ral, Ral effectors, and TBK1. This would be consistent with the decrease in Ral-GTP levels observed following depolarization and the previous reports demonstrating that Ral and TBK1 interact through the Ral effector, Sec5. It is also possible that the act of Ral relocalization itself affects TBK1 clustering. TBK1 becomes active when it undergoes autophosphorylation due to clustering of TBK1 molecules. Therefore, it may be that Ral inhibits TBK1 clustering and Ral relocalization relieves this inhibition, enabling TBK1 activity.

A potential limitation of our study is that our RalA-GTP pulldowns only pulled down a certain percentage (i.e. around 20%) of RalA-GTP from the total pool of RalA. It could be argued that a small percentage of RalA-GTP is not enough to basally inhibit TBK1. However, it is difficult to know the minimum amount of RalA-GTP required for TBK1 inhibition. This does not undermine our working model of Ral-mediated TBK1 inhibition as there are multiple ways that Ral could inhibit TBK1 independent of Ral-GTP loading and we have yet to determine a complete mechanism. For instance, as previously mentioned Ral may inhibit TBK1 by preventing clustering of TBK1 molecules and this could be independent of Ral-GTP loading. Alternatively, Ral may interact with certain proteins independent of its

GTP-status, which could inhibit TBK1 and Ral relocalization would physically remove these proteins away from TBK1 to enable TBK1 activity. Finally, perhaps clathrin-mediated endocytosis causes Ral to undergo a post-translational modification that relieves its inhibition of TBK1.

Our data raise the important question of how regulation of TBK1 activity contributes to the cellular response to mitochondrial depolarization, if at all. TBK1 is known to play roles in autophagy, through induction of p62 <sup>69</sup> and in the inflammatory response, through induction of IRF-3 and NFκB. It is plausible that the constitutive inhibition of TBK1 by RalA and RalB allows these response pathways to be poised and ready to respond rapidly in the case that mitochondrial damage occurs.

With this in mind, it is also possible that mitochondrial depolarization triggers an inflammatory response. The release of mitochondrial DNA (mtDNA) is seen as foreign to the body and results in an innate inflammatory response <sup>144</sup>. A previous study demonstrated that mtDNA activates the signaling molecule, STING, which then signals to TBK1 to promote type I interferon responses <sup>145</sup>. Ostensibly, sustained mitochondrial depolarization could result in the release of mtDNA, initiating a TBK1-mediated inflammatory response. Thus, it is possible that Ral inhibits TBK1 activity basally to hinder an inappropriate inflammatory response.

Although the functional consequences of Ral-mediated TBK1 inhibition remain to be determined, our data show that RalA and RalB localize to depolarized mitochondria in a CME-dependent process and inhibit TBK1 activity. We speculate that the redundant functions of RalA and RalB in inhibiting TBK1 activity

underscore the importance of TBK1 regulation in preventing an inappropriate inflammatory or autophagic response. Finally, this work provides another example of Ral functioning at mitochondria and may provide additional hints into how mitochondrial depolarization may affect diseases such as cancers and neurodegenerative disorders.

### **Future Directions**

Future work for this project can be divided into two categories: 1. Elucidating the functional consequences of TBK1 activation following mitochondrial depolarization and 2. Determining how Ral inhibits TBK1.

#### *1. What are the functional consequences of TBK1 activation?*

A previous study demonstrated that TBK1 activation following OA treatment does not result in phosphorylation of IRF-3, suggesting uncoupling from the innate immunity pathway<sup>68</sup>. However, we cannot exclude the possibility that TBK1 may result in an inflammatory response following mitochondrial depolarization as we have not examined this phenomenon. We would need to examine phosphorylation of IRF-3 following OA treatment to determine if our findings match those already in the literature. Moreover, phosphorylated IRF-3 is not the only target that should be evaluated to determine if depolarization-induced TBK1 activity results in an inflammatory response. For example, TBK1 also has been shown to phosphorylate IRF-7<sup>146</sup>.

It is noteworthy that shRala/RalB cells exhibit decreased STING levels compared to shScramble cells (Figure 2.12A). Currently, we do not understand why or what the consequences are of shRala/RalB cells having decreased STING levels. To further investigate decreased STING levels, future work should include studying STING mRNA levels in shRala/RalB cells to determine if Ral regulates transcription of STING. If this is the case then it is possible that Ral-dependent transcriptional regulation of STING is independent of the phospho-TBK1 phenotype.

However, an alternative explanation for decreased STING levels is that they may reflect the occurrence of an inflammatory response. Cytosolic DNA stimulates the cGAS-STING pathway, which ultimately results in STING ubiquitination and degradation to attenuate the response<sup>147</sup>. During activation of the cGAS-STING pathway, TBK1 phosphorylates p62 on Ser403, mediating ubiquitinated STING localization to autophagosomes for degradation<sup>147</sup>. Perhaps shRala/RalB cells basally exhibit an inflammatory response as increased TBK1 activity could then result in increased phosphorylation of p62 and subsequent STING degradation. To identify if shRala/RalB HeLa cells exhibit increased levels of phosphorylated p62, we performed immunoblotting and examined phosphorylated p62 (Ser403). However, our results were highly variable—some trials indicated no difference in phosphorylated p62 levels compared to shScramble control cells, while additional trials suggested otherwise. Due to the high variability in phosphorylated p62 levels, we were unable to determine if increased TBK1 activity in shRala/RalB cells results in increased phosphorylated p62 levels.

Another approach to study whether decreased STING levels are facilitated by increased TBK1 activity would be to pharmacologically inhibit TBK1 in shRala/RalB using a drug such as BX795. If TBK1 facilitates decreased STING levels then we expect that treating shRala/RalB HeLa cells with a TBK1 inhibitor will rescue STING levels. Understanding why shRala/RalB HeLa cells exhibit decreased STING levels and if they are related to increased TBK1 activity remains to be determined.

Although there is a chance that depolarization-induced TBK1 activation results in an inflammatory response, it seems more likely that TBK1 activation facilitates mitochondrial clearance. Given that TBK1 can phosphorylate Rab7a, which is required for Atg9a recruitment and mitophagy, it is possible that shRala/RalB double knockdown cells exhibit an increase in phosphorylated Rab7a. Increased TBK1 activity in shRala/RalB HeLa cells may result in an increase in phosphorylated Rab7a, resulting in increased Atg9a recruitment to depolarized mitochondria that ultimately leads to increased mitochondrial clearance. This would indicate that RalA and RalB inhibit mitophagy. Perhaps Ral basally inhibits mitophagy to limit inappropriate mitochondrial clearance. However, when mitophagy is triggered through sustained mitochondrial depolarization, Ral relocalizes releasing its inhibition of TBK1 and allows mitophagy to appropriate proceed.

In order to test if shRala/RalB cells have increased phosphorylated Rab7a levels we would examine phosphorylated Rab7a levels using Phos-tag and compare phosphorylated Rab7a levels in shRala cells to those of shScramble cells. Currently, Phos-tag technology is the only approach to evaluate phosphorylated Rab7a since

there currently is no antibody for phosphorylated Rab7a Ser72. If shRalA/RalB HeLa cells exhibit increased phosphorylated Rab7a levels then we would also expect to observe increased Atg9a recruitment to mitochondria. We would study Atg9a recruitment to mitochondria in shRalA/RalB HeLa cells with mitochondrial preps. We would expect to see an increase in Atg9a at mitochondria in shRalA/RalB cells compared to shScramble cells.

Finally, increased Atg9a recruitment to mitochondria suggests that the mitochondria are undergoing mitophagy, so we would study the rate of mitochondrial clearance in shRalA/RalB cells. It is possible that shRalA/RalB cells have an increased mitophagy rate compared to shScramble cells. Our previous studies indicate that shRalA/RalB cells undergo mitochondrial clearance similar to shScramble cells following 24 and 48 hours of mitochondrial depolarization. However, we have not conducted a comprehensive time course to definitively determine any alterations in mitophagy rates in shRalA/RalB cells. Future work should include performing a time course over a period of 24 hours on shRalA/RalB and shScramble HeLa cells to evaluate their mitophagy rates using an anti-DNA antibody to label mitochondrial DNA as previously described <sup>67</sup>.

In addition to facilitating mitophagy or an inflammatory response, it is also possible that TBK1 activation promotes cell survival. TBK1 can be recruited to the exocyst and phosphorylate AKT on Thr308 and Ser473, promoting tumorigenesis <sup>148</sup>. Perhaps increased TBK1 activity in shRalA/RalB cells promotes cell survival because the cells may be experiencing various types of stress (i.e. growth defects or mitochondrial damage) due to depleted Ral levels. We examined phosphorylation of

AKT on Ser473 in shRalA/RalB cells basally and in response to CCCP treatment. Our preliminary data indicated that the kinetics of phosphorylated AKT Ser473 may be different in shRalA/RalB cells in response to CCCP treatment, but these data were not robust. However, future work should also involve examining AKT phosphorylation on Thr308 to thoroughly establish whether TBK1 signals to AKT to promote cell survival in shRalA/RalB cells.

Further studying Ral relocalization with live-cell imaging may provide additional insight into how Ral inhibits TBK1. Studying Ral relocalization following mitochondrial depolarization with live-cell imaging will allow us to gain information about where Ral travels prior to localizing with depolarized mitochondria. Given that inhibition of clathrin impairs Ral trafficking to depolarized mitochondria and TBK1 activity, it will be interesting to determine if Ral colocalizes with clathrin. We performed preliminary live-cell imaging experiments using HeLa cells stably expressing mito-YFP and transiently expressing CFP-RalA and mCherry-Parkin that were treated with valinomycin for 4 hours. In the absence of mitochondrial depolarization, we found that RalA was relatively diffuse, but observed several RalA puncta moving throughout the cell. RalA also localized to what we presume are filopodia that touched each other on adjacent cells. Surprisingly, we did not observe RalA colocalized with depolarized mitochondria. mCherry-Parkin translocated from the cytosol to depolarized mitochondria, indicating that the valinomycin treatment worked. To account for the possibility that RalA localization to depolarized mitochondria may be an artifact of the fixation process, we repeated the experiment and fixed cells after 4 hours of valinomycin treatment. However, we

did not observe RalA localized at depolarized mitochondria, indicating that RalA relocation is not an artifact of fixation. It is likely that there is something about the conditions used during live-cell imaging that inhibit RalA relocation and further optimization is needed in the future.

Determining the functional consequences of TBK1 activation will provide insight into a particular cellular process such as mitophagy or the innate inflammatory response. It is important that we understand the cellular process TBK1 mediates following mitochondrial depolarization because these processes likely are altered in human diseases. After all, mitochondrial depolarization is involved in cellular processes such as mitochondrial dynamics and mitophagy and impairment in either of these processes is associated with various neurodegenerative disorders and cancers.

## *2. How does Ral inhibit TBK1?*

Although we know that Ral's localization is important for its ability to inhibit TBK1, we do not understand the mechanism that governs Ral-mediated TBK1 inhibition. Given that our working model is based on Ral relocation releasing its inhibition of TBK1, we predict that RalA-GTP interacts with TBK1. Following depolarization, RalA-GTP loading decreases (Figures 1.4A and 1.4B) and presumably RalA is no longer able to interact with TBK1. To test if RalA-GTP preferentially interacts with TBK1 versus RalA-GDP, we performed GST-RalA pulldowns in HeLa cells (Figure 2.13A). We detected a GST-RalA/GFP-TBK1 interaction that was not evident with GST control beads (Figure 2.13A). However,

we did not observe a difference in the GST-RalA/GFP-TBK1 interaction based on whether RalA was GTP- or GDP-bound (Figure 2.13A). We are not confident that GST-RalA beads were successfully loaded with either GTP or GDP because we detected a RalA-GTP/Sec5 interaction that was not dramatically impaired with RalA-GDP (Figure 2.13A).

These data have their limitations given that we performed the experiment using an *in vitro* approach and did not include an IP of endogenous RalA. Therefore, it is possible that our result from GST-RalA pulldowns may not reflect the true nature of a RalA/TBK1 interaction as RalA may undergo post-translational modifications that could affect its ability to interact with TBK1. Conversely, there may be no difference in RalA's ability to interact with TBK1 whether RalA is GTP- or GDP-bound. If that is the case then it is likely that the proteins that RalA binds regulates a RalA/TBK1 interaction. Perhaps prior to mitochondrial depolarization, RalA is in complex with proteins that facilitate RalA's inhibition of TBK1. In this case, RalA relocalization following depolarization could cause RalA to dissociate from these associated proteins, which could then affect RalA-mediated inhibition of TBK1. Consequently, future work may include performing a BioID screen to identify proteins that differentially interact with RalA before and after mitochondrial depolarization to obtain potential candidates for further study.

Another limitation of the GST-RalA pulldowns is that they do not account for RalA localization, which in turn may affect a RalA/TBK1 interaction. For example, RalA-GTP levels may differ when is RalA localized to mitochondria vs. RalA localized to the plasma membrane or other organelles. If this is the case then it is possible

that RalA at depolarized mitochondria may have decreased GTP loading and are unable to interact with TBK1 in contrast to RalA that is localized elsewhere within the cell. Future work should include biochemical studies to isolate untreated and depolarized mitochondria and examine RalA-GTP levels. We only measured total cellular RalA-GTP levels, but did not address how RalA localization may affect its GTP-loading status. However, biochemical isolation of RalA at mitochondria is difficult to achieve because RalA is located at multiple membranes within the cell. We attempted to examine RalA at isolated mitochondria, but the purity of our fraction made our results difficult to interpret. Future work also is needed to optimize the purity of mitochondrial preps to examine RalA.

Given that GST-RalA pulldowns have limitations, future work should also include performing co-immunoprecipitations of endogenous RalA to study a RalA/TBK1 interaction in the absence and presence of mitochondrial depolarization. We have made multiple attempts at immunoprecipitating RalA in HeLa cells using different buffer conditions and various versions of tagged-RalA (i.e. myc and flag). However, these IPs were highly inefficient as we only captured roughly 1% of RalA and were unable to detect a RalA and TBK1 interaction unlike the GST-RalA pulldown. Future IPs might be more successful if they included beads coated in lipids where RalA can be anchored into the lipids. This approach may increase the IP efficiency and detection of a RalA/TBK1 interaction.

Although we were unsuccessful in determining if RalA nucleotide-binding status affects its ability to interact with TBK1, we cannot exclude the possibility that GTP-loading status regulates Ral-mediated inhibition of TBK1. Given that RalA-GTP

loading decreases following mitochondrial depolarization, we predicted that RalA<sup>S28N</sup> (constitutively GDP-bound RalA) would not restore TBK1 inhibition in shRalA/RalB HeLa cells. Moreover, we speculated that RalA<sup>Q72L</sup> (constitutively GTP-bound RalA) would restore TBK1 inhibition. To test this, we generated HeLa cells that stably express shRNA-resistant wild-type RalA or RalA<sup>S28N</sup>. Surprisingly, we found that similar to wild-type Flag RalA, Flag RalA<sup>S28N</sup> partially restored TBK1 inhibition (Figure 2.14A). There are two possibilities that may account for this result. The first is that stably expressing Flag RalA<sup>S28N</sup> allows the cells to become accustomed to signaling that they do not normally experience such that they compensate for expressing Flag RalA<sup>S28N</sup>. In other words, this result may be an artifact. To validate this finding, future work should include performing transient restoration of TBK1 inhibition with GFP-RalA GTP/GDP mutants. We began performing these experiments with GFP-RalA<sup>S28N</sup> and GFP-RalA<sup>Q72L</sup>, however additional trials are needed to reach conclusions.

The second possibility that may explain how Flag RalA<sup>S28N</sup> partially restores endogenous TBK1 inhibition is that RalA regulates TBK1 activity through a mechanism that is independent of RalA-GTP loading status. However, this seems unlikely given that the current dogma of how small G proteins signal is through their effectors. If RalA inhibits TBK1 independently of GTP-loading status then RalA may undergo post-translational modifications (i.e. ubiquitination) that modulate its ability to inhibit TBK1. Instead, it appears more likely that RalA-GTP loading status will alter RalA's ability to inhibit TBK1 through RalA effectors. For example, RalA-GTP can bind Sec5, which may facilitate RalA's inhibition of TBK1. Following

mitochondrial depolarization, RalA becomes GDP-bound and no longer interacts with Sec5, so RalA becomes unable to inhibit TBK1 and TBK1 activity increases. To determine if effector proteins facilitate RalA-mediated TBK1 inhibition, we would generate stable knockdown cell lines for known RalA effectors such as Sec5, Exo84 and RalBP1. If knockdown of an effector protein resulted in increased TBK1 activity (i.e. phenocopies what we observed in shRalA/RalB cells) then we would propose that effector protein regulates TBK1 inhibition. Additional pulldown experiments would then be needed to confirm that the effector is in complex with RalA prior to depolarization.

In conclusion, we discovered a novel role for RalA and RalB where Ral proteins inhibit TBK1 and relocate to depolarized mitochondria in a clathrin-dependent process, enabling TBK1 activation. Elucidating both the functional consequences of TBK1 activation and the mechanism of Ral-mediated TBK1 inhibition will be necessary for fully understanding Ral's role in response to mitochondrial depolarization. Importantly, this project should be pursued further because expanding our knowledge about the molecular events surrounding mitochondrial depolarization may provide insight into a variety of diseases that are associated with processes that involve depolarization such as mitochondrial dynamics and mitophagy. Lastly, determining Ral's role in signaling to TBK1 may provide insight into diseases associated with TBK1 mutations such as ALS.

## **Materials and Methods**

### **Chemicals**

Carbonyl cyanidem-3-chlorophenylhydrazone (CCCP) was obtained from Calbiochem. Antimycin A was obtained from Sigma-Aldrich (ref. A8674). Oligomycin was obtained from MP Biomedicals, LLC (ref. 151786). Valinomycin was obtained from Thermo Fisher Scientific (ref. V1644). HeLa cells were treated with 10  $\mu$ M oligomycin and 4  $\mu$ M antimycin a, 10  $\mu$ M valinomycin or 10  $\mu$ M CCCP. Pitstop<sup>®</sup> 2 was obtained from Abcam and used at 20  $\mu$ M. BX795 was obtained from Enzo Life Sciences, Inc. (ref. 189-0005) and used at 2  $\mu$ M. BQU57 was obtained from Selleck Chemicals (ref. S7607) and used at 50  $\mu$ M. DMSO was obtained from VWR (ref. 0231). 16% formaldehyde was obtained from Cell Signaling Technology (ref. 12606S).

## **Cell Culture**

HeLa cells were obtained from the ATTC. HeLa cells were maintained in Dulbecco's Modified Eagle Medium (DMEM) (ref. 111965092, Life Technologies) supplemented with 10% Fetal Bovine Serum (FBS, ref. 16000044, GIBCO) and 1% Penicillin-Streptomycin (ref. 15140122, GIBCO). HeLa cells stably expressing mCherry-Parkin were generated using a retroviral system and selected using 2.5  $\mu$ g/mL Blastocidin (ref. R21001, GIBCO). shScramble, shRala/Ralb and shAP50 HeLa cells were generated using a retroviral system and selected using 1  $\mu$ g/mL Puromycin (ref. p8833, Sigma-Aldrich), while shRala/Ralb cells were further selected with 500  $\mu$ g/mL Neomycin (ref. 10131035, GIBCO). shRala/Ralb stably expressing WT Flag Rala (shRNA resistant) were selected with 180  $\mu$ g/mL Hygromycin B (ref. 10687010, Thermo Fisher Scientific). Cells were tested for

mycoplasma with the MycoAlert™ PLUS Mycoplasma Detection Kit (ref. LT07-701, Lonza).

### **Transfection/immunocytochemistry**

30,000 HeLa cells were seeded onto glass microslides (#1.5) (ref. 12541B, Fisher Scientific) and transfected 2 days later with the indicated constructs using FuGENE® 6 (ref. E269A, Promega). 24 hours post-transfection cells were treated as described with either CCCP or OA and fixed with 4% formaldehyde/PBS for 5 minutes at room temperature. Cells were mounted either with Prolong® Gold Antifade Mountant with DAPI (ref. P36931, Invitrogen™) or Prolong® Diamond Antifade Mountant (ref. P36930, Invitrogen™).

### **RNA interference and Constructs**

Oligonucleotides designed to generate short hairpin RNAs (shRNA) targeting the  $\mu 2$  subunit of AP2 (aka AP50) (5'-GTGGATGCCTTTCGGGTCA-3')<sup>149</sup> were cloned into pSUPER.retro.puro (OligoEngine, Inc.). pSUPER.retro.puro.RalA (shRalA--1: 5'-AAGACAGGTTTCTGTAGAAGA-3', and pSUPER.retro.puro.RalB (5'-GACTATGAACCTACCAAAG-3') were described previously<sup>11</sup>. S194A Flag RalA pbabe puro was made shRNA resistant using the following primers: 5'-TTTAGAAGATAAAAGGCAAGTCAGCGTGGAGGAGGCAAAAACAGA-3' and 5'-TCTGTTTTTTGCCTCCTCCACGCTGACTTGCCTTTTATCTTCTAAA-3'. This construct was then cloned into pbabe hygro by cutting pbabe hygro with BAMHI and Sall, while the insert was cut with BamH1 and XhoI. Upon obtaining S194A Flag RalA

pbabe hygro, site-directed mutagenesis was performed to convert S194A Flag RalA to wild-type RalA using the following primers: forward- 5'-AAAAAGAAGAGGAAAAGTTTAGCCAAGAGAAT-3' and reverse- 5'-ATTCTCTTGGCTAAACTTTTCCTCTTCTTTTT-3'. pSR neo RalB was a gift from Chris Counter (shRalB: 5'GACTATGAACCTACCAAAG -3'). HeLa cells were transiently transfected with FuGENE® 6 (ref. E269A, Promega) using 500 ng or 250 ng of the indicated fluorescent constructs: pEGFP (Clontech Laboratories, Inc.), pEGFP-C1-RalA, pEGFP-C1-RalB, mCherry-Parkin, mito-YFP or mito-BFP. pEGFP-TBK1 was a gift from Georgios Stathopoulos (Addgene plasmid # 87443). mCherry-Parkin was a gift from Richard Youle (Addgene plasmid # 23956). mCherry-Parkin was cloned into pWZL-blasti using the In-Fusion® HD Cloning Kit (Clontech Laboratories, Inc.). mito-BFP was a gift from Gia Voeltz (Addgene plasmid # 49151). mito-BFP was cloned into pBABE-puro (Millenium Pharmaceuticals) using XhoI and EcoR1. A Kozak sequence and EcoR1 site was introduced into mito-BFP using site-directed mutagenesis (Forward primer: 5'-TGCAGTCTCGAGGCCGCCACCATGCTTTCACTACGTCAA-3' and Reverse primer: 5'-GCTGACGAATTCTCAATTAAGCTTGTGCCC-3'). All stable cell lines were generated using the retroviral packaging vector, pCL-10A1 from Imgenex. pGEX-KG-RalBD was used to generate expression of glutathione *S*-transferase (GST)-RalBD<sup>150</sup>. S183A, S194A, S194A/S183A, S28N and Q72L mutant GFP-RalA constructs were generated from performing site-directed mutagenesis.

## **Western Blotting**

Whole cell lysates were prepared in RIPA buffer with protease inhibitors (2  $\mu\text{g}/\text{mL}$  Aprotinin, 2  $\mu\text{g}/\text{mL}$  Leupeptin, 1 mM PMSF, 1 mM  $\text{Na}_3\text{VO}_4$  and 50 mM NaF) and lysates were quantified using Bio-Rad Protein Assay Dye Reagent Concentrate (ref. 5000006). Equivalent protein amounts (generally 30 or 50  $\mu\text{g}$ ) were resolved by freshly cast 10% SDS-PAGE gels. Gels were run with either EZ-Run™ Prestained Rec Protein Ladder (ref. BP3603500, Fisher Scientific) or SeeBlue™ Plus2 Prestained Protein Standard (ref. LC5925, Invitrogen™). Gels were transferred to PVDF membranes (ref. IPVH00010, Immobilon®-P, Millipore) and immunoblotted with the following antibodies: mouse monoclonal  $\alpha$ -AP50 (ref. 611350, BD Transduction Laboratories, 1:500), mouse monoclonal  $\alpha$ -RalA (ref. 610221, BD Transduction Laboratories, 1:1000), rabbit monoclonal  $\alpha$ -GAPDH (ref. 5174, Cell Signaling Technology, 1:5000), mouse monoclonal  $\alpha$ -OPA1 (ref. 612606, BD Transduction Laboratories, 1:1000), rabbit monoclonal  $\alpha$ - $\beta$ -Actin (ref. 4970, Cell Signaling Technology, 1:2000), rabbit monoclonal  $\alpha$ -phospho-TBK1 (Ser172) (ref. 5483, Cell Signaling Technology, 1:1000), rabbit monoclonal  $\alpha$ - $\beta$ -tubulin (ref. 2128, Cell Signaling Technology, 1:2000), rabbit polyclonal  $\alpha$ -eGFP (ref. OSE00003G, Thermo Fisher Scientific) and mouse monoclonal  $\alpha$ -RalB (ref. 04-037, Millipore Sigma, 1:500). Goat  $\alpha$ -rabbit- or goat  $\alpha$ -mouse-HRP secondary antibodies were used (ref. 111-036-046, ref. 115-036-008, Jackson ImmunoResearch Laboratories, Inc., 1:5000) for visualization of blots enhanced chemiluminescence detection (WesternBright™ ECL). Band pixel intensity was quantified by using ImageJ and bands were normalized to the indicated controls.

## **Pitstop 2 Experiments**

50,000 HeLa cells were plated onto glass microslides (#1.5) (ref. 12541B, Fisher Scientific). Two days later, cells were transfected with 500 ng each of the indicated constructs using a 3:1 ratio of FuGENE® 6 (ref. E269A, Promega) to DNA. 24 hours post-transfection, cells were washed twice with 1X PBS and pre-treated with either DMSO or 20  $\mu$ M Pitstop® 2 (ref. ab120687) in serum-free DMEM supplemented with 10 mM HEPES (ref. 15630080, GIBCO) for 15 minutes at 37°C. Following the 15 minute pre-treatment, cells were treated with one of the following ways for 1 hour at 37°C: 1. DMSO, 2. 10  $\mu$ M oligomycin and 4  $\mu$ M antimycin A, 3. 20  $\mu$ M Pitstop 2 or 4. 20  $\mu$ M Pitstop 2 and 10  $\mu$ M oligomycin and 4  $\mu$ M antimycin A. Cells were then washed twice with 1X PBS and fixed with 4% formaldehyde/PBS for 5 minutes at room temperature. For image analysis, over 50 cells were counted per treatment to examine Parkin colocalization with the mitochondria (n=3).

## **Transferrin-Uptake**

### ***Microscopy***

50,000 HeLa cells were plated onto glass microslides (#1.5) (ref. 12541B, Fisher Scientific). Two days later, cells were washed twice with 1X PBS and treated for 15 minutes at 37°C with 0.1% DMSO or 20  $\mu$ M Pitstop® 2 in serum-free DMEM supplemented with 10 mM HEPES. Following the 15 minute pre-treatment, cells were treated with 10  $\mu$ g/mL Transferrin Alexa Fluor-647 (ref. T23366, Life Technologies) in the presence or absence of 20  $\mu$ M Pitstop 2 in serum-free DMEM supplemented with 10 mM HEPES for 15 minutes at 37°C. Cells were washed twice

with 1X PBS and fixed with 4% formaldehyde/PBS for 5 minutes at room temperature.

### ***Flow Cytometry***

For flow cytometric analysis of transferrin uptake, shScramble and shAP50 HeLa cells were serum-starved for 30 minutes in serum-free DMEM containing 25 mM HEPES and 0.5% Bovine Serum Albumin (BSA) (ref. BSA-50, Rockland Immunochemicals Inc.). Cells were detached using 10 mM EDTA/PBS, collected in serum-free DMEM and spun for 3 minutes at 1000 rpm at 4°C. Cells were then resuspended in cold serum-free DMEM containing 25 mM HEPES, 0.5% BSA and 50 µg/mL Transferrin Alexa Fluor-647. Cells were incubated at 4°C for 10 minutes and moved to 37°C for 15 minutes. Cells were then spun for 3 minutes at 1000 rpm at 4°C and washed twice with 1mL of cold 1X PBS/0.5% BSA. Following cold PBS/0.5% BSA washes, cells were acid washed twice with cold acidic buffer (0.1M glycine, 150 mM NaCl, pH 3). Cells were then washed with cold 1X PBS and fixed in 2% formaldehyde/PBS for 10 minutes at room temperature. Following fixation, cells were washed with cold 1X PBS, spun and resuspended in 500 µl cold 1X PBS. Unstained cells were also prepared as a negative control for flow cytometric analysis.

### ***Confocal Microscopy***

Fixed cells were mounted onto glass microslides (#1.5) (ref. 12541B, Fisher Scientific) and imaged on a Zeiss LSM 710 confocal microscope using the 63X oil

objective. Single color controls were tested to assess bleedover. For quantification of RalA or RalB recruitment to mitochondria in HeLa cells, 25 random images across 3 trials were analyzed. Ali Rohani developed the following methods to quantify our images. To quantify the colocalization of Ral and the mitochondria, we separated Ral and mitochondria from their respective background signals. Given that mitochondria and Ral contain exhibit different staining patterns, we separated different channels and saved each channel as an independent image. Following this, multiple preprocessing steps, including median, and top-hat filtering were applied to remove noise and other imperfections in each image. After preprocessing, a simple thresholding method was used for segmentation of the mitochondrial network and the RalA or RalB protein distribution. Threshold levels were chosen that effectively removed the noisy background from the real objects. The result of the thresholding step is a binary mask, with the value of 0 for background, and a value of 1 for the foreground mitochondrial or RalA or RalB contents.

Using the thresholded images, we determined percentage of overlap between the mitochondrial network and RalA or RalB, which we termed percent overlap. This was calculated using the following formula:

$$Overlap = \frac{common}{union}$$

The numerator is equal to the total number of pixels with the value of 1 after applying a logical AND between two images. These are the pixels where both mitochondria and RalA or RalB have a value of 1 after thresholding. The denominator is the sum of pixel values after applying a logical OR between the

thresholded channels. The pixels where either the mitochondria or RalA or RalB exist will have the value of 1 after applying the OR operation. Using this formula, the overlap has a value between 0 and 1, where 0 means no overlap, while the value of 1 means a complete overlap. By multiplying this value by 100, the overlap is represented as a percentage.

The other feature defined and used to quantify the colocalization of the mitochondria and RalA or RalB is the proximity index, which has a value between 0 and 1. The proximity index represents the similarity in the spatial distribution of the mitochondrial network and Ral proteins. The proximity index of 1 represents two completely overlapping structures, while an index of zero represents no similarity or absence of one channel.

To calculate the proximity index, we first average the values of the thresholded channels at each pixel. As a result, the pixels where both mitochondria and RalA or RalB exist (overlap) will have a value of 1, the pixels where either mitochondria or RalA or RalB exist will have the value of 0.5, and finally, the pixels where none of them exist, the pixel value will be 0. Following the averaging, we define a  $2^k \times 2^k$ ,  $2 \leq k \leq 10$ , sliding window to sweep the entire averaged image from top left to bottom right.

Starting from window one, we calculate the ratio of mitochondria to RalA or RalB and vice versa. The minimum of these ratios with a value between 0 and 1 is selected as the ratio factor for that window. Following this step, the ratio factor is multiplied to each individual pixel in the window. Finally, the average of the non-zero, weighted pixels in the window is defined as the proximity index for that

window and is stored for subsequent measurements. This process is repeated for each window until the whole image is scanned by the sliding window. Ultimately, the proximity index of RalA or RalB and mitochondria in the image is determined by summing up the proximity indices from different windows and dividing the result by the number of the windows with a non-zero proximity index.

The overlap measurement is independent of window size, but the proximity index is a function of the windows size as described earlier. Different window sizes define the proximity index at different granularities. By calculating and averaging the proximity indices of multiple cells with different treatments at different windows size we can identify the window size that results in the widest distinction between the treatment groups and use it to compare different treatments. We used a window size of 64 for our analyses.

### **RalA-GTP Pulldown**

GST-RalBD beads were generated as follows: 300 mL of BL21 bacteria expressing pGEX-KG-RalBD were induced with 0.3 mM IPTG and rocked for 3 hours at 37°C. Bacteria were then spun at 4°C at 6,000 g for 15 minutes and lysed with 40 mL of PBST with inhibitors (1% aprotinin, 1 mM PMSF and 0.5 mM DTT). Bacteria were sonicated (Output 4, Constant 50, 30 hits for 3 times) and spun at 4°C at 12,000 rpm for 20 minutes. Supernatant was combined with 500 µl of Glutathione Sepharose 4B (ref. 17-0756-01, GE Healthcare) beads and rocked overnight at 4°C. The beads were then spun at 2,000 rpm for 2 minutes each and washed 3 times with 10 mL of lysis buffer.

To perform the GST-RalBD pulldown, cells were serum starved overnight and treated with 10  $\mu$ M CCCP for 0, 30, 60 and 80 minutes. Cells were washed two times with cold 1X PBS, scraped and spun at 1,000 rpm for 5 minutes. Cells were lysed using 200  $\mu$ l of GTP lysis buffer (1% NP-40, 50 mM Tris pH 7.5, 200 mM NaCl, 10 mM MgCl<sub>2</sub>, 1% aprotinin, 1 mM PMSF, 0.5 mM DTT) on ice for 30 minutes. Samples were spun at 14,000 rpm for 10 minutes and a BCA was performed to quantify protein amounts. 500  $\mu$ g and 100  $\mu$ g of protein were used for pulldowns and inputs, respectively. For GST-RalBD pulldowns, 500  $\mu$ g of protein was combined with 30  $\mu$ l of GST-RalBD in a total volume of 500  $\mu$ l of GTP lysis buffer, rotating at 4°C for 45 minutes. Samples were washed two times with 500  $\mu$ l of GTP lysis buffer and spun at 2,000 rpm for 2 minutes. Total RalA and GTP-RalA levels were detected by SDS-PAGE and immunoblotting.

#### **GST-RalA Pulldown:**

GST-RalA and GST beads were generated as follows: 300 mL of BL21 or Rosetta bacteria expressing pGEX-6P1-RalA or pGEX-6P1 were induced with 0.3 mM IPTG and rocked for 3 hours at 37°C. Bacteria were then spun at 4°C at 6,000 g for 15 minutes and lysed with 40 mL of PBST with inhibitors (1% aprotinin, 1 mM PMSF and 0.5 mM DTT). Bacteria were sonicated (Output 4, Constant 50, 30 hits for 3 times) and spun at 4°C at 12,000 rpm for 20 minutes. Supernatant was combined with 500  $\mu$ l of Glutathione Sepharose 4B (ref. 17-0756-01, GE Healthcare) beads and rocked overnight at 4°C. The beads were then spun at 2,000 rpm for 2 minutes each and washed 3 times with 10 mL of lysis buffer.

To perform GST-RalA or GST pulldowns, GST-RalA and GST beads were washed twice with GST-lysis buffer (1% NP-40, 50 mM Tris pH 7.5, 200 mM NaCl, 10 mM MgCl<sub>2</sub>). The beads were then preloaded with an equal volume of 1 mM GTP or GDP in GTP/GDP loading buffer (20 mM Tris pH 7.4, 10 mM EDTA, 25 mM NaCl) for 20 minutes at 37°C. Beads were then spun for 2 minutes at 2000 rpm and resuspended in GTP-lysis buffer with inhibitors (1% aprotinin, 1 mM PMSF, 0.5 mM DTT). 50 µg of protein was used for input. 500 µg of protein from HeLa cells transiently expressing GFP-TBK1 was combined with 30 µl of GST-RalA or GST beads in a total volume of 400 µl of GTP lysis buffer. Pulldowns were performed for rotating at 4°C for 1 hour. All beads were then washed 3 times with GTP-lysis for 5 minutes and spun at 2000 rpm for 2 minutes. A TBK1/RalA interaction was detected by SDS-PAGE and immunoblotting.

## Figures

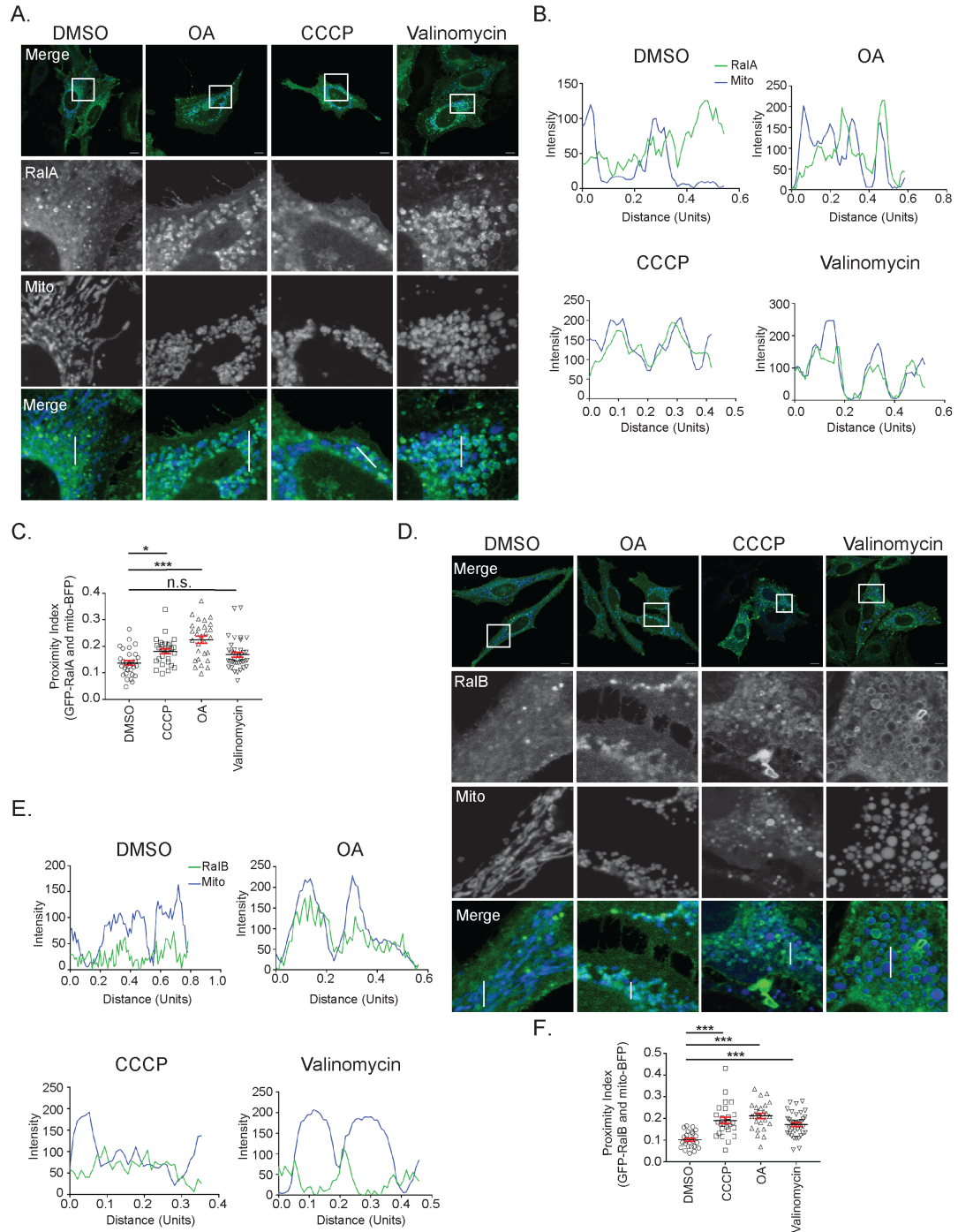


**Figure 2.1.** Both RalA and RalB are recruited to depolarized mitochondria. (A) HeLa cells transiently expressing mito-BFP and GFP-RalA were treated with vehicle control (DMSO), 10  $\mu$ M oligomycin and 4  $\mu$ M antimycin A (OA), 10  $\mu$ M CCCP or 10  $\mu$ M valinomycin for 3 hours and imaged with confocal microscopy (Scale bars = 10  $\mu$ M). White boxes indicate magnified sections. (B) Plot profiles of cells in A (1 Unit =

96 pixels). White lines in A indicate sections analyzed using ImageJ. (C) Quantification of RalA distance to mitochondria (One-way ANOVA using Dunnett's multiple comparisons test, mean  $\pm$  SEM, \* $p \leq 0.05$ , \*\*\* $p \leq 0.0001$ , n.s. = not significant,  $n = 3$ ). Each dot represents one cell. (D) HeLa cells transiently expressing mito-BFP and GFP-RalB were treated as in A. (E) Plot profiles of cells in D (1 Unit = 96 pixels). White lines in D indicate sections analyzed using ImageJ. (F) Quantification of RalB distance to mitochondria (One-way ANOVA using Dunnett's multiple comparisons test, mean  $\pm$  SEM, \*\*\* $p \leq 0.0001$ ,  $n = 3$ ). Each dot represents one cell.

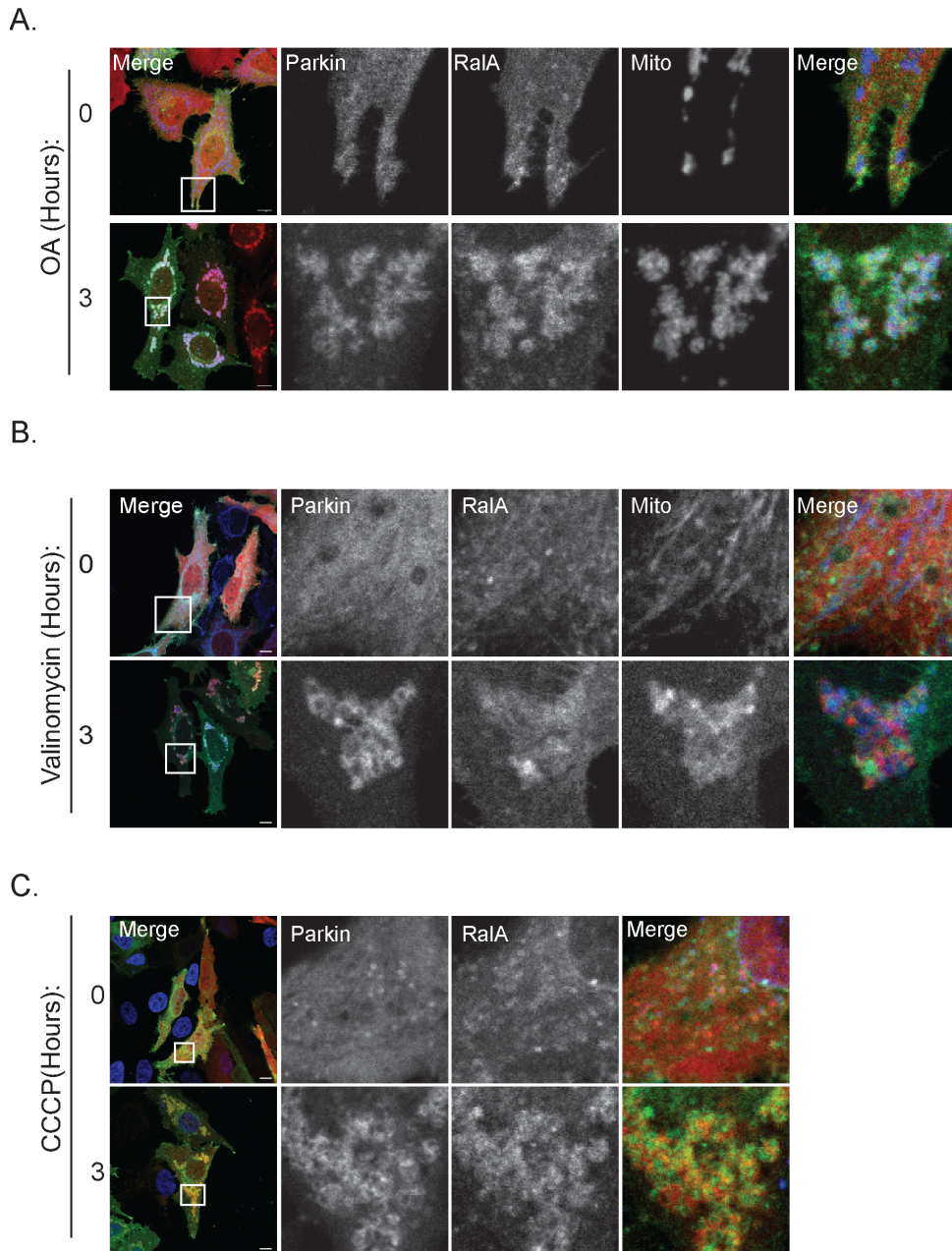


**Figure 2.2.** OA, Valinomycin and CCCP induce mitochondrial depolarization and RalA relocalization. (A) HeLa cells stably expressing mCherry-Parkin and transiently expressing mito-BFP and GFP-RalA were treated with 10  $\mu$ M oligomycin and 4  $\mu$ M antimycin A (OA) over 3 hours and imaged with confocal microscopy (Scale bars = 10  $\mu$ M). White boxes indicate magnified sections. (B) Same as A, except HeLa cells were treated with 10  $\mu$ M valinomycin (Scale bars = 10  $\mu$ M). (C) HeLa cells transiently expressing mCherry-Parkin and GFP-RalA were treated with 10  $\mu$ M CCCP for 3 hours and imaged with confocal microscopy (Scale bars = 10  $\mu$ M).

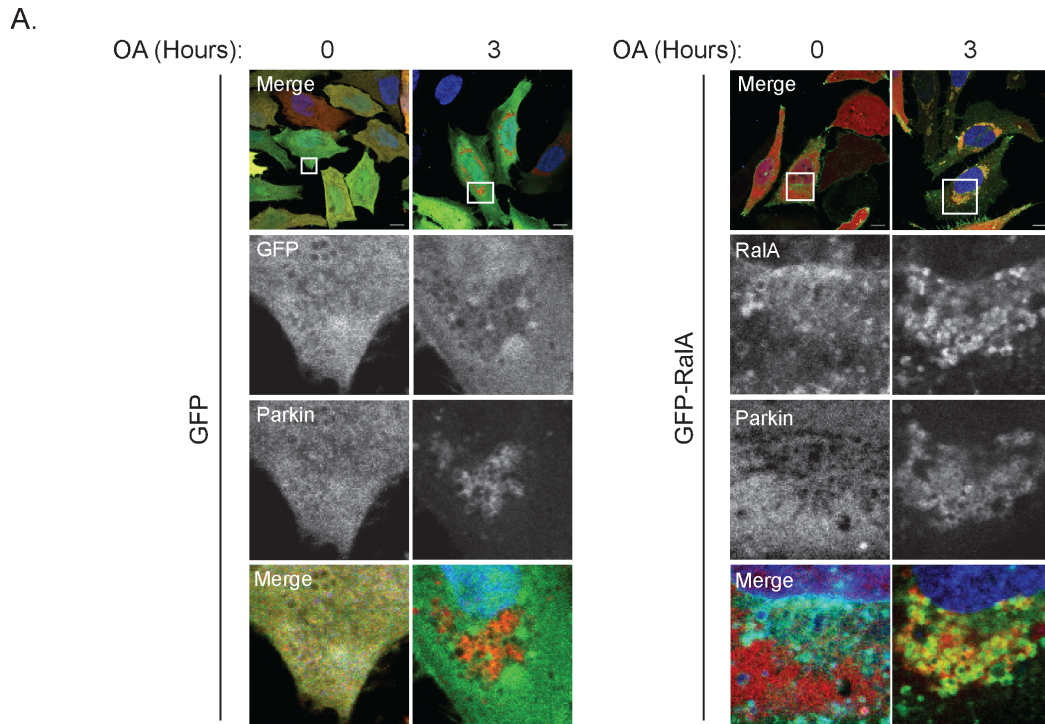


**Figure 2.3.** GFP does not relocate to depolarized mitochondria. (A) HeLa cells that transiently express mCherry-Parkin and either GFP or GFP-RalA were treated with 10  $\mu$ M oligomycin and 4  $\mu$ M antimycin A (OA) for 3 hours and imaged by confocal microscopy (Scale bars = 10  $\mu$ M). White boxes indicate magnified sections.

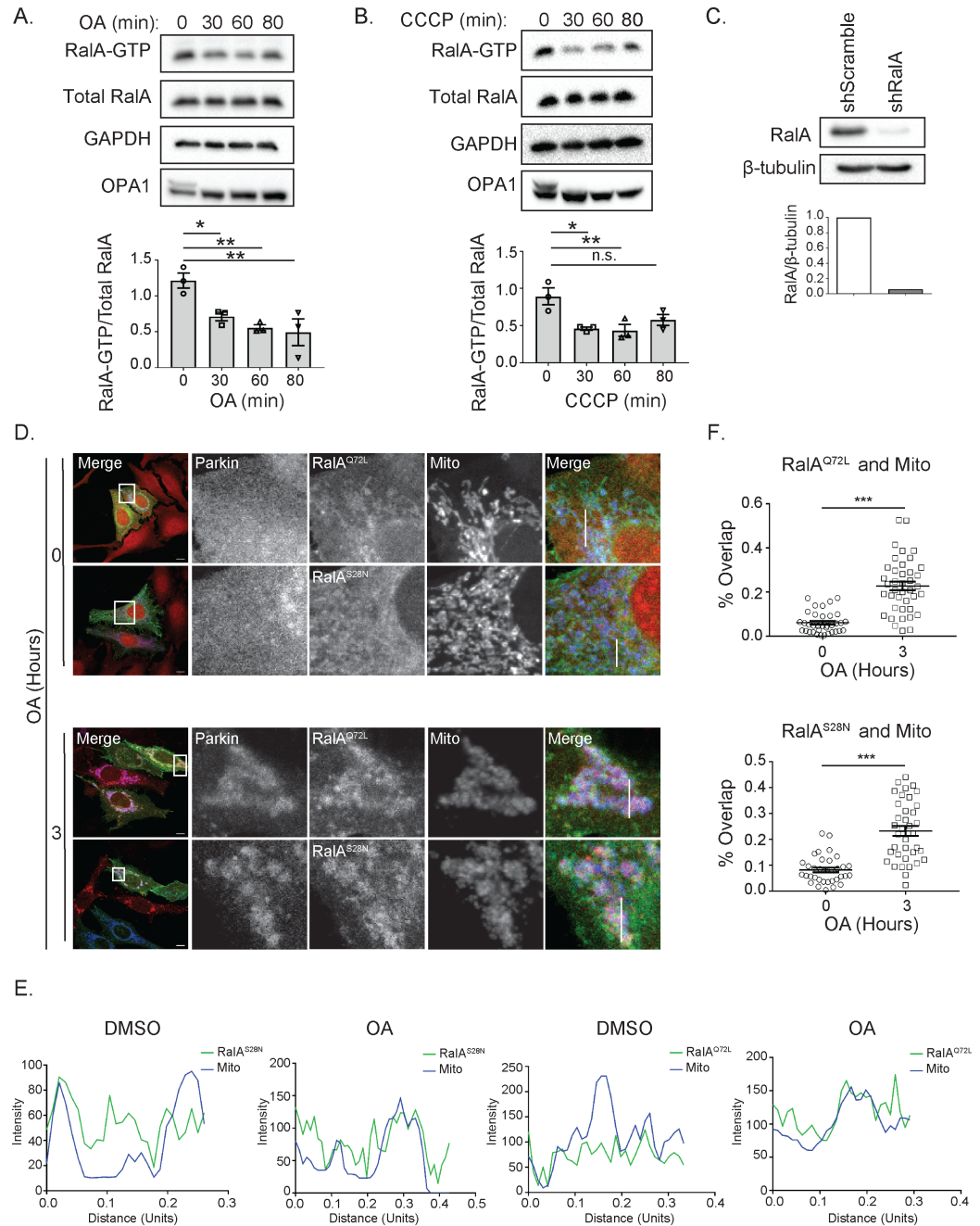


**Figure 2.4.** RalA GTP-loading decreases following mitochondrial depolarization, but does not regulate RalA localization. (A) HeLa cells were treated over an 80-minute time course with 10  $\mu$ M oligomycin and 4  $\mu$ M antimycin A (OA) and Ral-GTP levels were assessed by GST-RalBD pulldown. Ral-GTP levels were quantified and normalized to total RalA (One-way ANOVA using Dunnett's multiple comparisons test, mean  $\pm$  SEM, \* $p \leq 0.05$ , \*\*  $p \leq 0.005$ ,  $n = 3$ ). (B) Experiment in A was repeated using 10  $\mu$ M CCCP (One-way ANOVA using Dunnett's multiple comparisons test, mean  $\pm$  SEM, \* $p \leq 0.05$ , \*\* $p \leq 0.01$ ,  $n = 3$ ). (C) Immunoblot analysis of RalA in HeLa cells stably expressing the indicated shRNA constructs. RalA levels were quantified

and normalized to  $\beta$ -tubulin. (D) HeLa cells stably expressing mCherry-Parkin and transiently expressing mito-BFP and the indicated RalA-GTP mutants were treated with OA over 3 hours and imaged by confocal microscopy (Scale bars = 10  $\mu$ M). White boxes indicate magnified sections. (E) Plot profiles of cells in D (1 Unit = 96 pixels). White lines in D indicate sections analyzed using ImageJ. (F) Quantification of RalA and mitochondria colocalization in D (Two-tailed Unpaired t-test, mean  $\pm$  SEM, \*\*\* $p \leq 0.0001$ ,  $n = 3$ ). Each dot represents one cell.

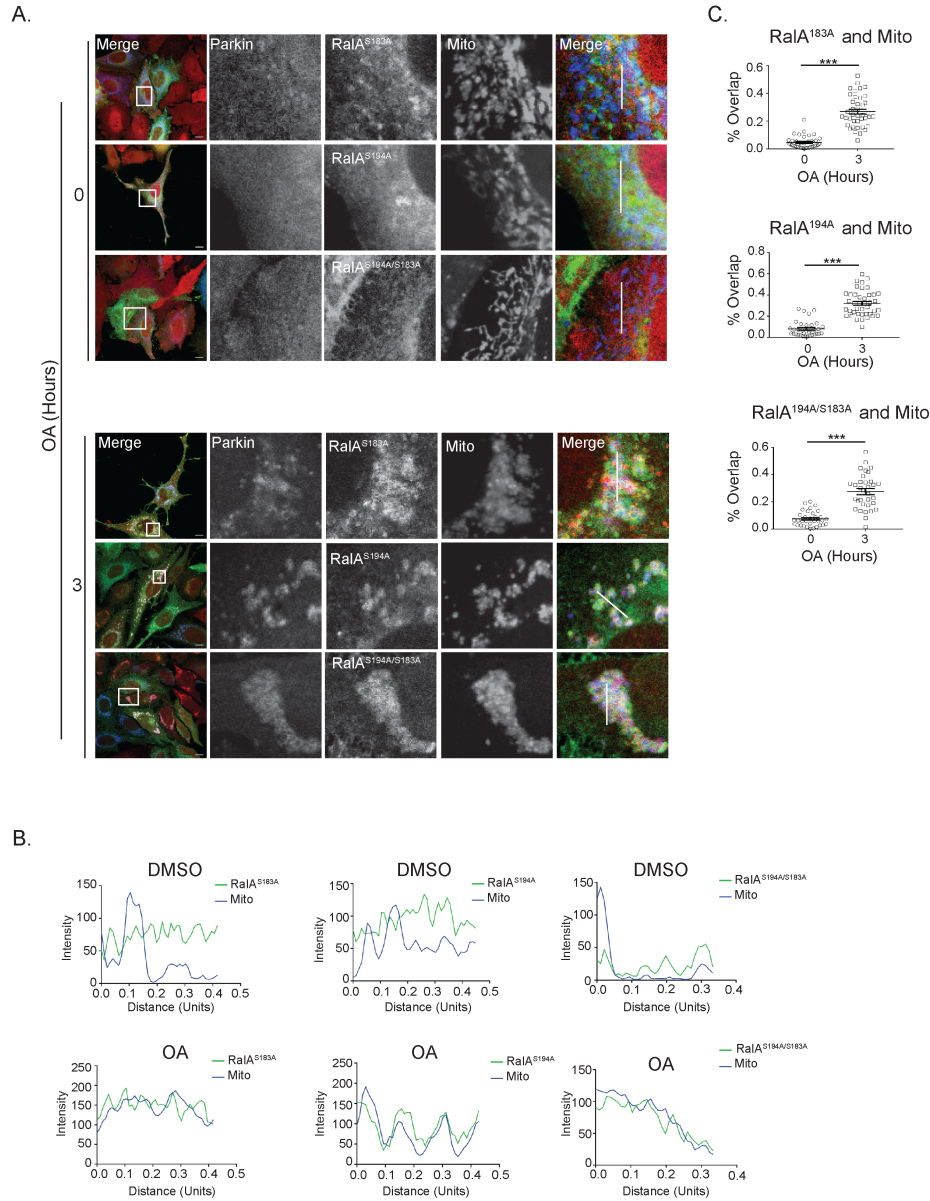


**Figure 2.5.** Phosphorylation of RalA on Ser194 or Ser183 does not regulate RalA subcellular localization in response to mitochondrial damage. (A) HeLa cells that stably express mCherry-Parkin and transiently express mito-BFP and the indicated GFP-RalA phosphorylation mutants were treated with 10  $\mu$ M oligomycin and 4  $\mu$ M antimycin A for 3 hours and imaged by confocal microscopy. DMSO was used as a vehicle control (Scale bars = 10  $\mu$ M). White boxes indicate magnified sections. (B) Plot profiles of cells in A. White lines in A indicate sections analyzed using ImageJ (1 Unit = 96 pixels). (C) Quantification of RalA and mitochondria colocalization in A (Two-tailed Unpaired t-test, mean  $\pm$  SEM, \*\*\* $p \leq 0.0001$ ,  $n = 3$ ). Each dot represents one cell.

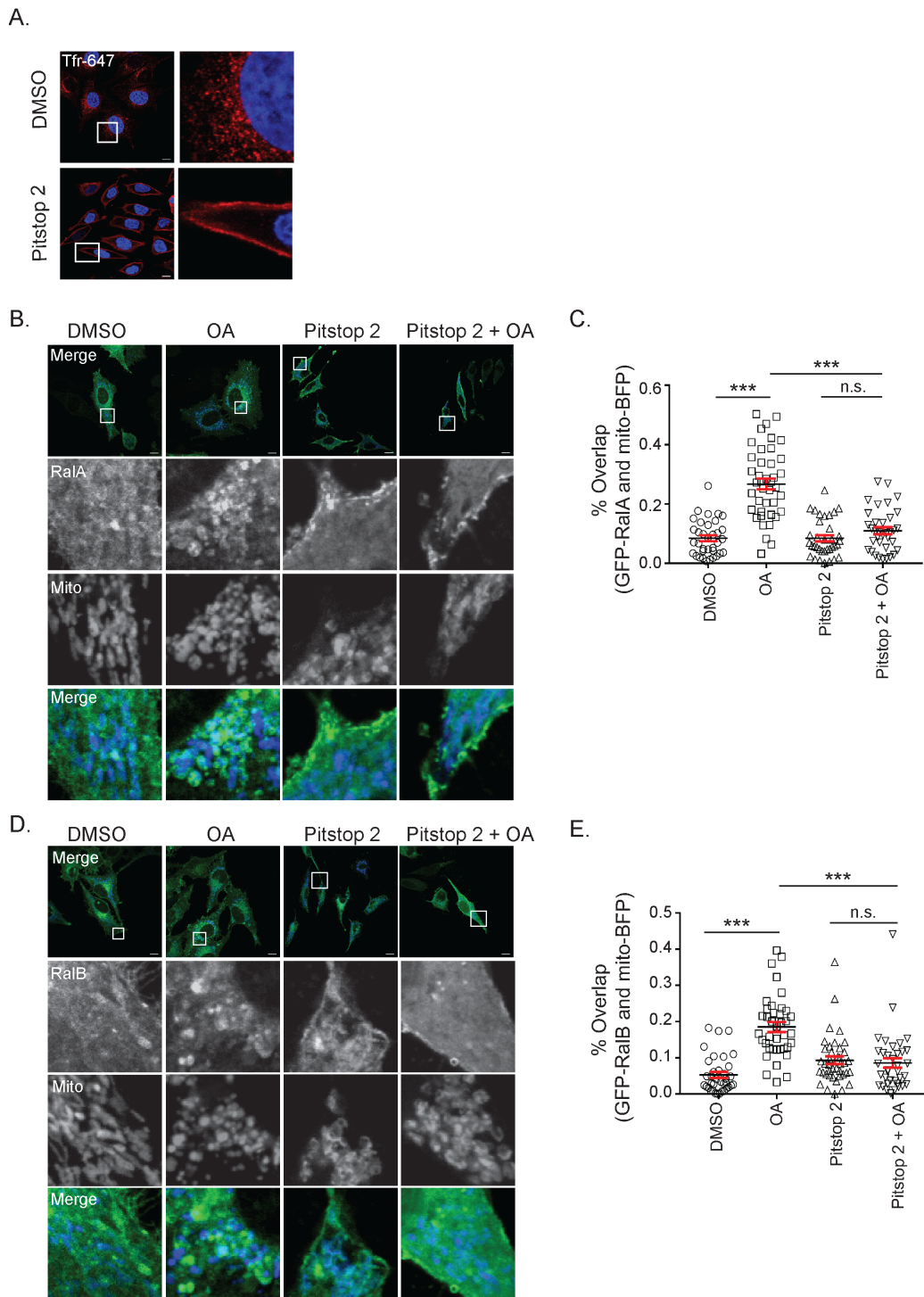


**Figure 2.6.** Clathrin-mediated endocytosis facilitates RalA and RalB recruitment to depolarized mitochondria. (A) HeLa cells were treated with 20  $\mu$ M Pitstop 2 or DMSO (vehicle control) for 15 minutes and transferrin Alexa Fluor-647 uptake was analyzed by confocal microscopy (Scale bars = 10  $\mu$ M). White boxes indicate

magnified sections. (B) HeLa cells transiently expressing mito-BFP and GFP-RalA were pre-treated for 15 minutes either with DMSO or 20  $\mu$ M Pitstop 2 for 15 minutes and then treated for 1 hour with Pitstop 2 and/or 10  $\mu$ M oligomycin and 4  $\mu$ M antimycin A (OA) as indicated and imaged by confocal microscopy (Scale bars = 10  $\mu$ M). White boxes indicate magnified sections. (C) Quantification of B to determine RalA colocalization with the mitochondria (One-way ANOVA using Tukey's multiple comparisons test, mean  $\pm$  SEM, \*\*\* $p \leq 0.001$ , n.s. = not significant,  $n = 3$ ). Each dot represents one cell. (D) Same as A, except HeLa cells transiently express GFP-RalB instead of GFP-RalA. (E) Quantification of D to determine the degree of RalB colocalization with the mitochondria (One-way ANOVA using Tukey's multiple comparisons test, mean  $\pm$  SEM, \*\*\* $p \leq 0.001$ , n.s. = not significant,  $n = 3$ ). Each dot represents one cell.

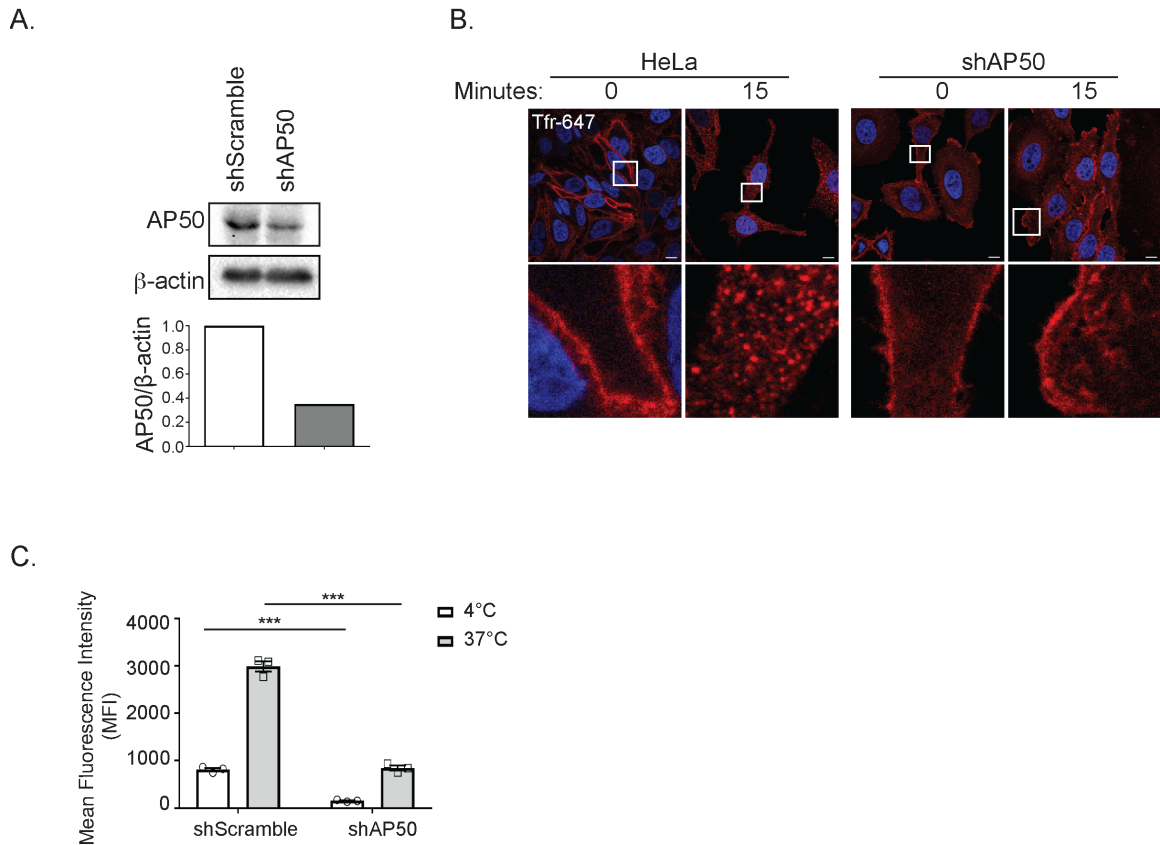


**Figure 2.7.** shAP50 cells exhibit impaired clathrin-mediated endocytosis. (A) Immunoblot analysis of AP50 in the indicated cells. AP50 levels were quantified and normalized to  $\beta$ -actin. (B) HeLa cells expressing the indicated shRNA constructs were incubated with transferrin Alexa Fluor-647 and either kept on ice ( $t = 0$ ) or shifted from 4°C to 37°C for 15 minutes ( $t = 15$ ) then analyzed by confocal microscopy (Scale bars = 10  $\mu$ M). White boxes indicate magnified sections. (C) Flow cytometric quantification of transferrin uptake in cells treated identically to those in B (Two-way ANOVA using Sidak's multiple comparisons test, mean  $\pm$  SEM, \*\*\* $p \leq 0.0001$ ,  $n = 3$ ).

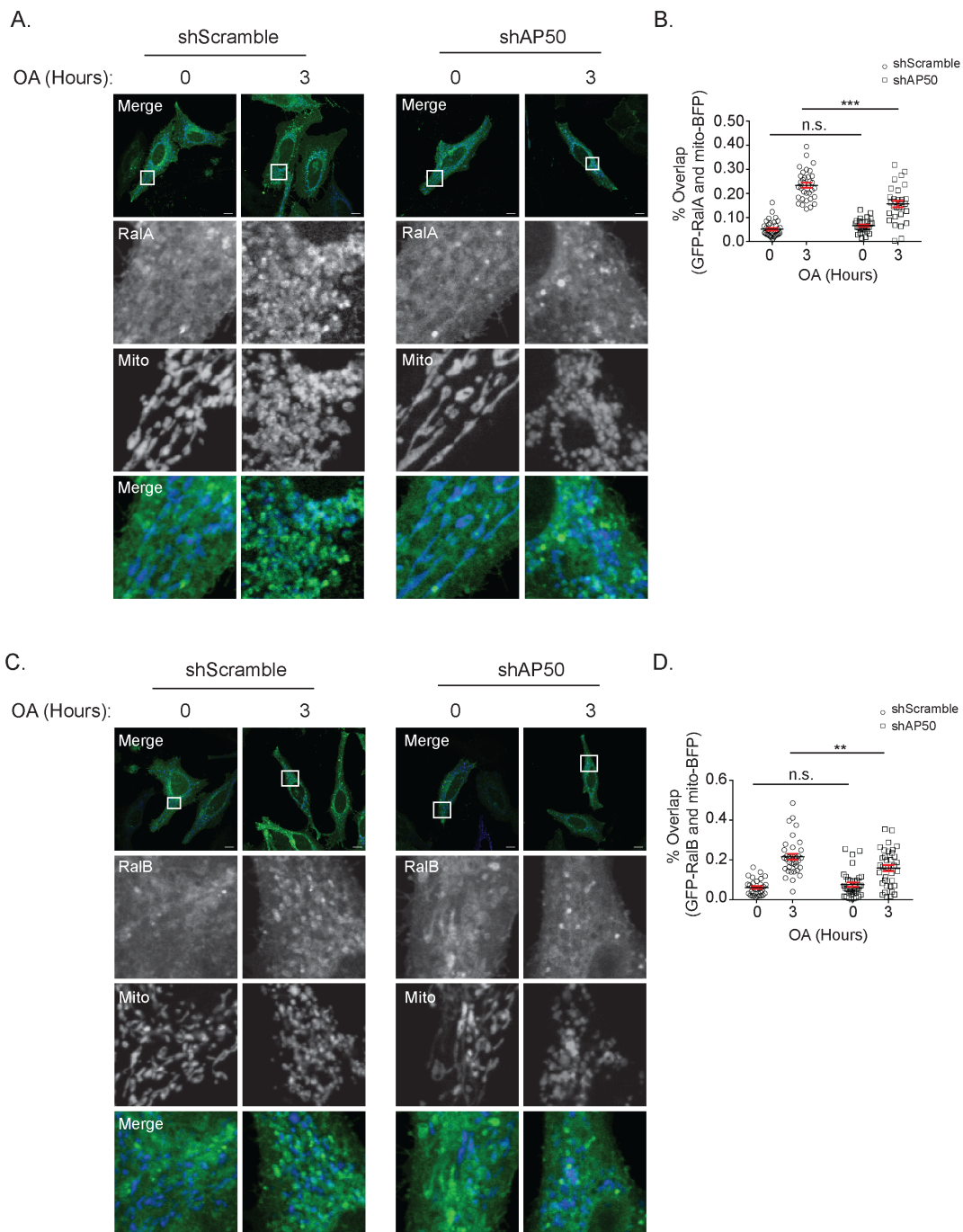


**Figure 2.8.** shAP50 cells exhibit impaired RalA and RalB localization to depolarized mitochondria. (A) shScramble and shAP50 HeLa cells transiently expressing GFP-RalA and mito-BFP were treated with 10  $\mu$ M oligomycin and 4  $\mu$ M antimycin A (OA) for 3 hours and imaged by confocal microscopy (Scale bars = 10  $\mu$ M). White boxes indicate magnified sections. (B) Quantification of RalA and mitochondria colocalization in A (Two-way ANOVA using Tukey's multiple comparisons test, mean  $\pm$  SEM, n.s. = not significant, \*\*\* $p \leq 0.0001$ ,  $n = 3$ ). Each dot represents one cell. (C)

Same as B, except HeLa cells express GFP-RalB instead of GFP-RalA (Scale bars = 10  $\mu$ M). (D) Quantification of RalB and mitochondria colocalization in C (Two-way ANOVA using Tukey's multiple comparisons test, mean  $\pm$  SEM, n.s.= not significant, \*\*p  $\leq$  0.001, n = 3). Each dot represents one cell.

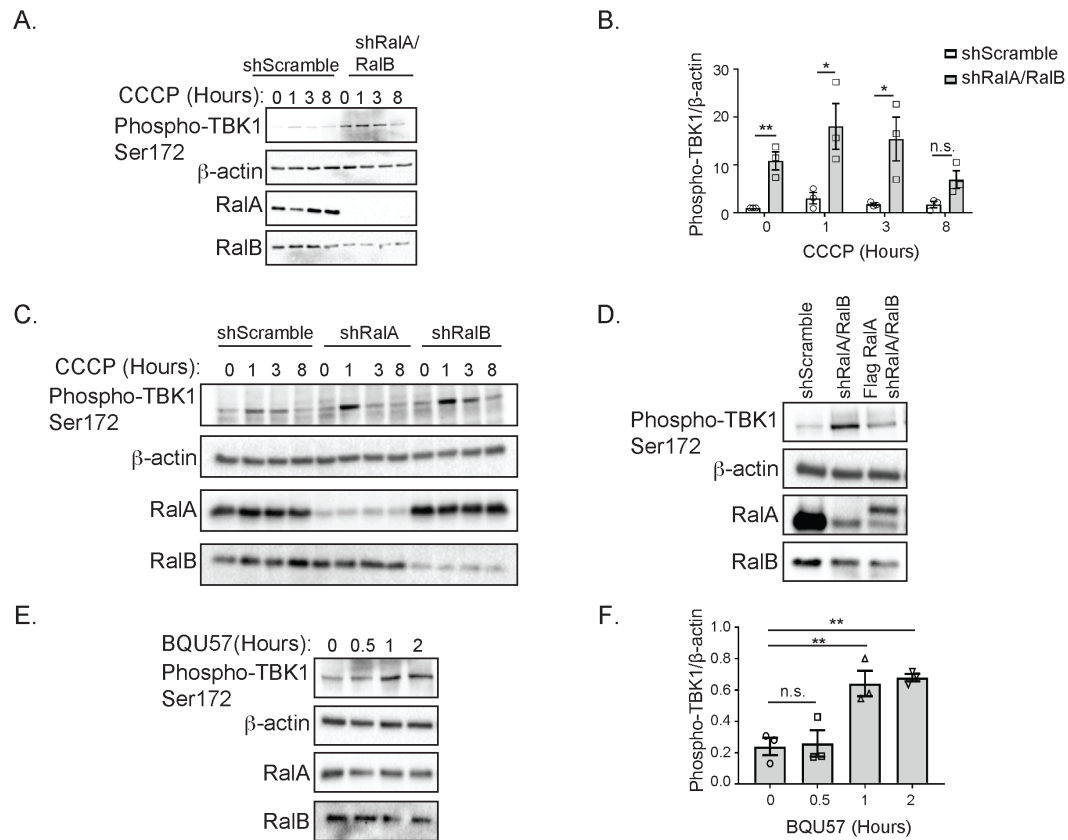


**Figure 2.9.** RalA and RalB negatively regulate TBK1 activity. (A) shScramble and shRalA/RalB HeLa cells were treated for 8 hours with 10  $\mu$ M CCCP. An Immunoblot was performed for the indicated proteins. (B) Phospho-TBK1 levels in A were quantified with ImageJ, normalized to  $\beta$ -actin and then further normalized to the untreated value obtained for shScramble cells (Two-tailed Unpaired t-test, mean  $\pm$  SEM, \* $p \leq 0.05$ , \*\* $p \leq 0.01$ , n.s. = not significant,  $n = 3$ ). (C) Stably expressing shScramble, shRalA and shRalB HeLa cells were treated with 10  $\mu$ M CCCP for 8 hours and immunoblotted for the indicated proteins. (D) HeLa cells stably expressing shScramble, shRalA/RalB or Flag RalA and shRalA/RalB constructs were immunoblotted for the indicated proteins. (E) HeLa cells were treated with 50  $\mu$ M BQU57 for 2 hours and an immunoblot was performed for the indicated proteins. (F) Phospho-TBK1 levels in E were quantified with ImageJ and normalized to  $\beta$ -actin (One-way ANOVA using Dunnett's multiple comparisons test, mean  $\pm$  SEM, \*\* $p \leq 0.01$ , n.s. = not significant,  $n = 3$ ).

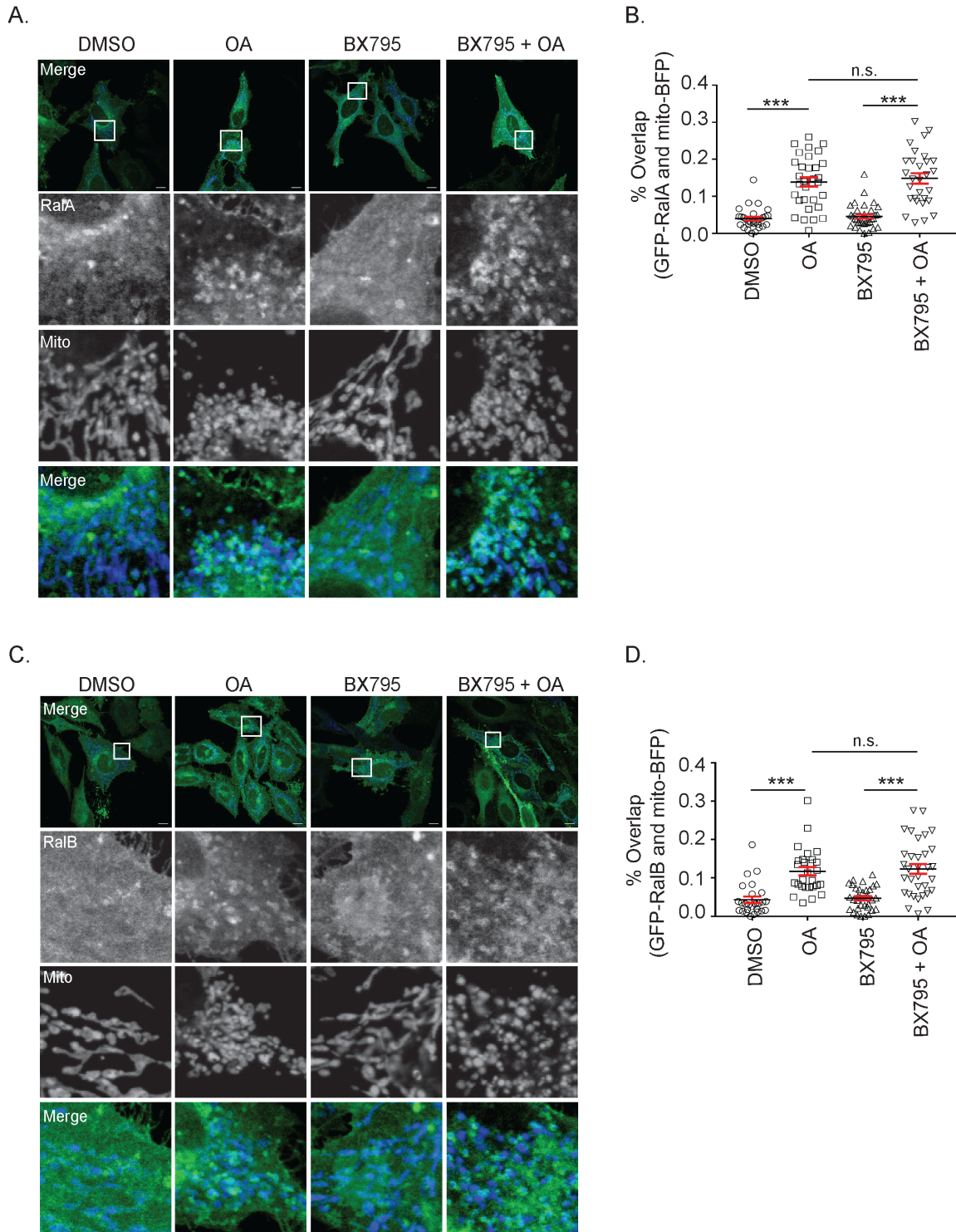


**Figure 2.10.** RalA and RalB relocation to depolarized mitochondria occurs upstream of TBK1 activation. (A) HeLa cells transiently expressing GFP-RalA and mito-BFP were pre-treated with vehicle control (DMSO) or 2  $\mu$ M BX795 for 1 hour

and then treated for an additional hour as indicated. Cells were imaged by confocal microscopy (Scale bars = 10  $\mu$ M). White boxes indicate magnified sections. (B) Quantification of A to determine the degree of RalA colocalization with mitochondria (One-way ANOVA using Tukey's multiple comparisons test, mean  $\pm$  SEM, \*\*\* $p \leq 0.001$ , n.s. = not significant, n = 3). Each dot represents one cell. (C) Same experiment as in A except HeLa cells express GFP-RalB instead of GFP-RalA. (D) Quantification of C to determine the degree of RalB colocalization with mitochondria (One-way ANOVA using Tukey's multiple comparisons test, mean  $\pm$  SEM, \*\*\* $p \leq 0.001$ , n.s. = not significant, n = 3). Each dot represents one cell.

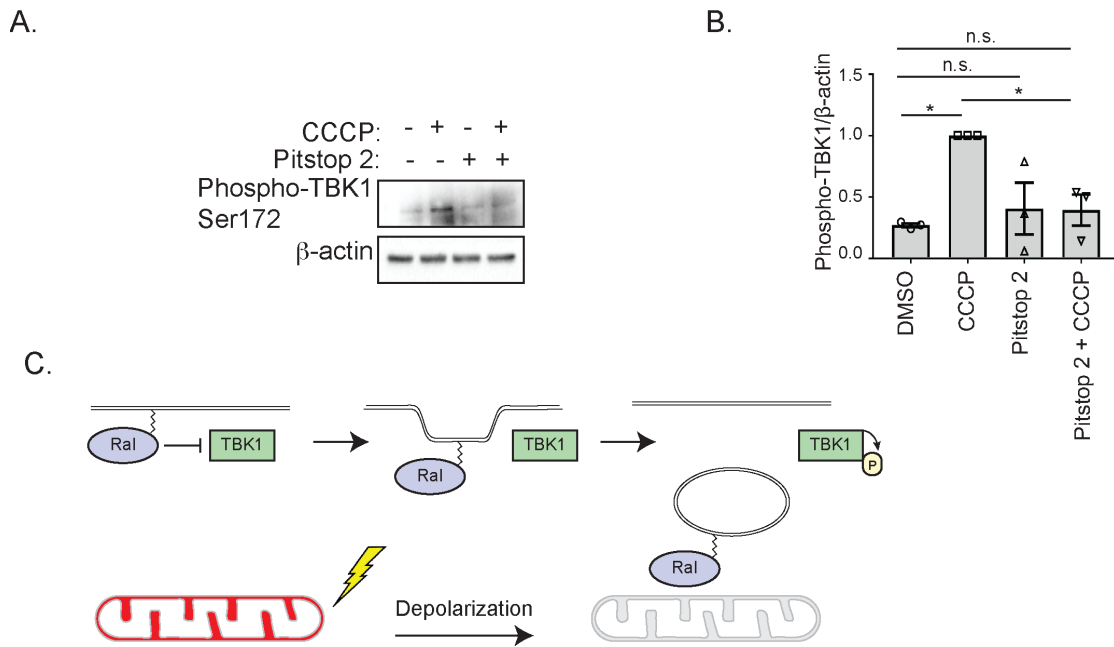


**Figure 2.11.** Ral relocation affects TBK1 activity. (A) HeLa cells were pre-treated either with vehicle control (DMSO) or 20  $\mu$ M Pitstop 2 for 15 minutes in serum-free DMEM containing 10 mM HEPES. Cells were then treated for 1 hour as indicated and immunoblotted for the indicated proteins. (B) Phospho-TBK1 levels in A were quantified with ImageJ, normalized to  $\beta$ -actin and then further normalized to the value obtained for cells treated 1 hour with CCCP treatment alone (One-way ANOVA using Tukey's multiple comparisons test, mean  $\pm$  SEM, \* $p \leq 0.05$ , n.s. = not significant,  $n = 3$ ). (C) Model of how RalA and RalB negatively regulate TBK1. Following mitochondrial depolarization, RalA and RalB localize to mitochondria via CME leading to a release of their inhibition of TBK1.

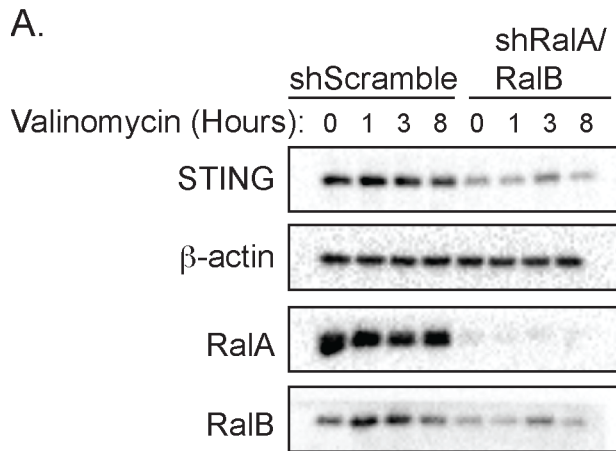


**Figure 2.12.** shRalA/RalB cells exhibit decreased STING levels. (A) HeLa cells stably expressing the indicated shRNA constructs were treated with 10  $\mu$ M Valinomycin over 8 hours. Immunoblotting was performed for the indicated proteins.

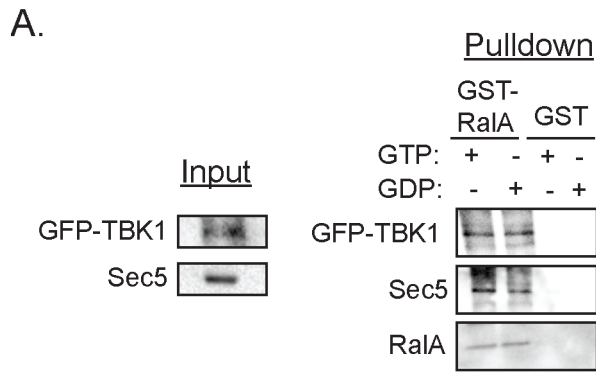


**Figure 2.13.** GST-RalA-GTP and GST-RalA-GDP interact similarly with GFP-TBK1. (A) Lysate from HeLa cells transiently expressing GFP-TBK1 was incubated with GST-RalA or GST beads that were preloaded with 1 mM GTP or GDP. An immunoblot was performed for the indicated proteins.

A.

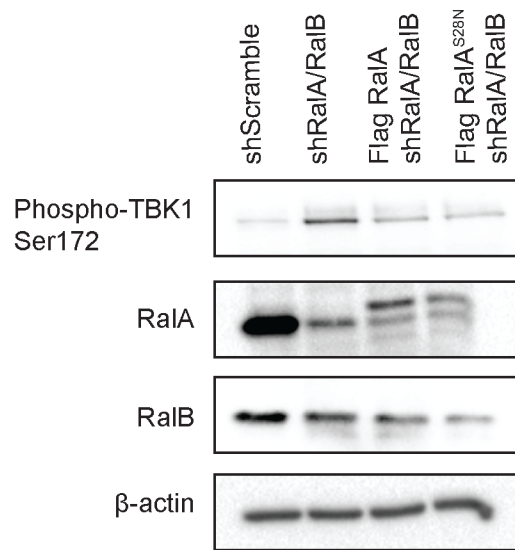


**Figure 2.14.** Stable expression of Flag RalA restores TBK1 inhibition in shRalA/RalB HeLa cells. (A) Lysate from untreated HeLa cells stably expressing the indicated constructs was obtained and immunoblot was performed for the described proteins.

## **Chapter Three: A novel role for RalA during PINK1-Parkin mitophagy**

### **Introduction**

In chapter 2, we demonstrated that both RalA and RalB relocate to depolarized mitochondria (Figures 2.1 and 2.2) with Parkin. These data indicate that Ral proteins may be involved in Parkin recruitment during PINK1-Parkin mitophagy. Interestingly, a proteomics screen identified RalA as a possible Parkin-interacting protein <sup>112</sup>. Given that RalA relocates and may interact with Parkin, we hypothesized that RalA mediates Parkin recruitment during PINK1-Parkin mitophagy. Although PINK1 kinase activity is required for Parkin recruitment, it remains unclear how Parkin traffics from the cytosol to PINK1 at the OMM following activation by phosphorylated ubiquitin chains <sup>114</sup>.

In this chapter we show that RalA, but not RalB mediates Parkin recruitment to depolarized mitochondria. Notably, knockdown or knockout of RalA impairs Parkin recruitment following mitochondrial depolarization, suggesting that RalA participates in this process and that PINK1 stabilization by itself is insufficient for full Parkin recruitment. Consistent with this, inhibition of clathrin-mediated endocytosis (CME) prevents both Parkin recruitment and RalA trafficking to mitochondria, implicating endosomal trafficking in mitophagy. Our study is the first to directly implicate RalA in PINK1-Parkin mitophagy. Furthermore, this finding provides yet another example of Ral proteins playing a broad role in various physiological processes following mitochondrial depolarization.

## **Both RalA and RalB colocalize with Parkin following mitochondrial depolarization**

We previously found that RalA relocates to depolarized mitochondria with Parkin and this relocalization occurs independently of Parkin (Figures 2.1A to 2.1F and 2.2A to 2.2C). It is possible that RalA and Parkin are two independent events with RalA having no effect on Parkin. Alternatively, RalA relocalization with Parkin may indicate that RalA affects Parkin in some manner. Given that RalB also relocates to depolarized mitochondria (Figures 2.1D to 2.1F), we sought to determine whether RalB also relocates to depolarized mitochondria with Parkin. To test this, we examined RalB relocalization in HeLa cells that stably or transiently express Parkin and transiently express GFP-RalB and/or mito-BFP that were treated with OA, valinomycin or CCCP (Figures 3.1A, 3.1B and 3.1C). We found that in response to all three depolarization methods, Parkin relocalized with RalB similar to RalA (Figures 3.1A, 3.1B and 3.1C). This suggests either that RalB has some effect on Parkin or that Parkin and RalB relocalization are two independent events.

## **RalA knockdown results in impaired Parkin recruitment**

The striking relocalization of RalA to mitochondrial membranes following mitochondrial depolarization and its colocalization with Parkin led us to ask whether RalA is required for Parkin recruitment to depolarized mitochondria. To test this, we transiently transfected mCherry-Parkin and mito-YFP into HeLa cells stably expressing shRNA targeting either RalA or a scramble control sequence (Figure 3.2A), then treated with CCCP over an 8-hour time course. As we expected,

scramble control cells exhibited perinuclear Parkin puncta that colocalized with the mitochondria 3 and 8 hours following CCCP treatment (Figure 3.2B). In contrast, only 40% of RalA knockdown cells exhibited Parkin recruitment following 8 hours of CCCP treatment (Figures 3.2B and 3.2C), compared with 90% of scramble control cells. We obtained similar results were obtained using an alternate shRalA construct, shRalA-2 (Appendix D).

To confirm our findings, we repeated this experiment using OA to induce mitochondrial depolarization. shRalA HeLa cells exhibited significantly impaired mitochondrial Parkin recruitment after 3 hours of OA treatment (71.6% vs. 90.4%) compared to shScramble HeLa cells (Figures 3.2D and 3.2E). After 8 hours of OA treatment, Parkin recruitment occurred at similar levels in both shScramble and shRalA HeLa cells (Figure 3.2E). Consequently, it appears that the extent of RalA involvement in mitochondrial Parkin recruitment is influenced by the method of depolarization and that impaired Parkin recruitment after 3 hours of OA treatment in shRalA cells likely reflects a delay rather than a complete inhibition. Interestingly, although Parkin recruitment was impaired in shRalA HeLa cells Parkin still was active as indicated by Parkin autoubiquitination (Figure 3.2F). Moreover, we observed comparable phospho-ubiquitin (Ser65) levels in stably expressing mCherry-Parkin shScramble and shRalA HeLa cells (Figure 3.2F). These data indicate that loss of RalA does not affect PINK1-dependent phosphorylation of ubiquitin and does not explain why shRalA cells exhibit impaired Parkin recruitment.

### **RalB knockdown does not impair Parkin recruitment**

To determine if RalB also facilitates Parkin recruitment to depolarized mitochondria, we examined Parkin recruitment in shRalB HeLa cells that were treated with OA for 3 hours (Figure 3.3A and 3.3B). Parkin recruitment in shRalB cells following mitochondrial depolarization was comparable to Parkin recruitment in shScramble cells (Figures 3.3B and 3.3C). There was no statistically significant difference in Parkin recruitment between shScramble and shRalB HeLa cells treated with OA for 3 hours, indicating that the potential involvement of Ral proteins in Parkin recruitment is specific for RalA (Figure 3.3C). However, it is possible that there was no significant impairment in Parkin recruitment in shRalB cells due to the fact that knockdown of RalB was not as robust as knockdown of RalA.

### **RalA knockout results in impaired Parkin recruitment**

We next sought to determine the necessity of RalA for Parkin recruitment to depolarized mitochondria in an additional cell type. As such, we generated RalA knockout (KO) mouse embryonic fibroblasts (MEFs) by expressing adenoviral Cre-recombinase in MEFs generated from RalA floxed embryos<sup>27</sup>. RalA KO MEFs and pre-Cre floxed MEFs (FL/FL) were then engineered to stably express mCherry-Parkin, treated for 8 hours with CCCP and stained with TOM20 to label the mitochondria (Figures 3.4A and 3.4B). While the timing and extent of Parkin recruitment we observed in MEFs differed from HeLa cells, we still observed a defect in Parkin recruitment in the absence of RalA (Figure 3.4B and 3.4C). Both RalA FL/FL and RalA KO MEFs exhibited increased Parkin recruitment to

depolarized mitochondria (Figure 3.4C). However, the degree of colocalization between Parkin and mitochondria in RalA KO MEFs as measured by Pearson's coefficient was significantly lower (40.2% lower) than that of RalA FL/FL MEFs following 8 hours of OA treatment (Figure 3.4C). Consequently, these data suggest that RalA facilitates Parkin recruitment to depolarized mitochondria.

Similar to shRalA HeLa cells, we did not observe impairment in phospho-ubiquitin (Ser65) levels in RalA KO MEFs compared to RalA FL/FL MEFs following 8 hours of CCCP treatment (Figure 3.5A). Once again, this suggests that the impairment in Parkin recruitment is due to a delay rather than complete inhibition. In contrast to HeLa cells, Parkin appeared as a doublet in MEFs both in the absence and presence of CCCP treatment (Figure 3.5A). However, increased phospho-ubiquitin levels in MEFs following depolarization suggests that Parkin must be active.

### **Imaging flow cytometry confirms that shRalA HeLa cells exhibit impaired Parkin recruitment**

Because knockdown or genetic knockout of RalA does not cause complete loss of Parkin recruitment following mitochondrial depolarization, we sought to develop an unbiased way to monitor Parkin recruitment to ensure that the effects we observe truly represent a Parkin recruitment defect. To that end, we treated shScramble or shRalA HeLa cells stably expressing mito-YFP and mCherry-Parkin with OA over 3 hours and analyzed Parkin and mitochondria colocalization using imaging flow cytometry. Consistent with our previous results, we observe a 30.9%

decrease in Parkin recruitment 1 hour after OA treatment in shRala cells compared to shScramble cells with a less robust decrease after three hours (Figures 3.6A and 3.6B). Additionally, we observed decreased Parkin recruitment following 3 hours of OA treatment, although this was not statistically significant ( $p$ -value = 0.05). Collectively, our results using three different quantification methods and examining two different cell types consistently reveal that loss of RalA impairs, but does not abolish Parkin recruitment to depolarized mitochondria.

### **Expression of GFP-RalA rescues Parkin recruitment in shRala HeLa cells**

To confirm that RalA is responsible for the observed defect in Parkin recruitment, we transiently transfected shRala HeLa cells that stably expressed mCherry-Parkin with shRNA-resistant GFP-RalA and treated them with OA for 3 hours (Figures 3.7A and 3.7B). Cells transfected with GFP-RalA rescued Parkin recruitment compared to untransfected cells (Figure 3.7B). These data indicate that the defect in Parkin recruitment is due to loss of RalA and not to an off-target effect of the shRNA.

### **Clathrin-mediated endocytosis facilitates Parkin recruitment following mitochondrial depolarization**

The coincident relocalization of Parkin and RalA to mitochondria following depolarization and the defect in Parkin recruitment following RalA inhibition led us to explore whether there were any common processes that could potentially link the two. Intriguingly, both RalA and Parkin have previously been identified at sites of

clathrin-mediated endocytosis (CME) and both have been implicated in the regulation of this process<sup>50,151</sup>. We previously found that Ral proteins relocate to mitochondria in a clathrin-dependent process (Figures 2.6B, to 2.6E and 2.8A to 2.8D). We speculated that perhaps CME facilitates Parkin recruitment to depolarized mitochondria. It is possible that we only observed a partial defect in Parkin recruitment in shRala HeLa cells and Rala KO MEFs because Rala is involved in CME and CME is the key force facilitating Parkin recruitment. If that is the case then we predicted that inhibiting CME would abolish Parkin recruitment.

To determine whether CME plays a role in recruiting Parkin to depolarized mitochondria, we treated HeLa cells transiently expressing mCherry-Parkin and mito-YFP with OA and Pitstop 2, a cell-permeable CME inhibitor, either alone or in combination (Figures 3.8A and 3.8B). While untreated cells and those treated with Pitstop 2 alone did not result in mCherry-Parkin and mito-YFP colocalization, we observed robust colocalization of mCherry-Parkin and mito-YFP following 1 hour of OA treatment (Figure 3.8A). Interestingly, cells treated with both OA and Pitstop 2 failed to exhibit Parkin relocation to mitochondria (Figures 3.8A and 3.8B). Parkin not only was unable to localize to depolarized mitochondria, but also did not activate as cells treated with both Pitstop 2 and OA did not exhibit Parkin autoubiquitination (Figure 3.8C). We also determined that cells treated with both Pitstop 2 and OA lack phosphorylated ubiquitin (Ser65), which is consistent with their abolished Parkin recruitment (Figure 3.8C).

OPA1 was used as a readout to confirm that mitochondrial depolarization occurs. Cells treated with Pitstop 2 alone exhibited preferential processing of OPA1,

indicating that Pitstop 2 itself may induce mitochondrial depolarization. However, PINK1 stabilization was only observed in cells treated with OA. Intriguingly, PINK1 stabilization in cells treated with both OA and Pitstop 2 were comparable to those in cells treated with OA alone (Figure 3.8D). Therefore, PINK1 stabilization occurs during CME inhibition, but PINK1 is unable to phosphorylate ubiquitin chains.

Furthermore, both RalA and Parkin relocalization in response to mitochondrial depolarization was significantly impaired in the presence of Pitstop 2 (Appendix E). This corresponds with our previous finding that RalA recruitment to depolarized mitochondria occurs in a clathrin-dependent process (Figures 2.6B to 2.6E, 2.8A to 2.8D). Consequently, these data suggest that clathrin activity is required for relocalization of both Parkin and RalA following mitochondrial depolarization.

Given that clathrin has additional roles outside of CME, and that any pharmacologic inhibitor will exhibit some degree of off-target effects, we repeated this set of experiments in HeLa cells that stably express an shRNA targeting AP50, the  $\mu$ 2 subunit of AP2 that is required for clathrin recruitment to sites of endocytosis (Figures 2.7A, 2.7B and 2.7C). shAP50 cells exhibited significantly impaired mitochondrial Parkin recruitment after both 1 and 3 hours of OA treatment compared to shScramble HeLa cells (Figures 3.9A and 3.9B). Collectively, these findings are consistent with the observed loss of Parkin recruitment in cells treated with both OA and Pitstop 2 and support the notion that CME mediates Parkin localization to mitochondria in response to mitochondrial depolarization.

## Discussion

There has been a great deal of interest in PINK1 and Parkin ever since the discovery that these proteins cooperate in the autophagic removal of damaged mitochondria <sup>109</sup>. While most of the studies have focused on mechanisms of PINK1 accumulation and retention and activation of mitochondrial Parkin, very few studies have explored the potential mechanisms through which Parkin traffics to depolarized mitochondria <sup>114-116,152</sup>. The prevailing hypothesis is that PINK1 accumulation and phosphorylation of resident ubiquitin chains is sufficient to cause mitochondrial accumulation of Parkin, presumably because freely diffusing Parkin that encounters phospho-ubiquitin is retained at the OMM. Once at the OMM, Parkin can then generate additional ubiquitin chains that act as PINK1 substrates and recruit additional Parkin molecules in a feedforward mechanism. This model is supported by data demonstrating that forced expression of PINK1 on the OMM is sufficient to recruit Parkin in the absence of depolarization and that mistargeting PINK1 to peroxisomes and lysosomes is sufficient to recruit Parkin to those organelles <sup>114,153</sup>.

On the surface, the data we present here seem to contradict the current accepted model of Parkin recruitment, as inhibition of CME, either through pharmacologic inhibition of clathrin or genetic inhibition of AP2, prevents Parkin relocalization following mitochondrial depolarization, even though PINK1 is stabilized. However, there are several potential models that could reconcile these findings. For example, plasma membrane associated Parkin may traffic to the endolysosomal network through CME, at which point it can be delivered to

mitochondria (or other organelles) through existing organelle-organelle contact sites. Under this scenario, Parkin would only accumulate at mitochondria in the presence of stabilized PINK1, though the trafficking could potentially occur under any circumstances in which endocytosis occurs. In support of this, Parkin has previously been identified at sites of CME and can regulate endocytosis through ubiquitination <sup>151</sup>. Furthermore, a study found that mitochondrial depolarization leads to transient calcium release that triggers massive endocytosis <sup>154</sup>. In turn, the increased rate of endocytosis may accelerate Parkin recruitment to depolarized mitochondria. Notably, while we observe pools of Parkin concentrated at distinct regions of the plasma membrane, we were unable to definitively identify Parkin colocalization with specific non-mitochondrial internal membranes at early time points following mitochondrial depolarization, as predicted by this model.

Previously, endocytosis has been implicated in PINK1-Parkin mitophagy to promote autophagy by regulating the assembly of Atg9a vesicles <sup>155</sup>. This study demonstrated that RABGEF1 recruits both Rab7a and Rab5 to depolarized mitochondria. We also identified Rab7 and Rab5 at depolarized mitochondria with Parkin (Figure 3.10A and 3.11A). Additionally, we found that both Rab7 and Rab5 colocalize with RalA in response to mitochondrial depolarization (Figure 3.10B and 3.11B). This suggests an association between RalA and endosomes, but does not directly show that RalA traffics to depolarized mitochondria through endocytosis. Our findings differ from the literature in that we propose a role for endocytosis upstream of mitochondrial clearance to aid Parkin recruitment. It is possible that

endocytosis not only regulates autophagosome assembly, but also controls Parkin localization to depolarized mitochondria.

The potential involvement of RalA in this process raises a number of important questions. Mostly studied in the context of cancer<sup>11,32</sup>, RalA is involved in a variety of membrane trafficking and remodeling activities, including exocytosis, endocytosis, and mitochondrial fission<sup>47,50,55,156,157</sup>. We find that mitochondrial depolarization leads to near complete relocalization of RalA to mitochondrial membranes that, like Parkin, depends on clathrin and AP2 (Figures 2.6B to 2.6E, 2.8A to 2.8D and Appendix E). In addition, Parkin recruitment to, or retention at, depolarized mitochondria is impaired in the absence of RalA.

It is clear that inhibition of RalA leads to defects in Parkin accumulation following mitochondrial depolarization. Because Ral function was previously implicated in endocytosis<sup>46,50</sup>, it is tempting to speculate that the defect in Parkin recruitment we observe is due to impaired endocytosis in the absence of RalA. We tested this hypothesis by analyzing the internalization of a variety of known endocytic cargoes, including Cholera Toxin Subunit B (Appendix F), but did not observe an obvious defect in the absence of RalA. It is plausible that RalA regulates endocytic trafficking of a cargo we did not measure or that our experimental setup did not provide the resolution to detect a partial phenotype. However, these data suggest RalA promotes Parkin accumulation at mitochondrial membranes through an alternative mechanism. For example, both RalA and Parkin may localize to depolarized mitochondria independently in a CME-dependent fashion, and then RalA promotes Parkin persistence or stability at the OMM.

Either of the two models described above would be consistent with a partial loss of Parkin recruitment even in the complete absence of RalA. In the first model, RalA would presumably affect only a subset of endocytic events, thus allowing some amount of Parkin to reach mitochondrial membranes through the remaining Ral-independent endocytosis. In the second model, Parkin localization would primarily be regulated through well-described direct interactions with phospho-ubiquitin and RalA would therefore play only an accessory role.

The regulation of mitophagy and the clearance of damaged mitochondria have important implications for a number of diseases, including neurodegeneration and cancer. Our work provides new insight into the mechanisms through which Parkin accumulates at depolarized mitochondria and for the first time, suggests that endocytic trafficking, rather than simple diffusion, is required for Parkin recruitment to the outer membrane of depolarized mitochondria. Intriguingly, PINK1 and Parkin are just two of a number of proteins whose genes are mutated in familial Parkinson's disease, and several of the other known genes, including Synj1, GAK, and LRRK2 have well defined roles in endocytosis or endocytic trafficking<sup>122-124,158-161</sup>. It will be interesting to test whether mutation or deletion of any of these other genes affects Parkin recruitment and whether defective PINK1-Parkin mitophagy may underlie more cases of familial Parkinson's disease than previously appreciated.

Finally, this work provides another example of RalA functioning at mitochondria and may provide additional hints into why RalA is important for Ras-driven cancers. It is becoming increasingly clear that mitochondrial function and

mitochondrial dynamics play important roles downstream of oncogenic Ras, and these data provide an additional link between Ras and the machinery that regulates mitochondrial function. Notably, several studies observed increased mitophagy in Ras-driven cancer cells and showed that mitophagy inhibition can block tumorigenic growth<sup>162,163</sup>. It will be interesting to explore whether RalA mediates mitophagy given the defect in Parkin recruitment if so, to determine whether loss of mitophagy explains the loss of tumor growth in the absence of RalA.

### **Future Directions**

It remains unclear whether the partial defect in Parkin recruitment in shRalA or RalA KO cells is due to RalA playing an accessory role in endocytosis or if RalA facilitates Parkin recruitment through an alternative mechanism. Perhaps RalB also mediates Parkin recruitment, which could account for the partial defect observed in shRalA and RalA KO cells. Future work should seek to address this question. Although we examined numerous endocytic cargoes in shRalA or RalA KO cells to determine if RalA depletion results in impaired endocytosis, we were only able to observe an impairment if that defect was obvious like what we observe with transferrin uptake in the presence of Pisp2 (Figure 2.6A). We should revisit these experiments using fluorescently tagged transferrin (or other fluorescent endocytic cargoes) and quantify transferrin uptake through flow cytometry, which enables robust quantification. We previously used this method to quantify transferrin uptake in shAP50 HeLa cells with great success (Figure 2.7C).

If loss of RalA does not result in an endocytic defect then RalA may regulate persistence or retention of Parkin at the OMM. To test this, we would depolarize HeLas or MEFs that stably express mCherry-Parkin and after 1 hour of inducing mitochondrial depolarization, treat cells with the Ral inhibitor, BQU57 for 2 hours (Appendix C). If BQU57 treatment results in decreased mitochondrial Parkin then this would suggest that RalA regulates retention or persistence of Parkin at the OMM. We previously found that RalA relocalization to depolarized mitochondria is independent of RalA-GTP loading status, so BQU57 should not impair RalA recruitment (Figures 2.4A to 2.4F).

Alternatively, it is possible that RalA may regulate persistence or retention of Parkin at the OMM through affecting PINK1 stabilization. We have not determined whether PINK1 stabilization is altered in shRalA HeLa cells or RalA KO MEFs. An impairment or delay in PINK1 stabilization could account for the observed Parkin recruitment defect that occurs in RalA knockdown or RalA KO cells. To address this, we would depolarize shScramble and shRalA HeLa cells and RalA FL/FL and RalA KO MEFs stably expressing mCherry-Parkin and perform immunoblotting to examine PINK1 stabilization over a period of 8 hours. If we observe a delay in PINK1 stabilization compared to control cells then this would explain the impairment in Parkin recruitment in the absence of RalA. Conversely, if loss of RalA does not impair PINK1 stabilization, then decreased Parkin recruitment is due to another mechanism.

In addition to studying the effect of RalA depletion on endocytosis, PINK1 stabilization and Parkin retention at the OMM, future work should also include

quantification of endocytosis in response to mitochondrial depolarization. In our current model, we hypothesize that mitochondrial depolarization results in upregulation of endocytosis through an increase in calcium release, which then facilitates both RalA and Parkin recruitment to mitochondria. To test this, we would quantify endocytosis in HeLa cells that stably express mCherry-Parkin in the presence and absence of mitochondrial depolarization through flow cytometric analysis of fluorescent transferrin uptake. We anticipate that depolarized cells would exhibit increased transferrin uptake, reflecting upregulation of endocytosis. Additionally, we would measure cytosolic calcium levels in the presence and absence of mitochondrial depolarization using the calcium indicator dye, Fura-2 AM. We predict that increased cytosolic calcium levels will correspond with upregulation of endocytosis.

If we do not observe upregulation of endocytosis following mitochondrial depolarization this does not negate our model of Parkin and RalA relocalization occurring in a CME-dependent process. Endocytosis occurs basally in cells. Therefore, perhaps endocytosis is not upregulated following mitochondrial depolarization. Instead, depolarization may induce post-translational modifications of certain proteins, which then facilitate association of Parkin and RalA with endosomes. Although we see RalA and Parkin in proximity with both Rab5 and Rab7 (Figures 3.10A, 3.10B, 3.11A and 3.12B), we do not know how RalA and Parkin associate with endosomes.

Additionally, colocalization of RalA and Parkin with Rab5 and Rab7 is not evidence that RalA and Parkin interact with endosomes. Consequently, we must

directly examine RalA and Parkin interactions with endosomes through a biochemical readout. To test this, we would purify endosomes from HeLa cells stably expressing Parkin and perform immunoblotting to detect Parkin and RalA levels at endosomes in the absence and presence of mitochondrial depolarization. We anticipate that we would detect an increase in RalA and Parkin levels at endosomes in response to mitochondrial depolarization. It seems unlikely that Parkin and RalA do not interact with endosomes given our Pistop 2 and shAP50 data, which suggests a role for CME in facilitating Parkin and RalA recruitment. However, if we are unable to detect Parkin and RalA at endosomes then we would need to reconsider how CME facilitates Parkin and RalA recruitment. For example, it may be that CME brings other proteins to Parkin and RalA, which then facilitate their relocation. This would mean that CME indirectly mediates Parkin and RalA relocation to depolarized mitochondria.

Our finding that CME facilitates both Parkin and RalA relocation to depolarized mitochondria raises a number of unanswered questions. It is important that we further understand the mechanism behind CME participation in RalA and Parkin relocation especially given that our work differs from the current dogma of Parkin recruitment. Additionally, further elucidating how the PINK1-Parkin pathway is regulated may provide additional insight into various neurodegenerative disorders including Parkinson's disease.

## **Materials and Methods**

### **Chemicals**

Carbonyl cyanidem-3-chlorophenylhydrazone (CCCP) was obtained from Calbiochem. Antimycin A and oligomycin were obtained from Sigma-Aldrich. Valinomycin was obtained from Thermo Fisher Scientific. HeLa cells were treated with 10  $\mu$ M oligomycin and 4  $\mu$ M antimycin A, 10  $\mu$ M valinomycin or 10  $\mu$ M CCCP. MEFs were treated with 30  $\mu$ M CCCP. Pitstop<sup>®</sup> 2 was obtained from Abcam and used at 20  $\mu$ M. Cholera Toxin Subunit B-Alexa Fluor 488 was obtained from Invitrogen<sup>™</sup> and used at 1  $\mu$ g/mL.

### **Cell Culture**

HeLa cells and MEFs were maintained in Dulbecco's Modified Eagle Medium (DMEM – Life Technologies) supplemented with 10% Fetal Bovine Serum (FBS – Life Technologies) and 1% Penicillin-Streptomycin (Gibco). HeLa cells were obtained from the ATTC. RalA FL/FL MEFs were a generous gift from Chris Counter's lab at Duke University School of Medicine. HeLa cells and MEFs stably expressing mCherry-Parkin were generated using a retroviral system and selected using 2.5  $\mu$ g/mL or 10  $\mu$ g/mL blasticidin, respectively. shScramble, shRalA and shAP50 HeLa cells were generated using a retroviral system and selected using 1  $\mu$ g/mL puromycin. shRalB HeLa cells were also generated using a retroviral system and selected using 500  $\mu$ g/mL neomycin. RalA KO MEFs were generated by infecting 200,000 RalA FL/FL MEFs with adeno-Cre-GFP (UNC Vector Core) for 24 hours with an MOI of 1000. RalA KO MEFs were then FACS sorted based on GFP expression to isolate single clones. MEFs were sorted using Basic Sorting Buffer (25 mM HEPES, 1

mM EDTA, 1% FBS, 1X PBS) into 96-well plates containing 100  $\mu$ l per well of pre-warmed DMEM.

### **Transfection/immunocytochemistry**

30,000 HeLa cells were seeded onto glass microslides (VWR) and transfected 2 days later with the indicated constructs using FuGENE<sup>®</sup> 6 (Promega). 24 hours post-transfection cells were treated as described with either CCCP or OA and fixed with 4% formaldehyde/PBS for 5 minutes at room temperature. Cells were mounted either with Prolong<sup>®</sup> Diamond Antifade Mountant with DAPI (Life Technologies) or Prolong<sup>®</sup> Diamond Antifade Mountant (Life Technologies). For immunocytochemistry, cells were permeabilized with 0.25% Triton<sup>®</sup> -X-100/PBS for 5 minutes at room temperature. Cells were stained with primary rabbit polyclonal TOM20 (ref. 11415, Santa Cruz Biotechnology, Inc., 1:400) overnight followed by  $\alpha$ -rabbit Alexa-488 secondary antibody (Life Technologies, 1:400) for 30 minutes at room temperature.

### **RNA interference and Constructs**

Oligonucleotides designed to generate short hairpin RNAs (shRNA) targeting the  $\mu$ 2 subunit of AP2 (aka AP50) (5'-GTGGATGCCTTTCGGGTCA-3')<sup>149</sup> were cloned into pSUPER.retro.puro (OligoEngine, Inc.). pSUPER.retro.puro.RalA (shRala--1: 5'-AAGACAGGTTTCTGTAGAAGA-3'; shRala-2: 5'-AACAGAGCTGAGCAGTGGAAT-3') and pSUPER.retro.puro.RalB (5'-GGTGATCATGGTTGGCAGC-3') were described previously<sup>11</sup>. HeLa cells were transiently transfected with FuGENE<sup>®</sup> 6 (Promega)

using 500 ng or 250 ng of the indicated fluorescent constructs: pEGFP-C1-RalA, pECFP-C1-RalA, mCherry-Parkin, mito-YFP, mito-BFP, pEGFP-Rab7 or pEGFP-Rab5. pEGFP-Rab7 and pEGFP-Rab5 were gifts from Marino Zerial's lab. mCherry-Parkin was a gift from Richard Youle (Addgene plasmid # 23956). mCherry-Parkin was cloned into pWZL-blasti using the In-Fusion® HD Cloning Kit (Clontech Laboratories, Inc.) mito-BFP was a gift from Gia Voeltz (Addgene plasmid # 49151). mito-BFP was cloned into pBABE-puro (Millenium Pharmaceuticals) using XhoI and EcoR1. A Kozak sequence and EcoR1 site was introduced into mito-BFP using site-directed mutagenesis (Forward primer: 5'-TGCAGTCTCGAGGCCGCCACCATGCTTTCACTACGTCAA-3' and Reverse primer: 5'-GCTGACGAATTCTCAATTAAGCTTGTGCCC-3'). mito-YFP was cloned into pBABE-neo using Sall and EcoRI. pBABE-neo was a gift from Hartmut Land & Jay Morgenstern & Bob Weinberg (Addgene plasmid #1767). All stable cell lines were generated using the retroviral packaging vector, pCL-10A1 from Imgenex.

### **Western Blotting**

Whole cell lysates were prepared in RIPA buffer with protease inhibitors (2 µg/mL Aprotinin, 2 µg/mL Leupeptin, 1 mM PMSF, 1 mM Na<sub>3</sub>VO<sub>4</sub> and 50 mM NaF) and equivalent protein amounts (generally 50 or 100 µg) were resolved by SDS-Page. Gels were transferred to PVDF membranes (Immobilin®-P) and immunoblotted with the following antibodies: mouse monoclonal α-Parkin (ref. 322282, Santa Cruz Biotechnology, Inc., 1:500), mouse monoclonal α-RalA (ref. 610221, BD Transduction Laboratories, 1:1000), rabbit monoclonal α-GAPDH (Cell

Signaling Technologies, #5174), mouse monoclonal  $\alpha$ -OPA1 (ref. 612606, BS Transduction Laboratories, 1:1000), mouse monoclonal  $\alpha$ -PINK1 (ref. AM6406a, Abgent, 1:500), rabbit monoclonal  $\alpha$ - $\beta$ -actin (ref. 4970, Cell Signaling Technology, 1:2000), rabbit monoclonal  $\alpha$ - $\beta$ -tubulin (ref. 2128, Cell Signaling Technology, 1:2000), rabbit polyclonal  $\alpha$ -phospho-ubiquitin (Ser65) (ref. 37642, Cell Signaling Technology, 1:1000) and mouse monoclonal  $\alpha$ -RalB (ref. 04-037, Millipore Sigma, 1:500). Rabbit- or mouse-HRP secondary antibodies were used at 1:5000 (Jackson ImmunoResearch Laboratories, Inc.). Band pixel intensity was quantified by using ImageJ and bands were normalized to the indicated controls.

## **Pitstop 2 Experiments**

50,000 HeLa cells were plated onto #1.5 glass microslides. Two days later, cells were transfected with 500 ng each of the indicated constructs using a 1:1 ratio of FuGENE<sup>®</sup> 6 (Promega) to DNA. 24 hours post-transfection, cells were washed twice with 1X PBS and pre-treated with either DMSO or 20  $\mu$ M Pitstop<sup>®</sup> 2 in serum-free DMEM supplemented with 10 mM HEPES for 15 minutes at 37°C. Following the 15 minute pre-treatment, cells were treated with one of the following ways for 1 hour at 37°C: 1. DMSO, 2. 10  $\mu$ M oligomycin and 4  $\mu$ M antimycin A, 3. 20  $\mu$ M Pitstop 2 or 4. 20  $\mu$ M Pitstop 2, 10  $\mu$ M oligomycin and 4  $\mu$ M antimycin A. Cells were then washed twice with 1X PBS and fixed with 4% formaldehyde/PBS for 5 minutes at room temperature. For image analysis, over 50 cells were counted per treatment to examine Parkin colocalization with the mitochondria (n=3).

## **Confocal Microscopy**

Fixed cells were mounted onto #1.5 glass microslides (VWR) and imaged on a Zeiss LSM 710 confocal microscope using the 63X oil objective. Single color controls were tested to assess bleedover. For quantification of Parkin recruitment HeLa cells, 20 random views were scored for Parkin colocalization with the mitochondria. Pearson's coefficients for Parkin and mitochondria (or RalA) colocalization were calculated using the Coloc2 plugin in ImageJ. To do this, images were split into 2 channels and a rolling ball radius of 50 pixels was subtracted from each channel. An ROI was drawn on the mitochondria and a PSF of 10 was used.

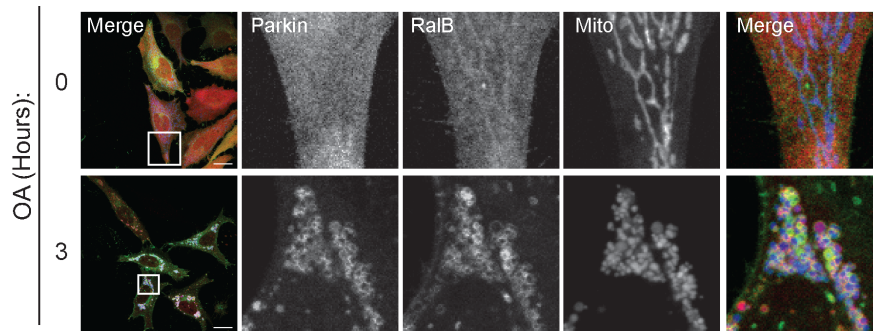
## **Imaging Flow Cytometry:**

8 million stably expressing mCherry-Parkin and mito-YFP shScram and shRalA HeLa cells were treated with 10  $\mu$ M oligomycin and 4  $\mu$ M antimycin A for 0, 1, and 3 hours. Following OA treatment, the cells were washed twice with 10 mL of PBS and dissociated with 2 mL of trypsin. The cells were collected with 10 mL of PBS and spun at 1,000 rpm for 5 minutes. The cells were then resuspended in 4 mL of PBS and gently filtered through 100  $\mu$ M filter mesh (Genessee) into 4 mL of 4% formaldehyde/PBS, so that the final concentration of the solution was 2% formaldehyde/PBS. The cells were allowed to fix at room temperature for 10 minutes with intermittent agitation. Following fixation, the cells were spun at 2,000 rpm for 5 minutes. The cells were resuspended in 8 mL of PBS and spun at 2,000 rpm for 5 minutes and resuspended in 1 mL of DAPI (1  $\mu$ g/mL, Thermo Fisher Scientific) in 0.1% Triton-X-100/PBS. The cells were spun one last time at 2,000

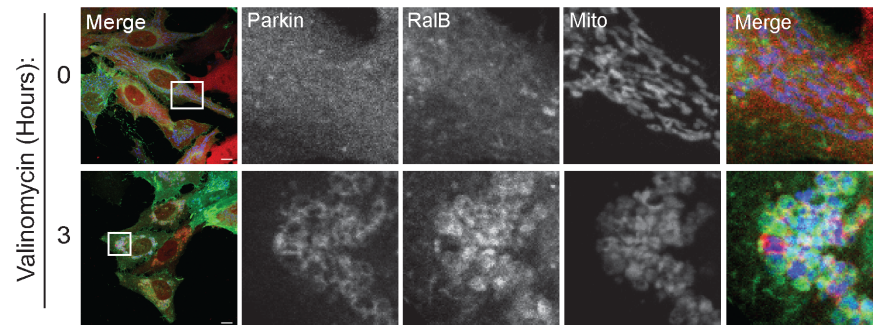
rpm for 5 minutes and resuspended in 80-100  $\mu$ l of DAPI/0.1% Triton-X-100/PBS. 8 million stably expressing mCherry-Parkin cells or mito-YFP and DAPI stained cells were used as compensation controls. The cells were stored in the dark at 4°C until they were run on the ISX MKII system. A 561 nm laser (xmW) was used to excite the mCherry and the emission detected in Channel 4 with a 595-640 nm band pass. YFP was excited with a 488 nm (xmW) and the emission detected in Channel 2 with a 480-560 nm band pass. Most samples were run until 10,000 events were collected or if the samples were running slowly then they were allowed to run to collect as many events as possible within 20 minutes. Using IDEAS software (ver. 6.2), an eroded mask of the YFP image (Ch02-mitochondria) was created and used to quantify the degree of Parkin colocalized with the mitochondria. A modified Pearson's correlation coefficient was used to determine the degree of similarity between the mCherry-Parkin (Ch04) and mito-YFP (Ch02) fluorescent images, indicating colocalization.

## Figures

A.



B.



C.

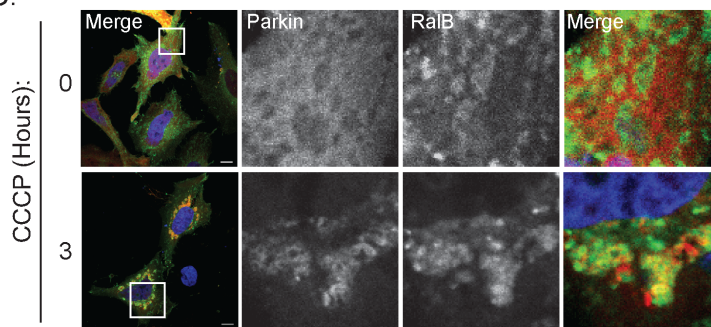


**Figure 3.1.** RalB and Parkin relocate in response to OA, Valinomycin and CCCP. (A) HeLa cells stably expressing mCherry-Parkin and transiently expressing mito-BFP and GFP-RalB were treated with 10  $\mu$ M oligomycin and 4  $\mu$ M antimycin A (OA) over 3 hours and imaged with confocal microscopy (Scale bars = 20  $\mu$ M). White boxes indicate magnified sections. (B) HeLa cells stably expressing mCherry-Parkin and transiently expressing mito-BFP and GFP-RalB were treated with 10  $\mu$ M valinomycin for 3 hours and imaged with confocal microscopy (Scale bars = 10  $\mu$ M). (C) HeLa cells transiently expressing mCherry-Parkin and GFP-RalB were treated with 10  $\mu$ M CCCP for 3 hours and imaged with confocal microscopy (Scale bars = 10  $\mu$ M).

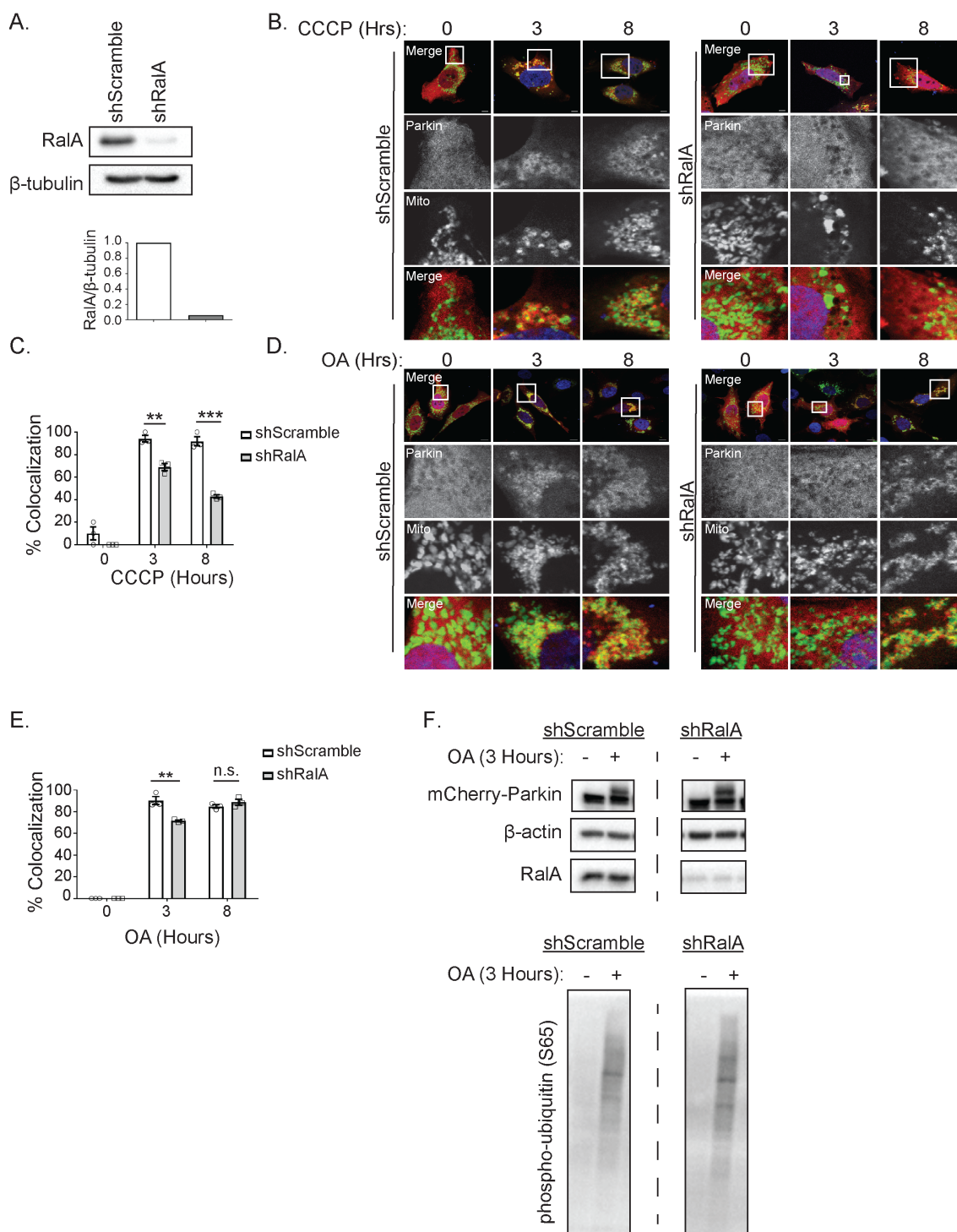


**Figure 3.2.** Genetic inhibition of RalA results in impaired Parkin recruitment following mitochondrial depolarization. (A) Immunoblot analysis of RalA in HeLa cells stably expressing the indicated shRNA constructs. RalA levels were quantified and normalized to  $\beta$ -tubulin. (B) shScramble and shRalA HeLa cells transiently expressing mCherry-Parkin and mito-YFP were treated with 10  $\mu$ M CCCP over 8

hours and imaged by confocal microscopy (Scale bars = 10  $\mu$ M). White boxes indicate magnified sections. (C) Parkin colocalization with mitochondria was assessed in the cells described in B for greater than 100 cells (Two-way ANOVA using Sidak's multiple comparisons test, mean  $\pm$  SEM, \*\*  $p \leq 0.005$ ,  $n = 3$ ). (D) shScramble and shRala HeLa cells transiently expressing mCherry-Parkin and mito-YFP were treated with 10  $\mu$ M oligomycin and 4  $\mu$ M antimycin A (OA) over 8 hours (Scale bars = 10  $\mu$ M). White boxes indicate magnified sections. (E) Parkin colocalization with mitochondria was assessed in cells described in C for greater than 100 cells (Two-way ANOVA using Bonferroni's multiple comparisons test, mean  $\pm$  SEM, \*\*  $p \leq 0.005$ ,  $n = 3$ , n.s. = not significant). (F) Immunoblot of the indicated proteins in stably expressing mCherry-Parkin shScramble and shRala HeLa cells were treated with 10  $\mu$ M oligomycin and 4  $\mu$ M antimycin A (OA) for 3 hours. Dashed lines represent cropped blots.

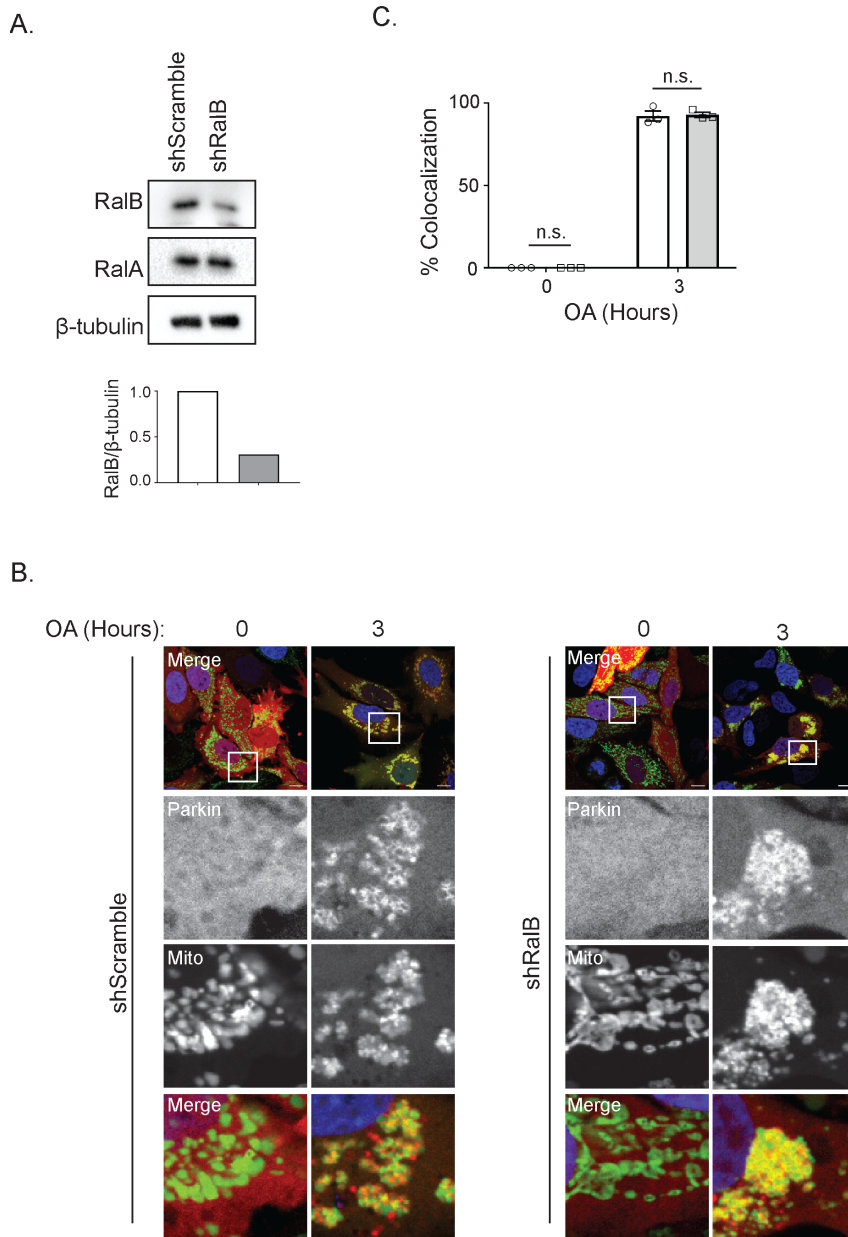


**Figure 3.3.** RalB knockdown does not affect Parkin recruitment following mitochondrial depolarization. (A) RalB and RalA levels were quantified by immunoblotting in the indicated cells. RalB levels were normalized to  $\beta$ -tubulin. (B) shScramble and shRalB HeLa cells transiently expressing mCherry-Parkin and mito-YFP were treated with 10  $\mu$ M oligomycin and 4  $\mu$ M antimycin A or DMSO (vehicle control) for 3 hours and imaged by confocal microscopy (Scale bars = 10  $\mu$ M). White boxes indicate magnified sections. (C) Quantification of B. Percentage of cells that exhibit Parkin recruitment to mitochondria in shScramble or shRalB HeLa cells (20 random views, Two-way ANOVA using Sidak's multiple comparisons test, mean  $\pm$  SEM, n.s. = not statistically significant, n = 3).





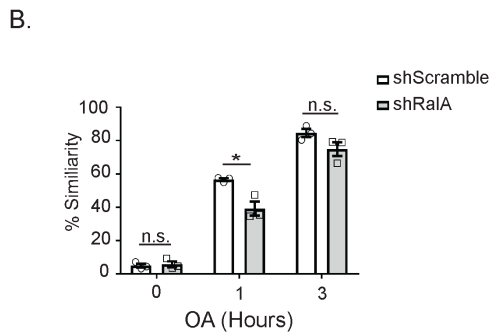
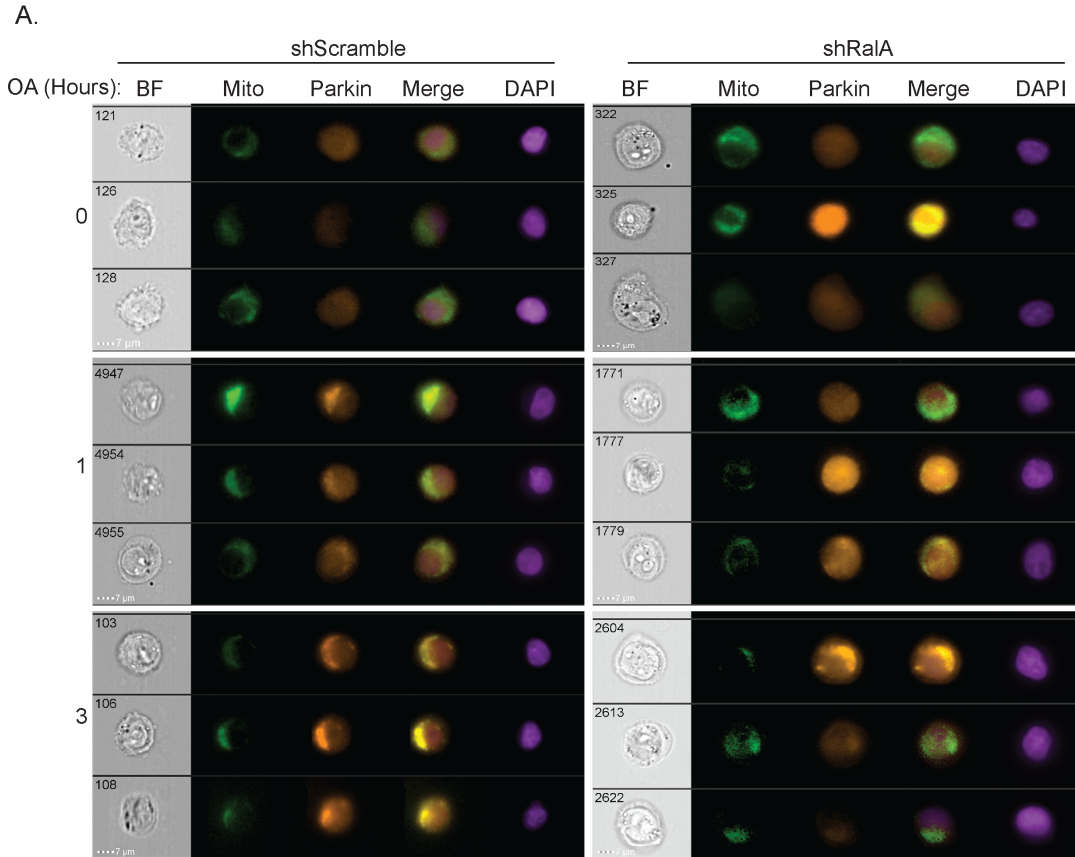


**Figure 3.6.** Imaging flow cytometry confirms that shRalA HeLa cells exhibit impaired Parkin recruitment. (A) shScramble and shRalA HeLa cells stably expressing mCherry-Parkin and mito-YFP were treated with 10  $\mu$ M oligomycin and 4  $\mu$ M antimycin A (OA) or DMSO (vehicle control) over 3 hours and imaged using confocal microscopy (BF = brightfield). (B) Quantification of percent total similarity between Parkin and mitochondria in the indicated cells in A (Two-way ANOVA using Sidak's multiple comparisons test, mean  $\pm$  SEM, \* $p \leq 0.01$ , n.s. = not statistically significant,  $n = 3$ ).

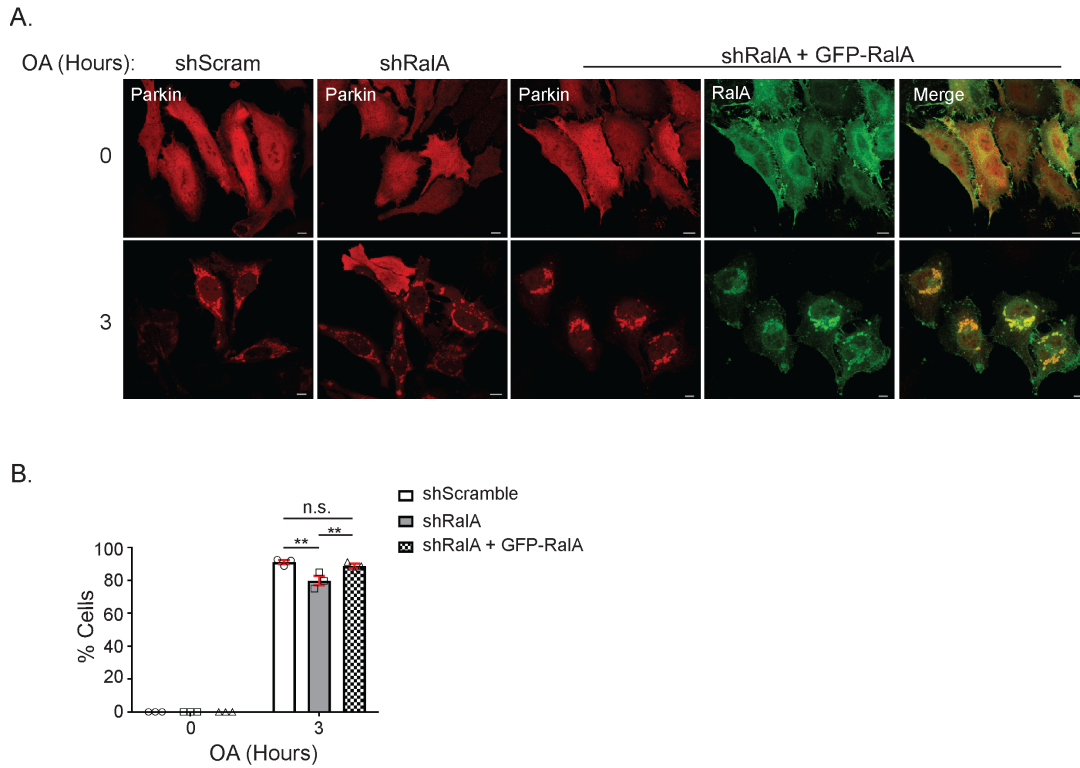


**Figure 3.7.** Expression of GFP-RalA rescues Parkin recruitment in shRala HeLa cells. (A) HeLa cells stably expressing the indicated shRNA constructs and transiently expressing mCherry-Parkin and shRNA-resistant GFP-RalA were imaged by confocal microscopy (Scale bars = 10  $\mu$ M). (B) The percentage of cells in A exhibiting Parkin puncta following 3 hours of OA treatment was calculated for shScramble and shRala HeLa cells and quantified in 20 random views (Two-way ANOVA using Tukey's multiple comparisons test, mean  $\pm$  SEM, \*\*p  $\leq$  0.001, n.s. = not statistically significant, n = 3).

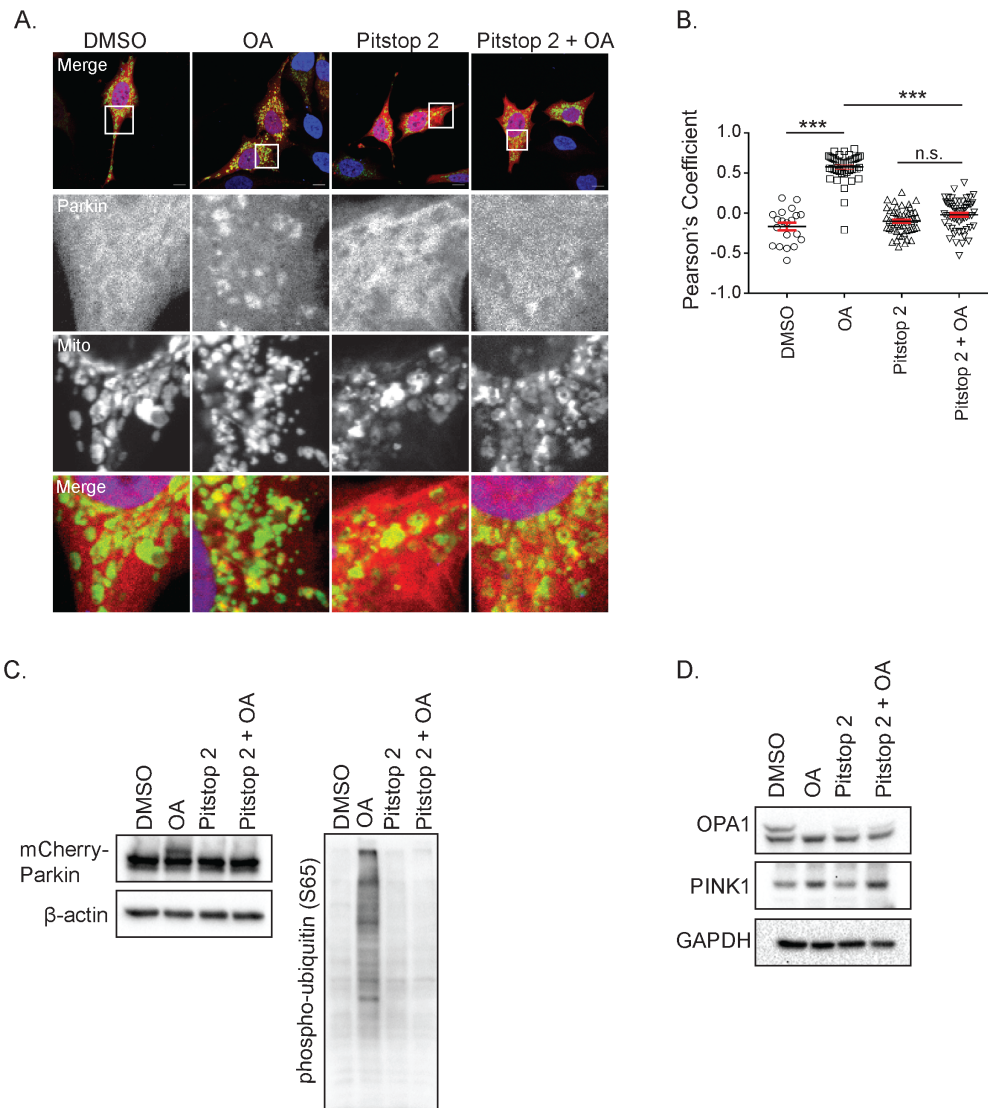
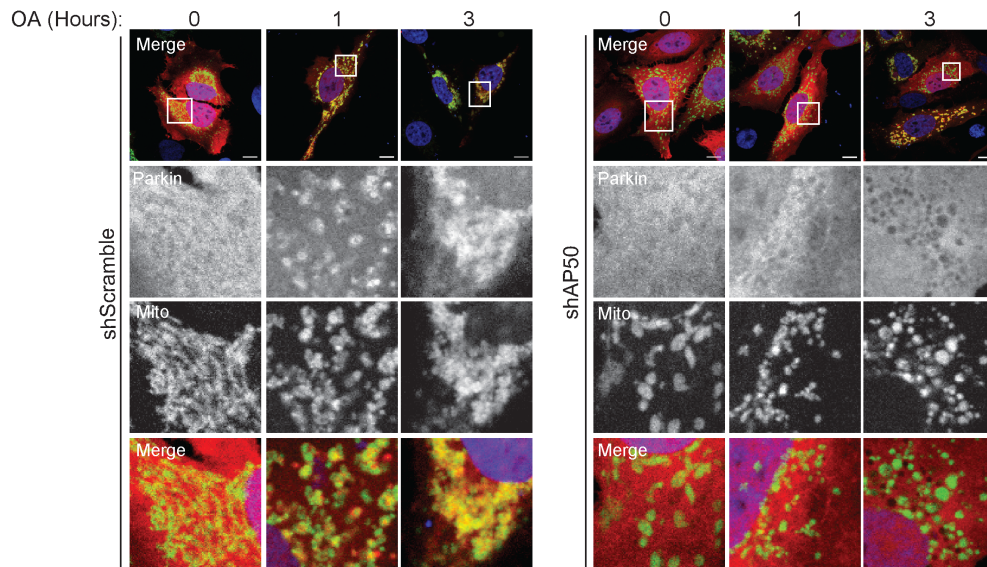


**Figure 3.8.** Clathrin-mediated endocytosis facilitates Parkin recruitment to depolarized mitochondria. (A) HeLa cells transiently expressing mito-YFP and mCherry-Parkin were pre-treated for 15 minutes either with DMSO or 20  $\mu$ M Pitstop 2 then treated for 1 hour with Pitstop 2 and/or 10  $\mu$ M oligomycin and 4  $\mu$ M antimycin A as indicated and imaged by confocal microscopy (Scale bars = 10  $\mu$ m). White boxes indicate magnified sections. (B) Quantification Parkin recruitment to the mitochondria in the cells described in A using Pearson's coefficients (One-way ANOVA using Tukey's multiple comparisons test, mean  $\pm$  SEM, \*\*\*p  $\leq$  0.0001, n.s. = not significant, n = 3). Each dot represents one cell. (C) Immunoblot analysis of mCherry-Parkin and phospho-ubiquitin (Ser65) in stably expressing mCherry-Parkin HeLa cells. Cells were pre-treated with 20  $\mu$ M Pitstop 2 or DMSO for 15 minutes and then treated with DMSO, 10  $\mu$ M oligomycin and 4  $\mu$ M antimycin A (OA), 20  $\mu$ M Pitstop 2 or Pitstop 2 and OA for 1 hour.  $\beta$ -actin was used as a loading control. (D) Immunoblot analysis of PINK1 in HeLa cells stably expressing mCherry-Parkin treated as in C. GAPDH was used as a loading control.

A.



B.

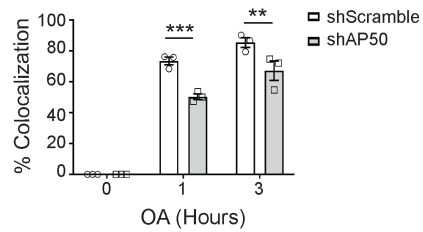
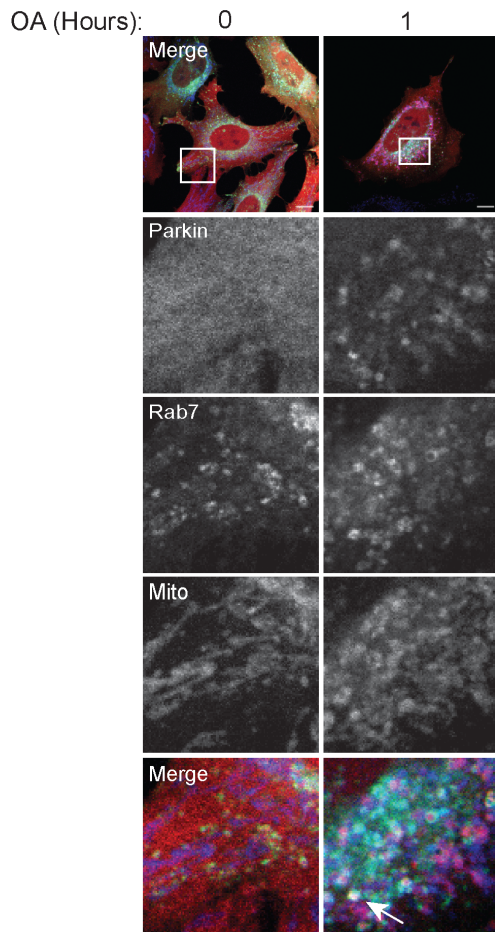


**Figure 3.9.** shAP50 cells exhibit impaired Parkin recruitment to depolarized mitochondria. (A) shScramble and shAP50 HeLa cells transiently expressing mito-YFP and mCherry-Parkin were treated with 10  $\mu$ M oligomycin and 4  $\mu$ M antimycin A for 3 hours and imaged by confocal microscopy (Scale bars = 10  $\mu$ M). White boxes indicate magnified sections. (B) Quantification of the percentage of cells that exhibit Parkin recruitment to the mitochondria in A (20 random views, Two-way ANOVA using Sidak's multiple comparisons test, mean  $\pm$  SEM, \*\*\* $p \leq 0.001$ , \*\* $p \leq 0.01$ ,  $n = 3$ ).

A.



B.

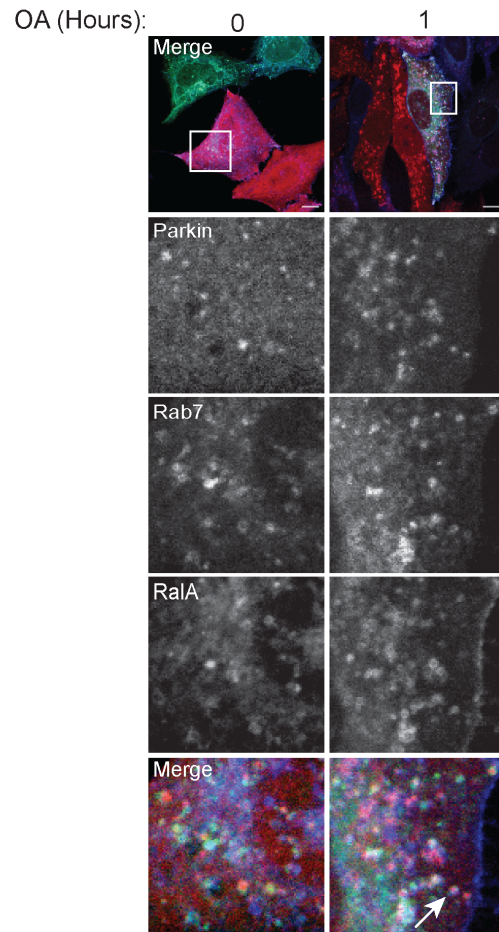


**Figure 3.10.** Rab7 colocalizes with mitochondria, RalA and Parkin following mitochondrial depolarization. (A) Stably expressing mito-BFP HeLa cells that transiently express mCherry-Parkin and GFP-Rab7 were treated with 10  $\mu$ M oligomycin and 4  $\mu$ M antimycin A (OA) for 1 hour. DMSO was used as a vehicle control. Cells were imaged with confocal microscopy (Scale bars = 10  $\mu$ M). White boxes indicate magnified sections. Arrow indicates a ring-like structure of GFP-Rab7 that is colocalized with mCherry-Parkin and mito-BFP. (B) Stably expressing mCherry-Parkin HeLa cells that transiently express GFP-Rab7 and CFP-RalA were treated as in A (Scale bars = 10  $\mu$ M). White boxes indicate magnified sections. Arrow indicates a ring-like structure of GFP-Rab7 that is colocalized with mCherry-Parkin and CFP-RalA.

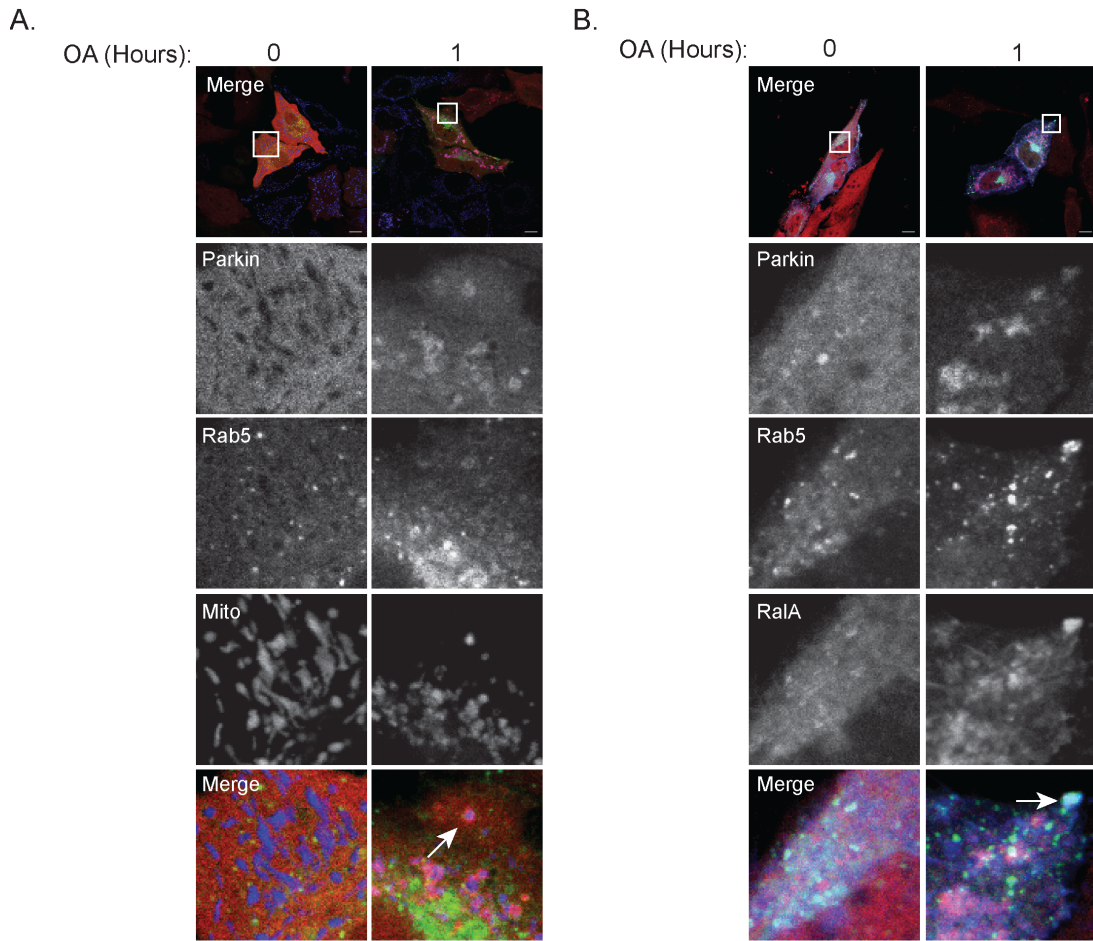


**Figure 3.11.** Rab5 is recruited to depolarized mitochondria with Parkin. (A) HeLa cells stably expressing mito-BFP and transiently expressing mCherry-Parkin and GFP-Rab5 were treated with 10  $\mu$ M oligomycin and 4  $\mu$ M antimycin A (OA) for 1 hour. DMSO was used as a vehicle control. Cells were imaged with confocal microscopy (Scale bars = 10  $\mu$ M). White boxes indicate magnified sections. Arrow indicates a ring-like structure of GFP-Rab5 that is colocalized with mCherry-Parkin and mito-BFP. (B) HeLa cells stably expressing mCherry-Parkin and transiently expressing GFP-Rab5 and CFP-RalA were treated as in A. Cells were imaged with confocal microscopy (Scale bars = 10  $\mu$ M). White boxes indicate magnified sections. Arrow indicates GFP-Rab5 colocalized with mCherry-Parkin and CFP-RalA.

## Chapter Four: Conclusions

Our findings demonstrate a novel role for both RalA and RalB in response to mitochondrial depolarization. We find that Ral proteins are recruited to depolarized mitochondria in a clathrin-dependent process as pharmacologic and genetic inhibition of CME impairs both RalA and RalB relocalization (Figures 2.6B to 2.6E and 2.8A to 2.8D). Previous studies have linked Ral with endocytosis<sup>50,164</sup>, but ours is the first to suggest a link between endocytosis and Ral trafficking.

Discovering that CME may facilitate Ral localization has implications for understanding additional cellular processes. For instance, Ral promotes the internalization of the Wnt pathway receptor complex to activate canonical Wnt signaling<sup>165</sup>. During Wnt signaling, Wnt ligands bind Frizzled and LRP receptor complexes, which destabilize the  $\beta$ -catenin destruction complex that contains various proteins such as APC. In the absence of the  $\beta$ -catenin destruction complex,  $\beta$ -catenin accumulates in the cytosol and translocates into the nucleus where it functions as a transcription factor.

However, it is unclear exactly how Ral signals through endocytosis to internalize the Wnt pathway receptor. Ral proteins are also required for intestinal stem cell proliferation following intestinal damage<sup>165</sup>. This finding begs the question, "Does endocytosis mediate a role for Ral in colorectal cancer?" A previous study demonstrated that RalA is required for colorectal cancer growth and is active in various colon cancer cell lines<sup>33</sup>. Perhaps aberrant RalA activation contributes to colorectal cancer progression by increased internalization of the Wnt pathway

receptor, thereby activating Wnt signaling. In support of this idea, the majority of colorectal cancers exhibit hyperactivated Wnt signaling <sup>166</sup>.

To test if RalA activates Wnt signaling to drive colorectal cancer, we could perform experiments using a mouse model of colorectal cancer. We would inducibly express RalA in the intestine and study if RalA overexpression results in accelerated tumor growth. It was previously demonstrated that wildtype RalA overexpression is sufficient to induce intestinal stem cell proliferation <sup>165</sup>. We would also examine Wnt receptor internalization in tumor-derived cells from the mouse model to test if RalA overexpression increases Wnt receptor internalization, corresponding with possible increased tumor growth. Wnt receptor internalization can be examined by incubating cells with biotinylated Wnt receptors such as Frizzled-7. Understanding how RalA, endocytosis and cancer may collectively function together will likely further our understanding of colorectal cancer and potentially other cancers (i.e. medulloblastoma, bladder cancer, etc.) in which RalA is aberrantly active.

We find that RalA and RalB not only relocate to depolarized mitochondria through a clathrin-dependent process, but also inhibit TBK1 (Figures 2.9A and 2.9B). Interestingly, HeLa cells depolarized with OA and treated with Pitstop 2 fail to exhibit increased TBK1 activity, indicating that CME is required for TBK1 activation (Figures 2.10A and 2.10B). Given that Pitstop 2 impairs Ral relocation in response to mitochondrial depolarization, this data further suggests Ral relocation mediates TBK1 activation. Furthermore, RalA and RalB inhibit TBK1 when they are in their GTP-bound form as Ral inhibition with BQU57 results in TBK1 activation (Figures 2.9E and 2.9F). Collectively, our data lends itself to a model

where RalA and RalB inhibit TBK1 and relocalization of Ral proteins releases this inhibition (Figure 2.10C).

TBK1 orchestrates either an inflammatory or autophagic response.

Autophagy and inflammation may be coordinated depending upon the severity of cellular stress and/or damage. Additionally, inflammation and autophagy are linked as immune responses often require autophagy to eliminate an identified target (i.e. foreign DNA). In the context of mitochondrial depolarization, it is likely that an autophagic response occurs rather than an inflammatory one because it is imperative that damaged mitochondria are removed. Consequently, RalA and RalB may basally inhibit TBK1 to prevent inappropriate activation of autophagy.

Additionally, basal inhibition of TBK1 can be a mechanism to aid a fast autophagic response. Perhaps basal inhibition of TBK1 allows it to be poised when needed following mitochondrial depolarization. Ral relocalization could then act as a quick release of TBK1 inhibition, prompting swift initiation of an autophagic response.

It remains to be determined exactly how TBK1 facilitates autophagy following mitochondrial depolarization if that is in fact the role that TBK1 plays. TBK1 previously has been shown to phosphorylate Rab7a, which recruits Atg9a to mitochondria and is required for mitochondrial clearance <sup>67</sup>. Given this finding, perhaps shRalA/RalB cells exhibit increased Rab7a phosphorylation and consequently, have increased mitophagy. We would use Phos-tag to determine if shRalA/RalB cells display elevated Rab7a phosphorylation levels compared to shScramble cells. Additionally, we anticipate that mitopreps of shRalA/RalB cells would indicate increased Atg9a at mitochondria compared to shScramble cells,

corresponding with the notion that Rab7a ultimately signals to Atg9a mediating mitophagy. Finally, we can quantify mitophagy rates in shScramble and shRalA/RalB HeLa cells by staining mitochondrial DNA and examining clearance over a timecourse. If shRalA/RalB cells exhibit increased mitochondrial clearance then this suggests that Ral proteins inhibit mitophagy possibly preventing unnecessary clearance. TBK1 also regulates autophagy through controlling autophagosome maturation and recruiting autophagy adaptors such as OPTN and NDP52 <sup>68,69</sup>. Consequently, there are multiple ways that TBK1 regulates autophagy and we have yet to determine how TBK1 affects autophagy in the context of mitochondrial depolarization and Ral signaling.

Although we speculate that TBK1 facilitates autophagy following mitochondrial depolarization, we cannot exclude the possibility that TBK1 regulates an inflammatory response. One study demonstrated that mitochondrial depolarization does not induce phosphorylation of IRF-3 thereby uncoupling an inflammatory response from depolarization <sup>68</sup>. However, we did not examine phosphorylation of TBK1-targeted interferon regulatory transcription factors (i.e. IRF-3 and IRF-7) to assess if TBK1 signals to the innate immune system following depolarization. Intriguingly, shRalA/RalB cells exhibit decreased STING levels (Figure 2.12A), which may indicate an inflammatory response. Following activation of the cGAS-STING pathway by cytosolic DNA, TBK1 phosphorylates IRF-3 to induce an innate immune response. However, TBK1 also phosphorylates p62, which mediates STING localization to autophagosomes to attenuate the inflammatory response <sup>147</sup>. Therefore, decreased STING levels may reflect the onset of an

inflammatory response given that decreased STING levels is a means by which the cell regulates the response. Alternatively, decreased STING levels may reflect Ral-regulated transcription of STING—independent of an inflammatory response.

Mutations in TBK1 are associated with neuroinflammatory diseases including Herpes Simplex Encephalitis (HSE), ALS and Normal Tension Glaucoma (NTG) <sup>167</sup>. Intriguingly, p62 and OPTN are linked to the pathogenesis of ALS, suggesting that aberrant autophagy may drive disease progression <sup>167</sup>. These findings implicate a potential relationship between, TBK1, inflammation and autophagy in neuroinflammatory diseases. Moreover, it will be important to determine Ral's role in neuroinflammatory diseases given that Ral inhibits TBK1. Discovering a potential role for RalA and RalB in neuroinflammatory diseases suggest that they could be therapeutic targets.

Ral proteins not only localize to depolarized mitochondria and inhibit TBK1, but RalA also mediates Parkin recruitment during PINK1-Parkin mitophagy (Figures 3.6A, 3.6B, 3.7A and 3.7B). We also find that CME regulates Parkin recruitment (Figures 3.8A, 3.8B, 3.9A and 3.9B). It is conceivable that we only observe a partial impairment in Parkin recruitment upon RalA knockdown or knockout because RalA plays an accessory role in endocytosis. Therefore, CME may serve as a driving force behind Parkin localization to depolarized mitochondria. Proposing that CME facilitates Parkin recruitment during mitophagy is in contrast with the current dogma in the PINK1-Parkin field. However, we are not suggesting that the current model of Parkin recruitment where PINK1 accumulates on the OMM and phosphorylates ubiquitin chains to promote Parkin recruitment is wrong. PINK1

accumulation and phosphorylated ubiquitin may work in combination with CME to regulate Parkin recruitment. The current model of Parkin recruitment is that Parkin passively diffuses throughout the cytosol and accumulates at the OMM when it encounters phosphorylated ubiquitin. However, we cannot distinguish between these two models based on current data in the literature.

Interestingly, patients with Parkinson's disease exhibit mutations in genes with endocytic roles including SYNJ1, GAK, DNAJC6 and LRRK2 <sup>113,123,159,168</sup>. Consequently, this makes sense in light of our finding that CME facilitates Parkin recruitment during PINK-Parkin mitophagy.

Our work has broader implications for better understanding the development of Parkinson's disease. Simple *in vitro* experiments can be performed to begin to assess the relationship of different endocytic proteins in facilitating Parkin localization. Single knockdowns of known endocytic genes that are mutated (i.e. SYNJ1, GAK, etc.) in Parkinson's disease can be introduced in HeLa cells that stably express mCherry-Parkin. Parkin recruitment in these cells can then be examined to determine if knockdown of commonly mutated endocytic genes results in impaired Parkin localization. Mutations in genes with endocytic functions in patients with Parkinson's disease is correlative, but does not demonstrate that these mutations are causative. Consequently, additional work is required to determine the *in vivo* requirement of CME for mediating Parkin recruitment.

Impaired mitophagy not only is associated with neurodegenerative disorders like Parkinson's disease, but also is linked to various human cancers <sup>169</sup>. Therefore, our work also has implications for understanding different types of cancers.

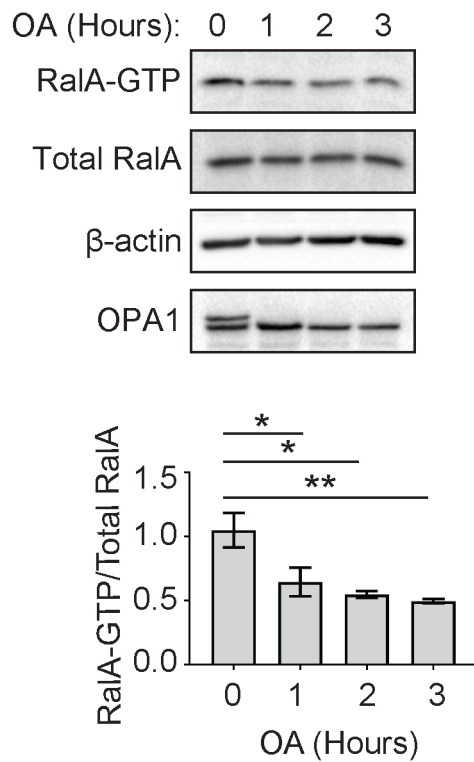
Autophagy traditionally is thought to act as a “double-edged sword” in cancer where depending on the specific type of cancer, it either promotes or prevents tumorigenesis. Similarly, the role for mitophagy in cancer is not well defined. It is believed that tumor cells may require mitophagy to manage levels of reactive oxygen species (ROS). Tumor cells already produce ROS and additional ROS from mitochondria may work synergistically to promote tumor cell death when mitophagy is impaired, enabling accumulation of dysfunctional mitochondria <sup>169</sup>. Additionally, Parkin knockout mice are susceptible to spontaneous hepatic tumors <sup>125</sup>. Parkin mutations occur in numerous cancers such as melanoma, colorectal cancer and gliomas, indicating that Parkin functions as a tumor suppressor <sup>125</sup>.

Both RalA and RalB previously have been linked to cancer <sup>11,37,38</sup>. Therefore, a major question that arises from our studies is “Does RalA contribute to tumorigenesis through its role in mediating PINK1-Parkin mitophagy?” Certainly, there is a lot of interest in targeting the Ras pathway as a potential treatment for numerous human cancers. If we can further identify a specific role for RalA in mediating tumorigenesis perhaps through its function in mitophagy then this may lead to new therapeutic treatments.

In conclusion, we have identified a novel role for RalA and RalB in response to mitochondrial depolarization. Ral proteins relocate to depolarized mitochondria in a clathrin-dependent process and inhibit TBK1. We also find that RalA and CME facilitate Parkin recruitment during PINK1-Parkin mitophagy. Our findings have important broader implications potentially for neurodegenerative diseases such as Parkinson’s disease and ALS as well as human cancers.

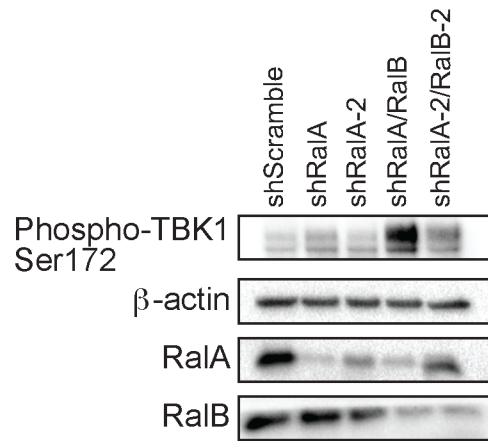
## APPENDIX

A.



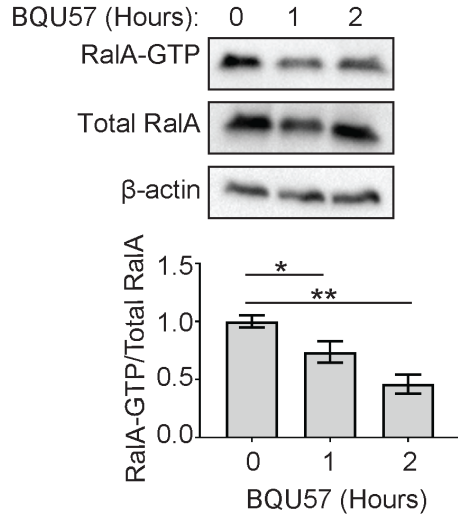
**Appendix A.** RalA-GTP levels remain decreased over 3 hours of OA treatment. (A) HeLa cells were treated with 10  $\mu$ M oligomycin and 4  $\mu$ M antimycin A (OA) for 3 hours and RalA-GTP levels were assessed by GST-RalBD pulldown. RalA-GTP levels were quantified and normalized to total RalA and then further normalized to the value for untreated cells (One-way ANOVA using Dunnett's multiple comparisons test, mean  $\pm$  SEM, \*p  $\leq$  0.05, \*\*p  $\leq$  0.01, n = 3).

A.

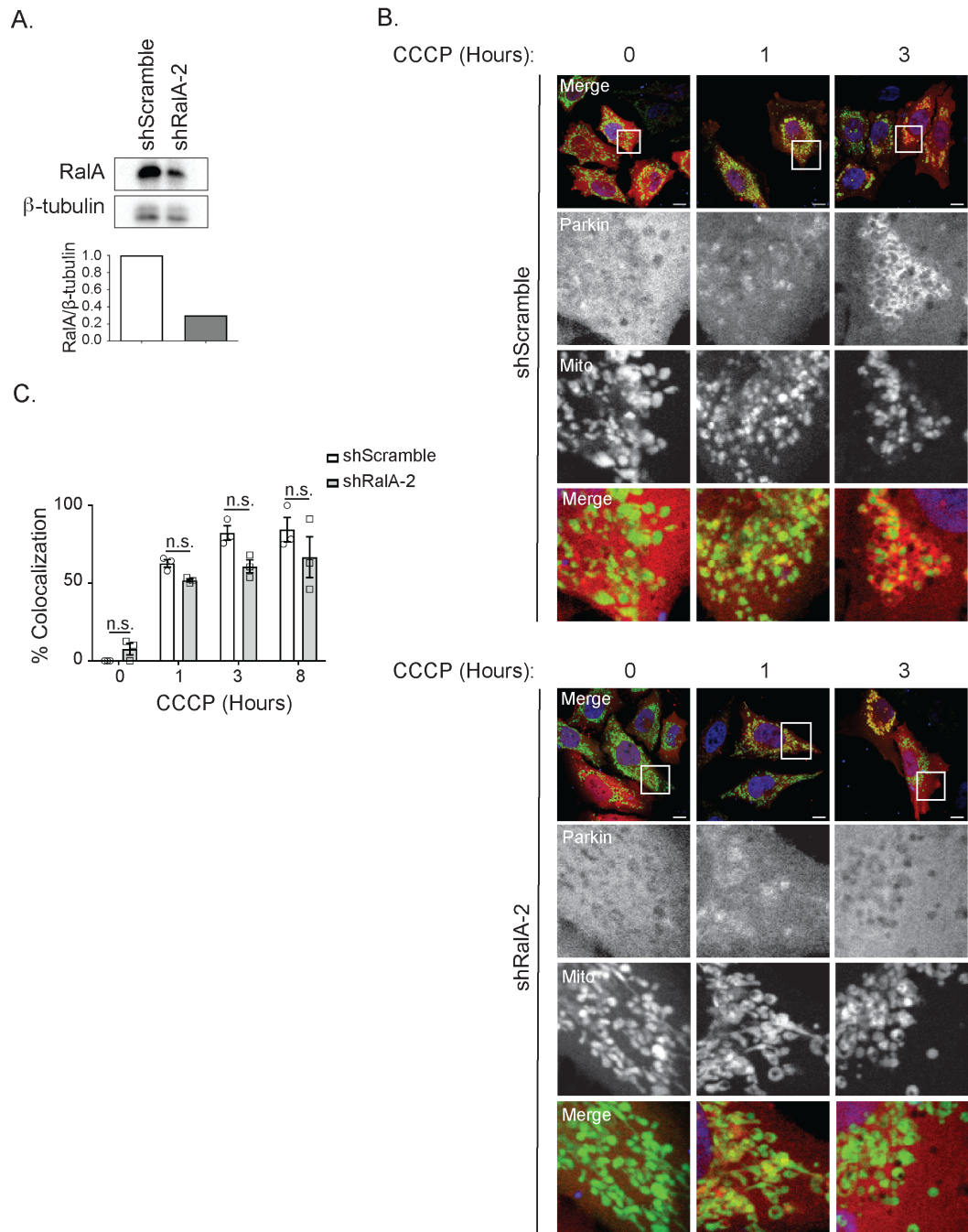


**Appendix B.** Alternate shRalA/RalB double knockdown HeLa cells exhibit increased TBK1 activity. (A) HeLa cells stably expressing the indicated shRNA constructs were immunoblotted for phospho-TBK1 Ser172,  $\beta$ -actin, RalA, and RalB.

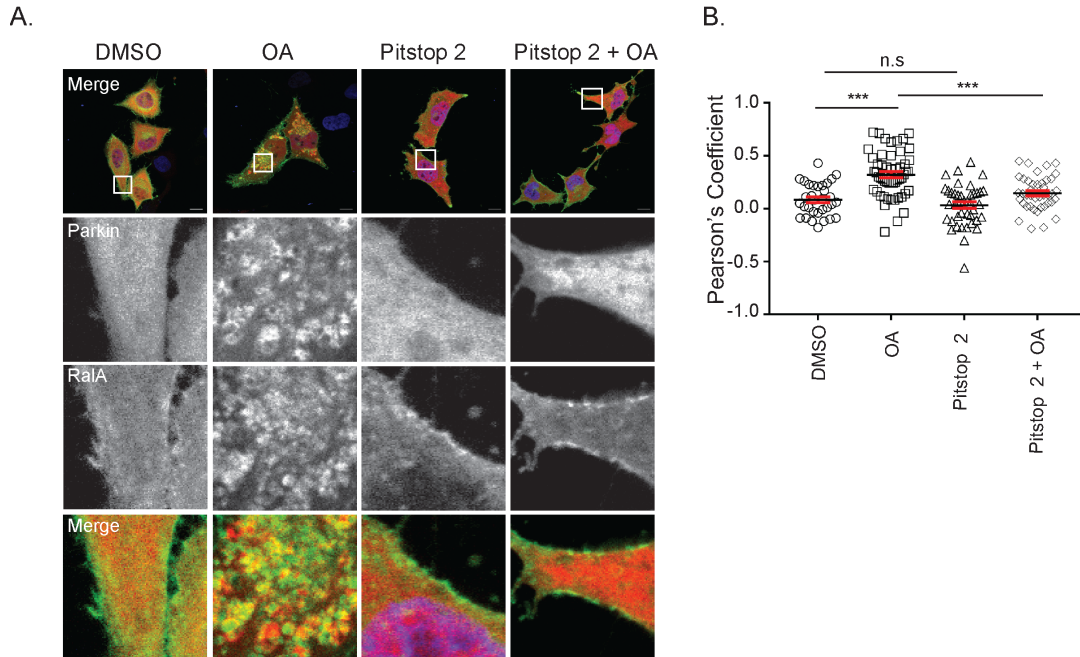
A.



**Appendix C.** BQU57 decreases RalA-GTP loading. (A) HeLa cells were treated with 50  $\mu$ M BQU57 for 2 hours and RalA-GTP levels were assessed by GST-RalBD pulldown. RalA-GTP levels were quantified, normalized to total RalA and then further normalized to the value for untreated cells (One-way ANOVA using Dunnett's multiple comparisons test, mean  $\pm$  SEM, \*p  $\leq$  0.05, \*\*p  $\leq$  0.001, n =3).

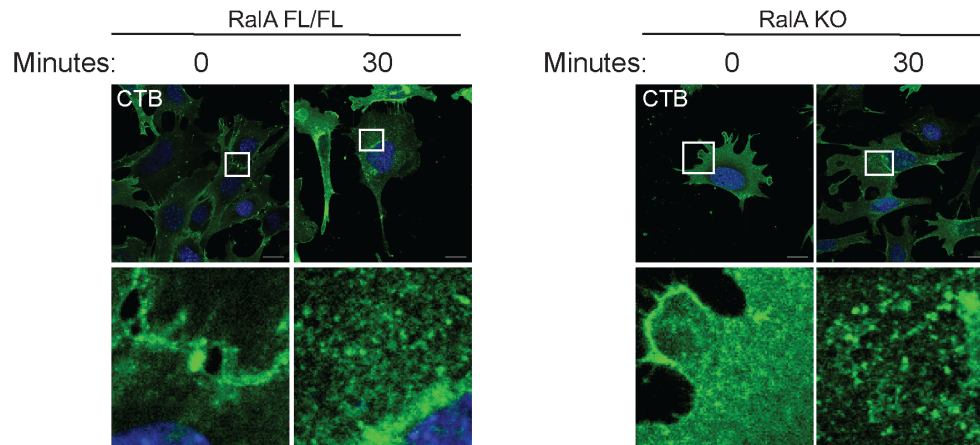


**Appendix D.** shRalA-2 HeLa cells exhibit impaired Parkin recruitment to depolarized mitochondria following CCCP treatment. (A) Immunoblot analysis of RalA in the indicated cells. RalA levels were quantified and normalized to  $\beta$ -tubulin. (B) shScramble and shRalA-2 HeLa cells transiently expressing mCherry-Parkin and mito-YFP were treated with 10  $\mu$ M CCCP or DMSO for 3 hours and imaged by confocal microscopy (Scale bars = 10  $\mu$ M). White boxes indicate magnified sections. (C) Parkin colocalization with mitochondria was assessed in the cells described in B for greater than 100 cells (Two-way ANOVA using Sidak's multiple comparisons test, mean  $\pm$  SEM, n.s. = not statistically significant, n = 3).



**Appendix E.** Clathrin-mediated endocytosis is required for both Parkin and RalA relocation to depolarized mitochondria. (A) HeLa cells transiently expressing mCherry-Parkin or GFP-RalA were pre-treated with DMSO or 20  $\mu$ M Pitstop 2 for 15 minutes and then treated for 1 hour with 10  $\mu$ M and 4  $\mu$ M (OA), DMSO, Pitstop 2 or Pitstop 2 and OA. Cells were imaged by confocal microscopy (Scale bars = 10  $\mu$ M). White boxes indicate magnified sections. (B) Quantification of A. Pearson's coefficients for RalA and Parkin colocalization were calculated using ImageJ (One-way ANOVA with Tukey's multiple comparisons test, mean  $\pm$  SEM, \*\*\* $p \leq 0.0001$ , n.s. = not statistically significant,  $n = 3$ ). Each dot represents one cell.

A.



**Appendix F.** RalA KO MEFs exhibit no defect in endocytosis of Cholera Toxin Subunit B. (A) RalA FL/FL and RalA KO MEFs were incubated with 1  $\mu\text{g}/\text{mL}$  Cholera Toxin Subunit B (CTB)-Alexa Fluor 488 for 15 minutes on ice and shifted from 4°C (t=0) to 37°C (t=30) for 30 minutes. Cells were imaged by confocal microscopy (Scale bars = 20  $\mu\text{M}$ ). White boxes indicate magnified sections.

## References

1. Chardin, P. & Tavitian, A. The ral gene: a new ras related gene isolated by the use of a synthetic probe. *The EMBO Journal* **5**, 2203–2208 (1986).
2. Chardin, P. & Tavitian, A. Coding sequences of human ralA and ralB cDNAs. *Nucleic Acids Res.* **17**, 4380 (1989).
3. Mirey, G. *et al.* A Ral guanine exchange factor-Ral pathway is conserved in *Drosophila melanogaster* and sheds new light on the connectivity of the Ral, Ras, and Rap pathways. *Molecular and Cellular Biology* **23**, 1112–1124 (2003).
4. Hsieh, C. L., Swaroop, A. & Francke, U. Chromosomal localization and cDNA sequence of human ralB, a GTP binding protein. *Somat. Cell Mol. Genet.* **16**, 407–410 (1990).
5. Kinsella, B. T., Erdman, R. A. & Maltese, W. A. Carboxyl-terminal isoprenylation of ras-related GTP-binding proteins encoded by rac1, rac2, and ralA. *Journal of Biological Chemistry* **266**, 9786–9794 (1991).
6. Falsetti, S. C. *et al.* Geranylgeranyltransferase I inhibitors target RalB to inhibit anchorage-dependent growth and induce apoptosis and RalA to inhibit anchorage-independent growth. *Molecular and Cellular Biology* **27**, 8003–8014 (2007).
7. Leung, K. F., Baron, R., Ali, B. R., Magee, A. I. & Seabra, M. C. Rab GTPases containing a CAAX motif are processed post-geranylgeranylation by proteolysis and methylation. *Journal of Biological Chemistry* **282**, 1487–1497 (2007).
8. Nishimura, A. & Linder, M. E. Identification of a novel prenyl and palmitoyl modification at the CaaX motif of Cdc42 that regulates RhoGDI binding. *Molecular and Cellular Biology* **33**, 1417–1429 (2013).
9. Gentry, L. R. *et al.* Divergent Roles of CAAX Motif-Signaled Posttranslational Modifications in the Regulation and Subcellular Localization of Ral GTPases. *J. Biol. Chem.* jbc.M115.656710 (2015). doi:10.1074/jbc.M115.656710
10. Shipitsin, M. & Feig, L. A. RalA but not RalB enhances polarized delivery of membrane proteins to the basolateral surface of epithelial cells. *Molecular and Cellular Biology* **24**, 5746–5756 (2004).
11. Lim, K.-H. *et al.* Activation of RalA is critical for Ras-induced tumorigenesis of human cells. *Cancer Cell* **7**, 533–545 (2005).
12. Wu, J.-C. *et al.* Identification of V23RalA-Ser194 as a critical mediator for Aurora-A-induced cellular motility and transformation by small pool expression screening. *Journal of Biological Chemistry* **280**, 9013–9022 (2005).
13. Wang, H. *et al.* Phosphorylation of RalB is important for bladder cancer cell growth and metastasis. *Cancer Research* **70**, 8760–8769 (2010).
14. Sablina, A. A. *et al.* The tumor suppressor PP2A A $\beta$  regulates the RalA GTPase. *Cell* **129**, 969–982 (2007).
15. Martin, T. D., Mitin, N., Cox, A. D., Yeh, J. J. & Der, C. J. Phosphorylation by protein kinase C $\alpha$  regulates RalB small GTPase protein activation, subcellular localization, and effector utilization. *J. Biol. Chem.* **287**, 14827–

- 14836 (2012).
16. Bivona, T. G. *et al.* PKC regulates a farnesyl-electrostatic switch on K-Ras that promotes its association with Bcl-XL on mitochondria and induces apoptosis. *Molecular Cell* **21**, 481–493 (2006).
  17. Neyraud, V. *et al.* RalA and RalB proteins are ubiquitinated GTPases, and ubiquitinated RalA increases lipid raft exposure at the plasma membrane. *Journal of Biological Chemistry* **287**, 29397–29405 (2012).
  18. Simicek, M. *et al.* The deubiquitylase USP33 discriminates between RALB functions in autophagy and innate immune response. *Nature Cell Biology* **15**, 1220–1230 (2013).
  19. Clough, R. R., Sidhu, R. S. & Bhullar, R. P. Calmodulin binds RalA and RalB and is required for the thrombin-induced activation of Ral in human platelets. *Journal of Biological Chemistry* **277**, 28972–28980 (2002).
  20. Wang, K. L. & Roufogalis, B. D. Ca<sup>2+</sup>/calmodulin stimulates GTP binding to the ras-related protein ral-A. *Journal of Biological Chemistry* **274**, 14525–14528 (1999).
  21. Wolthuis, R. M. *et al.* Activation of the small GTPase Ral in platelets. *Molecular and Cellular Biology* **18**, 2486–2491 (1998).
  22. Sidhu, R. S., Elsaraj, S. M., Grujic, O. & Bhullar, R. P. Calmodulin binding to the small GTPase Ral requires isoprenylated Ral. *Biochemical and Biophysical Research Communications* **336**, 105–109 (2005).
  23. Wildey, G. M., Viggewarapu, M., Rim, S. & Denker, J. K. Isolation of cDNA clones and tissue expression of rat ral A and ral B GTP-binding proteins. *Biochemical and Biophysical Research Communications* **194**, 552–559 (1993).
  24. Bhullar, R. P., Chardin, P. & Haslam, R. J. Identification of multiple ral gene products in human platelets that account for some but not all of the platelet G<sub>n</sub>-proteins. *FEBS Lett.* **260**, 48–52 (1990).
  25. Olofsson, B., Chardin, P., Touchot, N., Zahraoui, A. & Tavittian, A. Expression of the ras-related ralA, rho12 and rab genes in adult mouse tissues. *Oncogene* **3**, 231–234 (1988).
  26. Zhao, Z. & Rivkees, S. A. Tissue-specific expression of GTPases RalA and RalB during embryogenesis and regulation by epithelial-mesenchymal interaction. *Mech. Dev.* **97**, 201–204 (2000).
  27. Peschard, P. *et al.* Genetic Deletion of RALA and RALB Small GTPases Reveals Redundant Functions in Development and Tumorigenesis. *Current Biology* **22**, 2063–2068 (2012).
  28. Balakireva, M. *et al.* The Ral/exocyst effector complex counters c-Jun N-terminal kinase-dependent apoptosis in *Drosophila melanogaster*. *Molecular and Cellular Biology* **26**, 8953–8963 (2006).
  29. Sawamoto, K. *et al.* The *Drosophila* Ral GTPase regulates developmental cell shape changes through the Jun NH(2)-terminal kinase pathway. *The Journal of Cell Biology* **146**, 361–372 (1999).
  30. Hiatt, S. M. *et al.* De novo mutations in the GTP/GDP-binding region of RALA, a RAS-like small GTPase, cause intellectual disability and developmental delay. *PLoS Genet* **14**, e1007671 (2018).

31. Lim, K.-H. *et al.* Divergent roles for RalA and RalB in malignant growth of human pancreatic carcinoma cells. *Current Biology* **16**, 2385–2394 (2006).
32. Smith, S. C. *et al.* Expression of ral GTPases, their effectors, and activators in human bladder cancer. *Clin. Cancer Res.* **13**, 3803–3813 (2007).
33. Martin, T. D., Samuel, J. C., Routh, E. D., Der, C. J. & Yeh, J. J. Activation and involvement of Ral GTPases in colorectal cancer. *Cancer Research* **71**, 206–215 (2011).
34. Ginn, K. F. *et al.* RalA is overactivated in medulloblastoma. *J. Neurooncol.* 1–12 (2016). doi:10.1007/s11060-016-2236-4
35. Chien, Y. & White, M. A. RAL GTPases are linchpin modulators of human tumour-cell proliferation and survival. *EMBO rep* **4**, 800–806 (2003).
36. Hamad, N. M. *et al.* Distinct requirements for Ras oncogenesis in human versus mouse cells. *Genes Dev.* **16**, 2045–2057 (2002).
37. de Gorter, D. J. J. *et al.* The small GTPase Ral mediates SDF-1-induced migration of B cells and multiple myeloma cells. *Blood* **111**, 3364–3372 (2008).
38. Song, X. *et al.* Involvement of RalB in the effect of geranylgeranyltransferase I on glioma cell migration and invasion. *Clin Transl Oncol* **17**, 477–485 (2015).
39. Yin, J. *et al.* Activation of the RalGEF/Ral pathway promotes prostate cancer metastasis to bone. *Molecular and Cellular Biology* **27**, 7538–7550 (2007).
40. Thomas, J. C. *et al.* Inhibition of Ral GTPases Using a Stapled Peptide Approach. *J. Biol. Chem.* jbc.M116.720243 (2016). doi:10.1074/jbc.M116.720243
41. Chen, Y. *et al.* Autoantibodies to tumor-associated antigens combined with abnormal alpha-fetoprotein enhance immunodiagnosis of hepatocellular carcinoma. *Cancer Lett.* **289**, 32–39 (2010).
42. Li, J. *et al.* Evaluation and characterization of anti-RalA autoantibody as a potential serum biomarker in human prostate cancer. *Oncotarget* **5**, (2016).
43. Park, S. H. & Weinberg, R. A. A putative effector of Ral has homology to Rho/Rac GTPase activating proteins. *Oncogene* **11**, 2349–2355 (1995).
44. Cantor, S. B., Urano, T. & Feig, L. A. Identification and characterization of Ral-binding protein 1, a potential downstream target of Ral GTPases. *Molecular and Cellular Biology* **15**, 4578–4584 (1995).
45. Jullien-Flores, V. *et al.* Bridging Ral GTPase to Rho pathways. RLIP76, a Ral effector with CDC42/Rac GTPase-activating protein activity. *Journal of Biological Chemistry* **270**, 22473–22477 (1995).
46. Jullien-Flores, V. *et al.* RLIP76, an effector of the GTPase Ral, interacts with the AP2 complex: involvement of the Ral pathway in receptor endocytosis. *Journal of Cell Science* **113 ( Pt 16)**, 2837–2844 (2000).
47. Kashatus, D. F. *et al.* RALA and RALBP1 regulate mitochondrial fission at mitosis. *Nature Cell Biology* **13**, 1–10 (2011).
48. Ikeda, M., Ishida, O., Hinoi, T., Kishida, S. & Kikuchi, A. Identification and characterization of a novel protein interacting with Ral-binding protein 1, a putative effector protein of Ral. *Journal of Biological Chemistry* **273**, 814–821 (1998).

49. Campbell, L. J. *et al.* Thermodynamic mapping of effector protein interfaces with RalA and RalB. *Biochemistry* 150126162404003 (2015). doi:10.1021/bi501530u
50. Nakashima, S. *et al.* Small G protein Ral and its downstream molecules regulate endocytosis of EGF and insulin receptors. *The EMBO Journal* **18**, 3629–3642 (1999).
51. Yamaguchi, A., Urano, T., Goi, T. & Feig, L. A. An Eps homology (EH) domain protein that binds to the Ral-GTPase target, RalBP1. *Journal of Biological Chemistry* **272**, 31230–31234 (1997).
52. Shen, Y., Xu, L. & Foster, D. A. Role for phospholipase D in receptor-mediated endocytosis. *Molecular and Cellular Biology* **21**, 595–602 (2001).
53. Awasthi, S. *et al.* Novel function of human RLIP76: ATP-dependent transport of glutathione conjugates and doxorubicin. *Biochemistry* **39**, 9327–9334 (2000).
54. Moskalenko, S. *et al.* The exocyst is a Ral effector complex. *Nature Cell Biology* **4**, 66–72 (2002).
55. Moskalenko, S. *et al.* Ral GTPases regulate exocyst assembly through dual subunit interactions. *Journal of Biological Chemistry* **278**, 51743–51748 (2003).
56. Chen, X.-W., Leto, D., Chiang, S.-H., Wang, Q. & Saltiel, A. R. Activation of RalA is required for insulin-stimulated Glut4 trafficking to the plasma membrane via the exocyst and the motor protein Myo1c. *DEVCEL* **13**, 391–404 (2007).
57. Sánchez-Ruiz, J., Mejías, R., García-Belando, M., Barber, D. F. & González-García, A. Ral GTPases regulate cell-mediated cytotoxicity in NK cells. *J. Immunol.* **187**, 2433–2441 (2011).
58. Chien, Y. *et al.* RalB GTPase-mediated activation of the IkappaB family kinase TBK1 couples innate immune signaling to tumor cell survival. *Cell* **127**, 157–170 (2006).
59. Bodemann, B. O. *et al.* RalB and the Exocyst Mediate the Cellular Starvation Response by Direct Activation of Autophagosome Assembly. *Cell* **144**, 253–267 (2011).
60. Luo, J. Q. *et al.* Functional association between Arf and RalA in active phospholipase D complex. *Proc. Natl. Acad. Sci. U.S.A.* **95**, 3632–3637 (1998).
61. Vitale, N. *et al.* Calcium-regulated exocytosis of dense-core vesicles requires the activation of ADP-ribosylation factor (ARF)6 by ARF nucleotide binding site opener at the plasma membrane. *The Journal of Cell Biology* **159**, 79–89 (2002).
62. Frankel, P. *et al.* RalA interacts with ZONAB in a cell density-dependent manner and regulates its transcriptional activity. *The EMBO Journal* **24**, 54–62 (2005).
63. Ohta, Y., Suzuki, N., Nakamura, S., Hartwig, J. H. & Stossel, T. P. The small GTPase RalA targets filamin to induce filopodia. *Proc. Natl. Acad. Sci. U.S.A.* **96**, 2122–2128 (1999).
64. Arjonen, A., Kaukonen, R. & Ivaska, J. Filopodia and adhesion in cancer cell motility. *Cell Adh Migr* **5**, 421–430 (2011).
65. Shirai, Y. *et al.* Direct binding of RalA to PKC $\eta$  and its crucial role in

- morphological change during keratinocyte differentiation. *Mol. Biol. Cell* **22**, 1340–1352 (2011).
66. Helgason, E., Phung, Q. T. & Dueber, E. C. Recent insights into the complexity of Tank-binding kinase 1 signaling networks: the emerging role of cellular localization in the activation and substrate specificity of TBK1. *FEBS Lett.* **587**, 1230–1237 (2013).
  67. Heo, J.-M. *et al.* RAB7A phosphorylation by TBK1 promotes mitophagy via the PINK-PARKIN pathway. *Sci Adv* **4**, eaav0443 (2018).
  68. Heo, J.-M., Ordureau, A., Paulo, J. A., Rinehart, J. & Harper, J. W. The PINK1-PARKIN Mitochondrial Ubiquitylation Pathway Drives a Program of OPTN/NDP52 Recruitment and TBK1 Activation to Promote Mitophagy. *Molecular Cell* 1–15 (2015). doi:10.1016/j.molcel.2015.08.016
  69. Pilli, M. *et al.* TBK-1 promotes autophagy-mediated antimicrobial defense by controlling autophagosome maturation. *Immunity* **37**, 223–234 (2012).
  70. Oakes, J. A., Davies, M. C. & Collins, M. O. TBK1: a new player in ALS linking autophagy and neuroinflammation. *Mol Brain* **10**, 5 (2017).
  71. Uhm, M. *et al.* Phosphorylation of the exocyst protein Exo84 by TBK1 promotes insulin-stimulated GLUT4 trafficking. *Sci Signal* **10**, eaah5085 (2017).
  72. Lamb, C. A., Yoshimori, T. & Tooze, S. A. The autophagosome: origins unknown, biogenesis complex. *Nat. Rev. Mol. Cell Biol.* **14**, 759–774 (2013).
  73. Reggiori, F. & Klionsky, D. J. Autophagic processes in yeast: mechanism, machinery and regulation. *Genetics* **194**, 341–361 (2013).
  74. Davis, S., Wang, J. & Ferro-Novick, S. Crosstalk between the Secretory and Autophagy Pathways Regulates Autophagosome Formation. *Developmental Cell* **41**, 23–32 (2017).
  75. Hanada, T. *et al.* The Atg12-Atg5 conjugate has a novel E3-like activity for protein lipidation in autophagy. *Journal of Biological Chemistry* **282**, 37298–37302 (2007).
  76. Noda, N. N., Fujioka, Y., Hanada, T., Ohsumi, Y. & Inagaki, F. Structure of the Atg12-Atg5 conjugate reveals a platform for stimulating Atg8-PE conjugation. *EMBO rep* **14**, 206–211 (2013).
  77. Kuma, A., Mizushima, N., Ishihara, N. & Ohsumi, Y. Formation of the approximately 350-kDa Apg12-Apg5-Apg16 multimeric complex, mediated by Apg16 oligomerization, is essential for autophagy in yeast. *Journal of Biological Chemistry* **277**, 18619–18625 (2002).
  78. Glick, D., Barth, S. & Macleod, K. F. Autophagy: cellular and molecular mechanisms. *J. Pathol.* **221**, 3–12 (2010).
  79. Birgisdottir, Á. B., Lamark, T. & Johansen, T. The LIR motif - crucial for selective autophagy. *Journal of Cell Science* **126**, 3237–3247 (2013).
  80. Kirisako, T. *et al.* Formation process of autophagosome is traced with Apg8/Aut7p in yeast. *The Journal of Cell Biology* **147**, 435–446 (1999).
  81. Kimura, S., Noda, T. & Yoshimori, T. Dynein-dependent movement of autophagosomes mediates efficient encounters with lysosomes. *Cell Struct. Funct.* **33**, 109–122 (2008).
  82. Birgisdottir, Á. B., Lamark, T. & Johansen, T. The LIR motif - crucial for

- selective autophagy. *Journal of Cell Science* **126**, 3237–3247 (2013).
83. Tooze, S. A., Abada, A. & Elazar, Z. Endocytosis and autophagy: exploitation or cooperation? *Cold Spring Harbor Perspectives in Biology* **6**, a018358–a018358 (2014).
  84. Nakamura, S. & Yoshimori, T. New insights into autophagosome-lysosome fusion. *Journal of Cell Science* **130**, 1209–1216 (2017).
  85. Jäger, S. *et al.* Role for Rab7 in maturation of late autophagic vacuoles. *Journal of Cell Science* **117**, 4837–4848 (2004).
  86. Itoh, T., Kanno, E., Uemura, T., Waguri, S. & Fukuda, M. OATL1, a novel autophagosome-resident Rab33B-GAP, regulates autophagosomal maturation. *The Journal of Cell Biology* **192**, 839–853 (2011).
  87. Duman, J. G. & Forte, J. G. What is the role of SNARE proteins in membrane fusion? *Am. J. Physiol., Cell Physiol.* **285**, C237–49 (2003).
  88. Wang, H. *et al.* GABARAPs regulate PI4P-dependent autophagosome:lysosome fusion. *Proc. Natl. Acad. Sci. U.S.A.* **112**, 7015–7020 (2015).
  89. de Lartigue, J. *et al.* PIKfyve regulation of endosome-linked pathways. *Traffic* **10**, 883–893 (2009).
  90. Levine, B. & Kroemer, G. Autophagy in the pathogenesis of disease. *Cell* **132**, 27–42 (2008).
  91. Tracy, K., Velentzas, P. D. & Baehrecke, E. H. Ral GTPase and the exocyst regulate autophagy in a tissue-specific manner. *EMBO rep* **17**, 110–121 (2016).
  92. Friedman, J. R. & Nunnari, J. Mitochondrial form and function. *Nature* **505**, 335–343 (2014).
  93. Lane, N. & Martin, W. The energetics of genome complexity. *Nature* **467**, 929–934 (2010).
  94. Dudek, J., Rehling, P. & van der Laan, M. Mitochondrial protein import: common principles and physiological networks. *Biochim. Biophys. Acta* **1833**, 274–285 (2013).
  95. Youle, R. J. & van der Bliek, A. M. Mitochondrial Fission, Fusion, and Stress. *Science* **337**, 1062–1065 (2012).
  96. Twig, G. & Shirihai, O. S. The interplay between mitochondrial dynamics and mitophagy. *Antioxid. Redox Signal.* **14**, 1939–1951 (2011).
  97. Wai, T. & Langer, T. Mitochondrial Dynamics and Metabolic Regulation. *Trends in Endocrinology & Metabolism* **27**, 105–117 (2016).
  98. Shiota, T., Traven, A. & Lithgow, T. Mitochondrial biogenesis: cell-cycle-dependent investment in making mitochondria. *Curr. Biol.* **25**, R78–R80 (2015).
  99. Uren, R. T. *et al.* Mitochondrial release of pro-apoptotic proteins: electrostatic interactions can hold cytochrome c but not Smac/DIABLO to mitochondrial membranes. *Journal of Biological Chemistry* **280**, 2266–2274 (2005).
  100. Santo-Domingo, J. & Demaurex, N. Calcium uptake mechanisms of mitochondria. *Biochim. Biophys. Acta* **1797**, 907–912 (2010).
  101. Garrido, C. *et al.* Mechanisms of cytochrome c release from mitochondria.

- Cell Death and Differentiation* **13**, 1423–1433 (2006).
102. Du, C., Fang, M., Li, Y., Li, L. & Wang, X. Smac, a mitochondrial protein that promotes cytochrome c-dependent caspase activation by eliminating IAP inhibition. *Cell* **102**, 33–42 (2000).
  103. Paul, A., Krelin, Y., Arif, T., Jeger, R. & Shoshan-Barmatz, V. A New Role for the Mitochondrial Pro-apoptotic Protein SMAC/Diablo in Phospholipid Synthesis Associated with Tumorigenesis. *Mol. Ther.* **26**, 680–694 (2018).
  104. Hegde, R. *et al.* Identification of Omi/HtrA2 as a mitochondrial apoptotic serine protease that disrupts inhibitor of apoptosis protein-caspase interaction. *Journal of Biological Chemistry* **277**, 432–438 (2002).
  105. Mesmin, B. Mitochondrial lipid transport and biosynthesis: A complex balance. *The Journal of Cell Biology* **214**, 9–11 (2016).
  106. Scharwey, M., Tatsuta, T. & Langer, T. Mitochondrial lipid transport at a glance. *Journal of Cell Science* **126**, 5317–5323 (2013).
  107. Böttinger, L. *et al.* Phosphatidylethanolamine and cardiolipin differentially affect the stability of mitochondrial respiratory chain supercomplexes. *J. Mol. Biol.* **423**, 677–686 (2012).
  108. Lemasters, J. J. Variants of mitochondrial autophagy\_ Types 1 and 2 mitophagy and micromitophagy (Type 3). *Redox Biology* **2**, 749–754 (2014).
  109. Narendra, D., Tanaka, A., Suen, D. F. & Youle, R. J. Parkin is recruited selectively to impaired mitochondria and promotes their autophagy. *The Journal of Cell Biology* **183**, 795–803 (2008).
  110. Ding, W.-X. & Yin, X.-M. Mitophagy: mechanisms, pathophysiological roles, and analysis. *Biological Chemistry* **393**, 547–564 (2012).
  111. Zhang, J. & Ney, P. A. Role of BNIP3 and NIX in cell death, autophagy, and mitophagy. *Cell Death and Differentiation* **16**, 939–946 (2009).
  112. Sarraf, S. A. *et al.* Landscape of the PARKIN-dependent ubiquitylome in response to mitochondrial depolarization. *Nature* 1–7 (2013). doi:10.1038/nature12043
  113. Nuytemans, K., Theuns, J., Cruts, M. & Van Broeckhoven, C. Genetic etiology of Parkinson disease associated with mutations in the SNCA, PARK2, PINK1, PARK7, and LRRK2 genes: a mutation update. *Hum. Mutat.* **31**, 763–780 (2010).
  114. Narendra, D. P. *et al.* PINK1 Is Selectively Stabilized on Impaired Mitochondria to Activate Parkin. *PLoS Biol* **8**, e1000298 (2010).
  115. Koyano, F. *et al.* Ubiquitin is phosphorylated by PINK1 to activate parkin. *Nature* **510**, 162–166 (2015).
  116. Okatsu, K. *et al.* Phosphorylated ubiquitin chain is the genuine Parkin receptor. *The Journal of Cell Biology* **510**, 370 (2015).
  117. McDowell, G. S. & Philpott, A. Non-canonical ubiquitylation: mechanisms and consequences. *The International Journal of Biochemistry & Cell Biology* **45**, 1833–1842 (2013).
  118. Trempe, J. F. *et al.* Structure of Parkin Reveals Mechanisms for Ubiquitin Ligase Activation. *Science* **340**, 1451–1455 (2013).
  119. Lazarou, M. *et al.* The ubiquitin kinase PINK1 recruits autophagy receptors to induce mitophagy. *Nature* **524**, 309–314 (2015).

120. Richter, B. *et al.* Phosphorylation of OPTN by TBK1 enhances its binding to Ub chains and promotes selective autophagy of damaged mitochondria. *Proc. Natl. Acad. Sci. U.S.A.* 201523926 (2016). doi:10.1073/pnas.1523926113
121. Wild, P. *et al.* Phosphorylation of the autophagy receptor optineurin restricts Salmonella growth. *Science* **333**, 228–233 (2011).
122. Shin, N. *et al.* LRRK2 regulates synaptic vesicle endocytosis. *Experimental Cell Research* **314**, 2055–2065 (2008).
123. Krebs, C. E. *et al.* The Sac1 domain of SYNJ1 identified mutated in a family with early-onset progressive Parkinsonism with generalized seizures. *Hum. Mutat.* **34**, 1200–1207 (2013).
124. Quadri, M. *et al.* Mutation in the SYNJ1 gene associated with autosomal recessive, early-onset Parkinsonism. *Hum. Mutat.* **34**, 1208–1215 (2013).
125. Chang, J. Y., Yi, H.-S., Kim, H.-W. & Shong, M. Dysregulation of mitophagy in carcinogenesis and tumor progression. *Biochim Biophys Acta Bioenerg* **1858**, 633–640 (2017).
126. Sun, X. *et al.* Parkin deficiency contributes to pancreatic tumorigenesis by inducing spindle multipolarity and misorientation. *cc* **12**, 1133–1141 (2013).
127. da Silva-Camargo, C. C. V. *et al.* Parkin protein expression and its impact on survival of patients with advanced colorectal cancer. *Cancer Biol Med* **15**, 61–69 (2018).
128. O'Flanagan, C. H. & O'Neill, C. PINK1 signalling in cancer biology. *BBA - Reviews on Cancer* **1846**, 590–598 (2014).
129. Ginn, K. F. RalA is overactivated in medulloblastoma. *J. Neurooncol.* **130**, 99–110 (2016).
130. Yan, C. *et al.* Discovery and characterization of small molecules that target the GTPase Ral. *Nature* **515**, 443–447 (2015).
131. Martin, T. D. *et al.* Ral and Rheb GTPase activating proteins integrate mTOR and GTPase signaling in aging, autophagy, and tumor cell invasion. *Molecular Cell* **53**, 209–220 (2014).
132. Moore, A. S. & Holzbaur, E. L. F. Dynamic recruitment and activation of ALS-associated TBK1 with its target optineurin are required for efficient mitophagy. *Proc. Natl. Acad. Sci. U.S.A.* **113**, E3349–58 (2016).
133. Dupuis, L. *et al.* Mitochondria in amyotrophic lateral sclerosis: a trigger and a target. *Neurodegener Dis* **1**, 245–254 (2004).
134. Mouli, P. K., Twig, G. & Shirihai, O. S. Frequency and Selectivity of Mitochondrial Fusion Are Key to Its Quality Maintenance Function. *Biophysj* **96**, 3509–3518 (2009).
135. Rainbolt, T. K., Lebeau, J., Puchades, C. & Wiseman, R. L. Reciprocal Degradation of YME1L and OMA1 Adapts Mitochondrial Proteolytic Activity during Stress. *CellReports* **14**, 2041–2049 (2016).
136. Frech, M., Schlichting, I., Wittinghofer, A. & Chardin, P. Guanine nucleotide binding properties of the mammalian RalA protein produced in Escherichia coli. *Journal of Biological Chemistry* **265**, 6353–6359 (1990).
137. Emkey, R., Freedman, S. & Feig, L. A. Characterization of a GTPase-activating

- protein for the Ras-related Ral protein. *Journal of Biological Chemistry* **266**, 9703–9706 (1991).
138. Lim, K. H. *et al.* Aurora-A phosphorylates, activates, and relocalizes the small GTPase RalA. *Molecular and Cellular Biology* **30**, 508–523 (2010).
  139. Pollock, S. R. & Kashatus, D. F. in *Encyclopedia of Signaling Molecules* **39**, 4424–4433 (Springer, Cham, 2018).
  140. Elkin, S. R., Lakoduk, A. M. & Schmid, S. L. Endocytic pathways and endosomal trafficking: a primer. *Wien Med Wochenschr* 1–9 (2016). doi:10.1007/s10354-016-0432-7
  141. Han, K. *et al.* Regulated RalBP1 binding to RalA and PSD-95 controls AMPA receptor endocytosis and LTD. *PLoS Biol* **7**, e1000187 (2009).
  142. Landry, M.-C. *et al.* A functional interplay between the small GTPase Rab11a and mitochondria-shaping proteins regulates mitochondrial positioning and polarization of the actin cytoskeleton downstream of Src family kinases. *J. Biol. Chem.* **289**, 2230–2249 (2014).
  143. Hamacher-Brady, A., Choe, S. C., Krijnse-Locker, J. & Brady, N. R. Intramitochondrial recruitment of endolysosomes mediates Smac degradation and constitutes a novel intrinsic apoptosis antagonizing function of XIAP E3 ligase. *Cell Death and Differentiation* **21**, 1862–1876 (2014).
  144. Collins, L. V., Hajizadeh, S., Holme, E., Jonsson, I.-M. & Tarkowski, A. Endogenously oxidized mitochondrial DNA induces in vivo and in vitro inflammatory responses. *J. Leukoc. Biol.* **75**, 995–1000 (2004).
  145. West, A. P. *et al.* Mitochondrial DNA stress primes the antiviral innate immune response. *Nature* **520**, 553–557 (2015).
  146. Sharma, S. *et al.* Triggering the interferon antiviral response through an IKK-related pathway. *Science* **300**, 1148–1151 (2003).
  147. Prabakaran, T. *et al.* Attenuation of cGAS-STING signaling is mediated by a p62/SQSTM1-dependent autophagy pathway activated by TBK1. *The EMBO Journal* **37**, e97858 (2018).
  148. Ou, Y.-H. *et al.* TBK1 directly engages Akt/PKB survival signaling to support oncogenic transformation. *Molecular Cell* **41**, 458–470 (2011).
  149. Dugast, M., Toussaint, H., Dousset, C. & Benaroch, P. AP2 clathrin adaptor complex, but not AP1, controls the access of the major histocompatibility complex (MHC) class II to endosomes. *Journal of Biological Chemistry* **280**, 19656–19664 (2005).
  150. Lim, K.-H. *et al.* Aurora-A phosphorylates, activates, and relocalizes the small GTPase RalA. *Molecular and Cellular Biology* **30**, 508–523 (2010).
  151. Fallon, L. *et al.* A regulated interaction with the UIM protein Eps15 implicates parkin in EGF receptor trafficking and PI(3)K-Akt signalling. *Nature Cell Biology* **8**, 834–842 (2006).
  152. Wauer, T., Simicek, M., Schubert, A. & Komander, D. Mechanism of phospho-ubiquitin-induced PARKIN activation. *Nature* **524**, 370–374 (2015).
  153. Lazarou, M., Jin, S. M., Kane, L. A. & Youle, R. J. Role of PINK1 Binding to the TOM Complex and Alternate Intracellular Membranes in Recruitment and Activation of the E3 Ligase Parkin. *DEVCEL* **22**, 320–333 (2012).

154. Hilgemann, D. W., Fine, M., Linder, M. E., Jennings, B. C. & Lin, M.-J. Massive endocytosis triggered by surface membrane palmitoylation under mitochondrial control in BHK fibroblasts. *Elife* **2**, 299–16 (2013).
155. Yamano, K. *et al.* Endosomal Rab cycles regulate Parkin-mediated mitophagy. *Elife* **7**, 2006 (2018).
156. Vitale, N. *et al.* The Small GTPase RalA controls exocytosis of large dense core secretory granules by interacting with ARF6-dependent phospholipase D1. *Journal of Biological Chemistry* **280**, 29921–29928 (2005).
157. Lalli, G. & Hall, A. Ral GTPases regulate neurite branching through GAP-43 and the exocyst complex. *The Journal of Cell Biology* **171**, 857–869 (2005).
158. Li, N.-N. *et al.* GWAS-linked GAK locus in Parkinson's disease in Han Chinese and meta-analysis. *Hum. Genet.* **131**, 1089–1093 (2012).
159. Nagle, M. W. *et al.* The 4p16.3 Parkinson Disease Risk Locus Is Associated with GAK Expression and Genes Involved with the Synaptic Vesicle Membrane. *PLoS ONE* **11**, e0160925 (2016).
160. Schreij, A. M. A. *et al.* LRRK2 localizes to endosomes and interacts with clathrin-light chains to limit Rac1 activation. *EMBO rep* **16**, 79–86 (2015).
161. Schreij, A. M. A., Fon, E. A. & McPherson, P. S. Endocytic membrane trafficking and neurodegenerative disease. *Cellular and Molecular Life Sciences* **73**, 1529–1545 (2016).
162. Lu, H. *et al.* Regulation and function of mitophagy in development and cancer. *autophagy* **9**, 1720–1736 (2013).
163. Kim, J.-H. *et al.* Involvement of mitophagy in oncogenic K-Ras-induced transformation: Overcoming a cellular energy deficit from glucose deficiency. *autophagy* **7**, 1187–1198 (2011).
164. Jullien-Flores, V. *et al.* RLIP76, an effector of the GTPase Ral, interacts with the AP2 complex: involvement of the Ral pathway in receptor endocytosis. *Journal of Cell Science* **113 ( Pt 16)**, 2837–2844 (2000).
165. Johansson, J. *et al.* RAL GTPases Drive Intestinal Stem Cell Function and Regeneration through Internalization of WNT Signalosomes. *Cell Stem Cell* (2019). doi:10.1016/j.stem.2019.02.002
166. Schatoff, E. M., Leach, B. I. & Dow, L. E. Wnt Signaling and Colorectal Cancer. *Curr Colorectal Cancer Rep* **13**, 101–110 (2017).
167. Ahmad, L., Zhang, S.-Y., Casanova, J.-L. & Sancho-Shimizu, V. Human TBK1: A Gatekeeper of Neuroinflammation. *Trends in Molecular Medicine* **22**, 511–527 (2016).
168. Edvardson, S. *et al.* A deleterious mutation in DNAJC6 encoding the neuronal-specific clathrin-uncoating co-chaperone auxilin, is associated with juvenile parkinsonism. *PLoS ONE* **7**, e36458 (2012).
169. Chourasia, A. H. Mitophagy and cancer. 1–11 (2015). doi:10.1186/s40170-015-0130-8